On the Decay Interactions of Neutral K_{e3} and $K_{\mu3}$.

S. FURUICHI

Department of Physics, Hiroshima University - Hiroshima

Summary. — The decay interactions of the processes $K^0 \to e + \nu + \pi^0$ and $K^0 \to \mu + \nu + \pi^0$ are investigated. Under the assumption that these processes occur through the weak Fermi interaction the analysis has been performed about the energy spectra and angular correlations of charged secondaries in order to obtain some information about the decay interactions.

1. – Preliminary.

Some efforts have been devoted to check the adequacy of the universal weak Fermi interaction in explaining all weak decay processes. One of these is performed about the decay processes of $K^c_{\mu(e)3}$ [1] where the type of decay interactions and type of spin of $K^c_{\mu(e)3}$ are investigated under the assumption that the weak Fermi interaction is participating in the decays. (This is referred to as I). The analysis which is based on the Lorentz invariance requirements and one point interaction for lepton pair has been presented in I to obtain information about the dynamics of these weak decay processes. There we have mainly discussed about the energy spectrum of the secondary electron or muon which appears in the decay.

---

[1] S. FURUICHI, T. KODAMA, S. OGAWA, Y. SUGAHARA, A. WAKASA and M. YONEZAWA: *Prog. Theor. Phys.*, **17**, 89 (1957).

This paper constitutes the complementary part of the previous analysis in which the charged K-particle is discussed, and the neutral counter particle is treated. The existence of the neutral K-meson with electron and pion secondaries has recently been found ([2]) and it may seem reasonable to assume its decay mode as $K^0 \to e + \nu + \pi^c$ analogously as in the case of K^c_{e3}. The study of weak interaction in the case of neutral K-particles not only provides the complementary data to the case of charged K, but might serve for the investigation of the charge relation of weak interactions.

In the neutral K decay process, besides the momentum of charged lepton, we can obtain directly from the experiments the data about the momentum distribution of the pion and lepton and the angular correlation between them. In the following section we give an analysis about them, using the same method as used in I. One of the most important matter in the investigation is to decide the type of Fermi interactions which are observed in the natural occurences.

In this paper we assume that the spin of the K-meson is 0. From the analysis of some recently accumulated data about K^c_{e3} we are informed that the spin 0 possibility is larger than other spin possibilities ([3]), and the recent experimental data on the θ and τ mesons are in favor of the spin 0 assumption for these particles. The application of the present method to the case of high spin K-meson is easy, but in general much involved owing to the increase in the number of possible types of interaction.

The effective transition matrix M for the process is written as (for the spin 0 K-meson)

$$(1) \qquad M \propto F^s \overline{\psi}^c(p)\, \psi^\nu(q) \varphi^*(e)\, \Phi(k) + F^V \overline{\psi}^c(p) \gamma_\varrho \psi^\nu(q) \varphi^*(l)\, \Phi(k)\, s_\varrho +$$
$$+ F^T \overline{\psi}^c(p)\, \gamma_{[\varrho} \gamma_{\sigma]} \psi^\nu(q) \varphi^*(l)\, \Phi(k)\, s_\varrho t_\sigma ,$$

where $\Phi(k)$, $\psi^\nu(q)$, $\psi^c(p)$ and $\varphi(l)$ are the wave functions of K-meson, neutrino, electron (muon) and pion respectively. γ_μ is the ordinary Dirac matrix. s_ϱ and t_σ are the two independent momenta in the problem. The effective couplings F are the invariant functions of these independent momenta.

We can not know at present about the detailed structure of F owing to the complication of strong interaction. However we have made an approximation in I which replaces them by a momentum-independent constants. The same approximation is assumed here *a priori*.

In the following we give the discussion on the energy distribution of the

([2]) C. D'ANDLAU, R. ARMENTEROS, A. ASTIER, H. C. DeSTAEBLER, B. P. GREGORY, L. LEPRINCE-RINGUET, F. MULLER, C. PEYROU and H. TINLOT: *Nuovo Cimento*, **4**, 917 (1956).

([3]) S. FURUICHI, Y. SUGAHARA, A. WAKASA and M. YONEZAWA: *Nuovo Cimento*, **5**, 285 (1957).

secondary neutrino, charged pion and the distribution of the angle between two charged secondaries (*) using the expression (1) for the interaction. And some related problem to the present discussion of K-meson shall also be examined in Sect. 4.

2. – Energy distribution.

2˙1. *Neutrino energy distribution*. – In the neutral K event the data obtained from experiment are the pion and charged lepton momenta as well as the angle between them. Unfortunately these data are laboratory data and can not be easily compared with theory, since we can get in the ordinary experiments only vague information about the momentum or direction of the incident neutral K-meson which decays in flight.

However we can evaluate the neutrino momentum in the K-meson rest system from these laboratory data on the secondary by the equation

$$(2) \qquad q_0 = [\, m_K^2 - (p_0 + l_0)^2 + (\boldsymbol{p} + \boldsymbol{l})^2 \,]/2m_K \, ,$$

where m_K is the mass of the K-meson. p_0, $\boldsymbol{p}$ and l_0, $\boldsymbol{l}$ are the observed laboratory energy and the momenta of electron (muon) and pion respectively.

So whatever the value of the incident K-meson momentum, we can get the spectrum of the neutrino in the center of mass system of the K-meson and easily compare the experiment with theory.

The shape of the distribution is much like the distribution of the electrons and the most characteristic feature is the distribution in the case of tensor interaction.

The spectra of the final neutrino for the matrix elements (1) are given in Fig. 1. The curves are given for pure S, V and T interaction.

We do not give the K_{e3}^0 curve, for the distribution agrees well with the electron distribution on account of the small rest mass of the electron.

There have been several reports on the anomalous V^0 events including some cases which can be interpreted as K_{e3}^0 but they are rather fragmental and a systematical survey seems to be not yet performed.
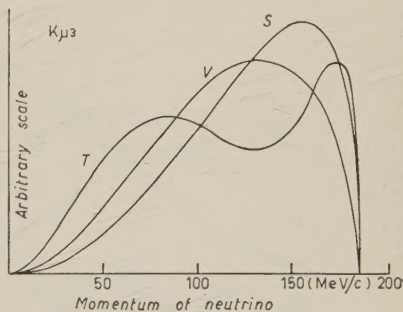

Fig. 1. – Theoretical energy spectra for the secondary neutrino in $K_{\mu3}^0$-decay processes. The curves are given for pure S, V and T interactions in the rest system of the K-meson.

(*) The calculation of angular correlation is very complicated by the appearence of elliptic integrals; we do it by numerical integration.

The reason for this may lie in the difficulty of obtaining high intensity neutral K-meson beams. Unfortunately we can not at present compare theory with experiment and must expect the future development of experiments.

2·2.1. *Charged lepton distribution.* – We have discussed in I the energy distribution of the secondary charged lepton in the case of charged $K \to$ $\to \mu + \nu + \pi^0$ and $K \to e + \nu + \pi^0$. For the present case the curve of these distributions are also valid by making a very small correction due to the mass difference between neutral and charged pion, and since the general features of the distribution are not changed we do not repeat it again.

In both the charged lepton and neutrino distributions, one of the most significant features of the distribution is the shape in the case of tensor interaction—the two peak shape—and it seems to be an easy task to clarify whether the tensor interaction exists or not, And we have met such a situation in the K^c_{e3} decay process which requires the existence of tensor interaction.

2·2.2. *Pion distribution.* – Besides the charged leptons (electron or muon) there appears another charged particle—charged pion—in the neutral K decay processes, and we can know its momentum from the experiment. We give here the energy distribution of the secondary pion in the center of mass system of the K-meson. The spectra are given in Fig. 2a and 2b. In the pion energy spectra the S-T interference term vanishes after angular integration, furthermore, in the K_{s3} case, S-V, V-T interference terms are very small.
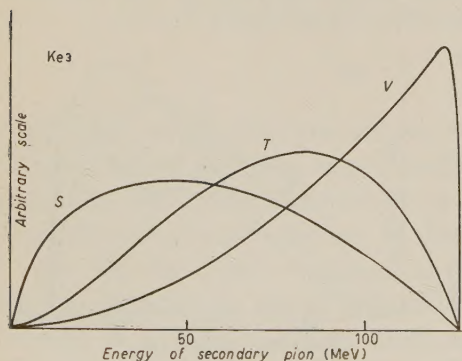

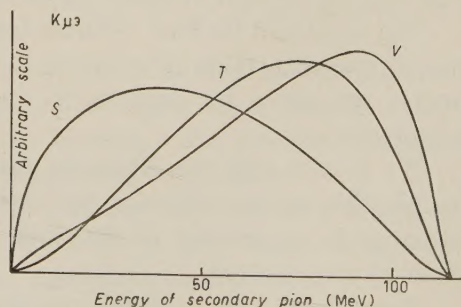Fig. 2a. – Theoretical energy spectra for secondary pion in K_{e3}.

Fig. 2b. – Theoretical energy spectra for secondary pion in $K_{\mu3}$.

This is independent of the approximation to replace F's by simple momentum dependent constants. Then, comparison of the pion energy spectrum with experiment is rather easy and type determination is simple.

It may be the indication of scalar interaction if the experimental distribution has a steep rise toward the low energy end, because the steep rise of the distribution is established only by the existence of scalar interaction. While if the distribution has large probability toward the high energy side it may indicate the existence of vector interaction. In the practical analysis of experimental data the K_{e3} is easier to be treated than the $K_{\mu3}$, because of the small interference term and the large difference between each type of distribution. However it must be remarked that the statement may be valid only if the assumption that only the lowest momentum dependent term is dominated is not strongly violated. While in the lepton energy spectrum the situation is a little different, because there always appear the muon momentum p and the neutrino momentum q in the combination $p+q$ and inclusion of higher order terms might not change the lowest feature appreciably. However if the types of Fermi interactions are known from other investigations, the simple structure of this function might be convenient for the analysis of the contribution from the dynamics of « loop » process.

3. – Angular correlations ([4]).

In this section we investigate the distribution of the angle between the final pion and electron (muon).

For the discussion of the angular correlation it is important to take two appropriate momenta in order to simplify the angular dependence of the invariant F functions. For example, if we take the K-meson momentum (k_ϱ) and the pion momentum (l_ϱ) as two independent variables, the function F becomes independent of the angle of these two charged particles and dependent only on $m_K l_0$ in the rest system of the K-meson. If we calculate the angular correlation for some fixed pion, as performed by PAIS and TREIMAN ([5]), we get the distribution which is completely free from the complication of momentum dependence of F which might be caused by strong dynamics.

However in Figs. 3a and 3b we

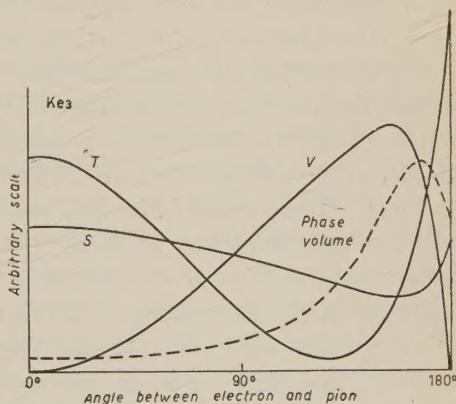Fig. 3a. – Theoretical angle distribution between pion and electron in K_{e3}^0 events. The curves divided by the distribution by phase volume of the final state are given.

([4]) A more detailed investigation of angular correlation covering the high spin case has been performed by HORI and WAKASA (private communication).

([5]) A. PAIS and B. TREIMAN: *Phys. Rev.*, **105**, 1616 (1957).

give the distribution integrated over the pion momentum by taking the same approximation as in the discussion of the energy spectrum, in order to obtain a rough feature of the situation and to check the relative consistency of the approximation, and to save the expected scarcity of experimental data.
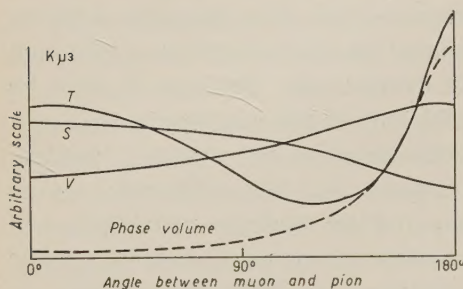

Fig. 3b. – Angular correlation of pion and muon in $K^0_{\mu 3}$ decay.

The distribution is dominated by phase volume distribution and owing to the large mass difference between secondary particles the distribution shows a maximum near 180°.

In order to make clear the difference between various types of the Fermi interaction we present the distribution divided by the phase volume of the final state.

The conclusive answer from angular correlations for the Fermi coupling type might be obtained in the kind of analysis of PAIS and TREIMAN although it requires much data.

4. – Some remarks on the hypothesis of Fermi interaction.

In this paper we have analysed the K_{e3} and $K_{\mu 3}$ events, assuming that the weak Fermi interaction is participating in the decay. The weak Fermi interaction concerned here is the Fermi interaction operating between one pair of baryons and one pair of leptons. If the assumption that the Fermi interaction causes the decay by co-operating with strong interaction is valid, it predicts the β-decay of Λ or Σ particles. Thus the experimental detection of these β-decay events has very significant implications to the present model. The relative frequency of these β-decay process in respect to the ordinary decay mode $\Lambda(\Sigma) \to N + \pi$ is $1/60 \div 1/200$ (^{6}), if we assume the same coupling constant as for the β-decays of the nucleon.

At present we have only one event which may be interpreted as β-decay of Σ (^{7}), and this supports our model. Further experimental investigation of β-decay events of Λ and Σ is very important and desirable.

In connection with the Fermi interaction assumption the problems of π-e decay and K_{e2}-decay are also important ones. It has been possible to inter-

(^{6}) K. IWATA, S. OGAWA, H. OKONOGI, B. SAKITA and S. ONEDA: *Prog. Theor. Phys.*, **13**, 19 (1955).

(^{7}) J. HORNBOSTEL and E. O. SALANT: *Phys. Rev.*, **102**, 502 (1956).

prete the absence of π-e-decay in so far that the interaction type of β-decay of nucleon is only S and T, and the process may be forbidden by parity conservation assuming the π-e-decay is due to those Fermi interactions. However it becomes clear that space-parity does not conserve in the weak β-decay process ([8]). So it may seem that this fact could open new questions on the π-e-decay puzzle even if we take the above explanation. However this space parity non-conservation may not cause trouble to the above interpretation of the π-e puzzle, as is seen in the perturbational calculations, if the strong pion baryon interaction has pseudo-character (γ_5 or $\gamma_5\gamma_\mu$ interaction) and only S and T Fermi interactions (here S and T means the coupling type between baryon pairs) realize, and this is independent whether we take Lee-Yang's theory of the neutrino or not. Anyway this puzzle must be further investigated both in its dynamical and kinematical character.

If the neutrinos appearing in the $K_{e(\mu)3}$ decay are two component neutrinos the emerging muons are generally polarized. The investigation of polarization may serve also to clarify the decay interaction ([9]).

In connection with the space parity non-conservation, there also rises the question whether time reversal invariance and charge conjugation invariance are valid or not. In the analysis of the charged K_{e3}-decay process the S and T interactions seem to be required in order to explain the observed experimental energy distribution of secondary electrons. In such a case we may check the invariance principles by studying the magnitude of the interference terms, since these invariance principles impose a restriction on the relative phase of the effective coupling constant (see Appendix).

Finally we should like to make some observation on the experiments of K_{e3}^0 and $K_{\mu3}^0$. Since the K^0 events are mainly decays in flight, the data obtained are not of K-events at rest, so the theoretical distribution must be transformed in the moving system of K or conversely experimental data into the rest system. And in order to know the momentum of the initial K-meson from the information about the decay secondaries it is required to know the direction of the incident K-beam. However it may be very difficult to decide the origin of the K and identify the charged secondaries simultaneously. Thus the only practical data which are available for comparison are the momentum distributions of the neutrino, and for the present the check of the theory must be done with this quantity.

([8]) T. D. LEE and C. N. YANG: *Phys. Rev.*, **104**, 254 (1956); C. S. WU, E. AMBLER, R. W. HAYWARD, D. D. HOPPES and R. P. HUDSON: *Phys. Rev.*, **105**, 1413 (1957).
([9]) J. WERLE: *Report of 7th Rochester Conference*; S. FURUICHI, S. SAWADA and M. YONEZAWA: *Nuovo Cimento*, **6**, 1416 (1957).

* * *

The author would like to express his deep gratitude to Mr. M. YONEZAWA for his kind collaboration and valuable discussion throughout this work. He is also grateful to Prof. K. SAKUMA, Drs. S. OGAWA and K. SENBA for their continual interest, to Miss Y. SUGAHARA for her assistance in carrying out the calculation in Sect. **3**, to Messers S. HORI and A. WAKASA for informing hmi about their calculations. He is also indebted to Dr. S. TANAKA at Rikkyo University for his kind teaching of the mutual relation between various formulations of time reversal.

APPENDIX

Here we show that the requirements of time reversibility impose on the effective coupling constants F's certain conditions. We follow WATANABE's [10] formulation of time reversal. Under the Wigner type of time reversal the condition that the system be invariant under time reversal is given by

$$(A.1) \qquad\qquad (RH(-t)R^{-1})^T = H(t) ,$$

where R is the unitary operator of time reversal.

Under time reversal the field operators transform as

$$(A.2) \quad \begin{cases} (R\,\psi(-t)\,R^{-1})^T = \varrho\gamma_5\gamma_4\,\overline{\psi}C(t) & \text{for the spinor field,} \\ (R\,\Phi(-t)\,R^{-1})^T = \varrho'\,\Phi^*(t) & \text{for the boson field.} \end{cases}$$

Now we take the effective interaction Hamiltonian corresponding to transition matrix (1) as

$$(A.3) \quad H_{\text{int}}(t) = f_s\,\overline{\psi}^e(t)\psi^\nu(t)\varphi^*(t)\,\Phi(t) - if_\nu\overline{\psi}^e(t)\gamma_\varrho\,\psi^\nu(t)\varphi^*(t)\,\frac{\partial\Phi(t)}{\partial x_\varrho} +$$

$$+ f_T\overline{\psi}^e(t)\gamma_{[\sigma}\gamma_{\sigma]}\psi^\nu(t)\,\frac{\partial\varphi^*(t)}{\partial x_\sigma}\,\frac{\partial\Phi(t)}{\partial x_\varrho} + \text{H.C.}$$

[10] S. WATANABE: *Phys. Rev.*, **84**, 1008 (1951); H. UMEZAWA, S. KAMEFUCHI and S. TANAKA: *Prog. Theor. Phys.*, **12**, 383 (1954); S. WATANABE: *Rev. Mod. Phys.*, **27**, 40 (1955).

If we substitute the expression (A.3) to the equation (A.1) and compare the left and right sides of equation (A.1), we get the following conditions between phase factors and effective coupling constants. (Compare the transformed one with its corresponding H.C. term of $H(t)$).

(A.4)
$$\begin{cases} f_{\mathrm{S}}\varrho_e^* \varrho_\nu \varrho_\pi^* \varrho_{\mathrm{K}} = f_{\mathrm{S}}^* \,, \\[4pt] -f_{\mathrm{V}}\varrho_e^* \varrho_\nu \varrho_\pi^* \varrho_{\mathrm{K}} = f_{\mathrm{V}}^* \,, \\[4pt] f_{\mathrm{T}}\varrho_e^* \varrho_\nu \varrho_\pi^* \varrho_{\mathrm{K}} = f_{\mathrm{T}}^* \,. \end{cases}$$

Then we get the following conditions for the effective coupling constants f_{S}, f_{V} and f_{T},

(A.5)
$$\begin{cases} (f_{\mathrm{S}}/f_{\mathrm{T}}) = \quad (f_{\mathrm{S}}^*/f_{\mathrm{T}}^*) & \text{(reality)}\,, \\[4pt] (f_{\mathrm{S}}/f_{\mathrm{V}}) = -\,(f_{\mathrm{S}}^*/f_{\mathrm{V}}^*) & \text{(imaginarity)}\,, \\[4pt] (f_{\mathrm{V}}/f_{\mathrm{T}}) = -\,(f_{\mathrm{V}}^*/f_{\mathrm{T}}^*) & \text{(imaginarity)}\,. \end{cases}$$

Consequently, when interaction Hamiltonian (1) is invariant under time reversal, the interference terms (cf. espression (6) in I) take maximum value on account of a relative phase (A.5), and we may be able to check the validity of time reversibility by observing the magnitude of interference term. From the data of K_{e3}^c [11] up to now, we have not obtained the definite indication whether time reversibility is violated or not in K_{e3} processes. It must be remarked that the space parity non-conserving theory does not make any objection to our present analysis. But it must also be noted that all of the parity violating interactions which are obtained from (1) replacing ψ^ν by $(1+a\gamma_5)\psi^\nu$ are not in general compatible with the requirement of time reversibility. However for the real a all the interactions are compatible with this requirement. Charge conjugation invariance imposes the same condition as (A.5) for effective coupling iconstant.

---

[11] Ref. [3].

RIASSUNTO (*)

Si esaminano le interazioni di decadimento dei processi $K^0 \to e + \nu + \pi^c$ e $K^0 \to \mu + \nu + \pi^c$. Facendo l'ipotesi che questi processi avvengano tramite l'interazione di Fermi debole, l'analisi è stata portata sugli spettri energetici e le correlazioni angolari dei secondari carichi onde ottenere informazioni sulle interazioni di decadimento.

Some Remarks on Parity Non-Conservation and the τ - Θ Dilemma.

S. GOTÔ

Institute of Physics, Tokyo Gakugei University - Tokyo, Japan

Summary. — LEE and YANG have succeeded in ascribing the parity non-conservation in the weak interactions to the singular nature of the mass zero neutrino—a screwon theory of two component neutrino. In this paper we introduce two kinds of neutrinos—the right circularly polarized neutrino and the left circularly polarized neutrino in the normal particle state—in order to forbid the unwanted processes such as $\mu^{\pm} \to e^{\pm} + e^{+} + e^{-}$ and $\mu^{-} + p \to p + e^{-}$ which are not forbidden in the Lee-Yang's original formulation, and discuss a possibility of solving the so-called τ-Θ dilemma by virtue of the virtual neutrino's effect.

1. – Introduction.

Recently LEE and YANG ([1,2]) have discussed a possibility of parity non-conservation in the weak interaction as a method of solving the so-called τ-Θ dilemma, and suggested a number of possible experimental tests of the violation of parity conservation. In fact, C. S. WU *et al.* ([3]), performing the experiment suggested by LEE and YANG, found a violation of the law of space inversion invariance in case of ^{60}Co.

To ascribe the parity non-conservation in the weak interactions to the singular nature of mass zero neutrino, LEE and YANG ([4]) examined a screwon theory of neutrino which essentially originates from the zero mass of neutrino.

([1]) T. D. LEE and C. N. YANG: *Phys. Rev.*, **104**, 254 (1956).

([2]) T. D. LEE, R. OEHME and C. N. YANG: preprint.

([3]) C. S. WU *et al.*: *Phys. Rev.*, **105**, 1413 (1957).

([4]) T. D. LEE and C. N. YANG: preprint; L. LANDAU: *Nuclear Physics*, **3**, 127 (1957); A. SALAM: *Nuovo Cimento*: **5**, 299 (1957).

According to their theory, the neutrino has been considered to be a source of the non-conservation of parity, so that we have a natural understanding of the violation of parity conservation in processes involving the neutrino. But unfortunately their theory, as it stands, shows that an understanding of the τ-Θ puzzle presents now a problem on a new level, because no neutrino is involved in the decay of $K_{\pi 3}$ and $K_{\pi 2}$.

Lee and Yang's theory of the two component neutrino gives that the μ-e decay consistent with the known experimental result is

$$(1.1) \qquad \mu^- \to e^- + \nu + \tilde{\nu}$$

and not

$$(1.2) \qquad \mu^- \to e^- + 2\nu$$

$$(2.3) \qquad \to e^- + 2\tilde{\nu},$$

where ν and $\tilde{\nu}$ mean respectively a screwon neutrino and its antiscrewon neutrino. If we assume here lepton number conservation by assigning the same lepton number for both μ^- and e^- to allow the process (1.1) on the one hand and forbid the processes (1.2) and (1.3) on the other, the unwanted processes

$$(1.4) \qquad \mu^\pm \to e^\pm + e^+ + e^-$$

and

$$(1.5) \qquad \mu^- + p \to p + e^-$$

become to be allowable by the lepton number conservation. Therefore we are obliged to set a different selection rule from the conservation law of lepton number in order to forbid the processes (1.4) and (1.5), but it will be hardly possible for us to perform this task unless a vast alteration be undertaken of some of the currently used physical concepts.

In this note we introduce two kinds of neutrino—the right circularly polarized neutrino ν_1 and the left circularly polarized neutrino ν_2—in the normal particle state in order to forbid the unwanted processes (1.4) and (1.5), and examine an interaction model being shown schematically in Fig. 1 in connection with the τ-Θ puzzle.

2. – Fundamental assumptions.

First we assume in accordance with LEE and YANG as follows:

I.   *The neutrino is an essentially two component Dirac particle* [5] *whose mass is necessarily exactly zero.*

---

[5] C. L. COWAN *et al.*: *Nature*, **178**, 446 (1956); *Nuovo Cimento*, **3**, 649 (1956).

II.   *The lepton number (n) is conserved in all allowable processes*:

(2.1) $\Delta n = 0$.

This selection rule was first used by KONOPINSKI and MAHMOUD ([6]) to forbid the unwanted processes (1.4) and (1.5). We have no experiments showing the violation of the lepton number conservation.

III.   *A new quantum number, lepton strangeness (u), is assigned for every lepton* ([7]).

The assignment of lepton number (n), lepton iso-spin (I) and lepton strangeness (u) is the same as that in the paper (G) ([7]).

IV.   *In the normal particle state, two kinds of neutrinos, the right circularly polarized neutrino ν_1 and the left circularly polarized neutrino ν_2, are introduced.*

Since the mass of neutrino is assumed in I to be exactly zero, it is allowable to introduce two kinds of neutrinos ν_1 and ν_2 in the normal particle state. The ν_1 and ν_2 are distinguishable from each other, because they are the different eigen states of the γ_5-operator.

V.   *The primary interactions in the strong ones are of the Yukawa type and those in the weak interactions of the Fermi type.*

By use of this assumption the various interactions realized in nature can be classified into either the primary or the secondary processes.

VI.   *The interaction scheme is assumed to be like that given in Fig. 1.*
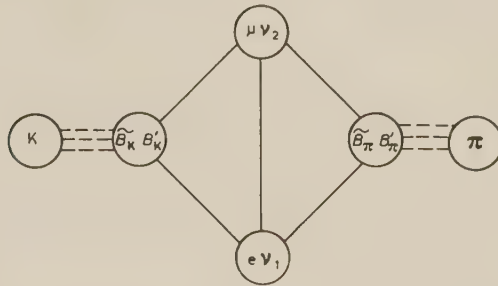
Fig. 1. – Interaction model. ———— weak Fermi type interaction $(f^2 \sim 10^{-14})$; ·········· strong Yukawa type interaction $(G^2 \sim 1)$.

The selection rules governing the strong and weak interactions have been

([6]) E. J. KONOPINSKI and H. M. MAHMOUD: *Phys. Rev.*, **92**, 1045 (1953).

([7]) S. GOTÔ: *Prog. Theor. Phys.*, **17**, 107 and 517 (1957); *Nuovo Cimento*, **5**, 1573 (1957). We call this paper as (G).

given in the paper (G). According to this interaction scheme the neutrino is the source of all the weak interactions and at the same time is also the source of parity non-conservation in the lepton processes.

3. – The weak lepton processes (involving real neutrino).

As is shown in the paper (G), the positive muon μ^+ and the electron e^-, are assumed to be normal particles. Therefore the μ-e decay occurs through

$$(3.1) \qquad \mu^- \rightarrow e^- + \tilde{\nu}_1 + \tilde{\nu}_2$$

and not

$$(3.2) \qquad \left\{ \begin{array}{l} \mu^- \rightarrow e^- + \nu_1 + \nu_2 \\ \quad\;\rightarrow e^- + \tilde{\nu}_1 + \nu_2 \\ \quad\;\rightarrow e^- + \nu_1 + \tilde{\nu}_2 \end{array} \right.$$

by the lepton number conservation.

Now the decay coupling of the process (3.1) can be written with the notation defined by

$$(3.3) \qquad O_\nu = \gamma_\mu , \qquad O_A = \gamma_5 \gamma_\mu$$

as follows

$$(3.4) \qquad H_{\text{int}} = \sum_{i=\nu,A} f_i (O_i^\top C^{-1} \psi_{\mu+} \psi_{e-})(O_i^\top C^{-1} \psi_{\nu_1} \psi_{\nu_2})^* + \text{h. c.} ,$$

where ψ_{ν_1} and ψ_{ν_2} denote respectively the conventional four component wave functions of the right circularly polarized neutrino ν_1 and of the left circularly polarized neutrino ν_2 (with violation of parity). C means the charge conjugation operator of the Dirac spinor and $C^{-1}\psi\psi$ is defined by

$$(3.5) \qquad C^{-1}\psi\psi = \sum_{\alpha,\beta=1}^{4} C^{-1}_{\alpha\beta}\psi_\alpha\psi_\beta .$$

The energy spectrum of the emitted electron in the μ-e decay results to be the same as that in reference (^{4}).

In the β-decay there are two possibilities

$$(3.6a) \qquad n \rightarrow p + e^- + \tilde{\nu}_1$$

or

$$(3.6b) \qquad n \rightarrow p + e^- + \tilde{\nu}_2 .$$

The choice of the two possibilities (3.6a) and (3.6b) can be determined by measuring the sign of the asymmetry parameter. The experiment made by C. S. Wu *et al.* shows that the β-decay occurs through (3.6a) and not through (3.6b), because the sign of the asymmetry parameter is negative. Corresponding to the β-decay (3.6a), the μ-capture, the π-μ-decay, the $K_{\mu 2}$ decay, the $K_{\mu 3}$ decay and the K_{e3} decay are given respectively as follows:

(3.7) $\mu^- + p \rightarrow n + \tilde{\nu}_2$

(3.8) $\pi^+ \rightarrow \mu^+ + \tilde{\nu}_2$

(3.9) $K^+ \rightarrow \mu^+ + \tilde{\nu}_2$

(3.10) $\rightarrow \mu^+ + \tilde{\nu}_2 + \pi^0$

(3.11) $\rightarrow e^+ + \nu_1 + \pi^0$.

We note here that in the μ-e decay the ratio of the parity conserving term to the parity non-conserving term is always one.

To explain the various decay modes of K-mesons by a single kind of K-particle, for example with odd parity and zero spin, we assume that the interaction Hamiltonians in the Minkowski space are given by

(3.12) $H_s = G_1 \overline{\Psi}_a \gamma_5 \overline{\Psi}_b \varphi + G_2 \Psi_a \gamma_5 \gamma_\mu \Psi_b \dfrac{\partial \varphi}{\partial x_\mu} + \text{h. c.}$

(for the strong Yukawa interaction)

(3.13) $H_{we} = \sum_{i=S,T} f_i \overline{\Psi}_a O_i \Psi_b \overline{\psi}_{e^-} O_i \psi_{\nu_1} + \text{h. c.}$

(for the weak Fermi interaction involving electron)

(3.14) $H_{w\mu} = \sum_{i=V,A} f_i \overline{\Psi}_a O_i \Psi_b \overline{\psi}_{\mu^+} O_i \psi_{\nu_2} + \text{h. c.}$

(for the weak Fermi interaction involving moun)

where Ψ_a, Ψ_b, ψ_{e^-}, ψ_{μ^+}, ψ_{ν_1}, and ψ_{ν_2} are the fields describing the baryon a, the baryon b, the electron, the positive muon, the neutrino ν_1 and the neutrino ν_2. If we use $\hbar = c = \lambda = 1$ with $\lambda = \hbar/m_\pi c \sim 10^{-13}$ cm (the Compton wave length for pion), we obtain $G_1^2 \sim G_2^2 \sim 1$, $f^2 \sim 10^{-14}$.

From the interaction Hamiltonian given by (3.12) we see that there are two possibilities of the intrinsic parity assignment for the stronglys, because in all the strong interactions parity is strictly conserved. To make our discussion simple, we consider the case only where the K has odd parity. We assume the intrinsic spin of the K-particle to be zero.

Thus we can obtain the non-zero transition matrix for any one of the processes $(3.8) \sim (3.11)$. In our case the branching ratios

$$\varrho_\pi = w(\pi^+ \to e^+ + \nu_1)/w(\pi^+ \to \mu^+ + \widetilde{\nu}_2),$$

$$\varrho_{\pi\gamma} = w(\pi^+ \to e^+ + \nu_1 + \gamma)/w(\pi^+ \to \mu^+ + \widetilde{\nu}_2)$$

and

$$\varrho_K = w(K^+ \to e^+ + \nu_1)/w(K^+ \to \mu^+ + \widetilde{\nu}_2),$$

$$\varrho_{K\gamma} = w(K^+ \to e^+ + \nu_1 + \gamma)/w(K^+ \to \mu^+ + \widetilde{\nu}_2)$$

can be made to be consistent with the known experimental results ([8]), because the decay processes $\pi^+ \to e^+ + \nu_1$ and $K^+ \to e^+ + \nu_1$ are forbidden for the S and T type couplings of four fermions involving (e^+, ν_1).

4. – The weak stronglys processes (involving no real neutrino).

Since in the present model all the weak decay interactions between the stronglys (the baryon, the K and π-mesons) are assumed to be realized only through the (μ, ν_2) loop, it will be expected that the τ and Θ decay modes of K-meson should be derived from a single kind of K-meson on account of the parity non-conserving virtual neutrino.

In the first place we consider the $K_{\pi 2}$ decay mode of K-meson with odd parity and zero spin. One type of Feynman diagrams of $K_{\pi 2}$ ($K_{\pi 3}$) decay is shown in Fig. 2. The transition matrix element for the process $K^+ \to \pi^+ + \pi^0$ is given by
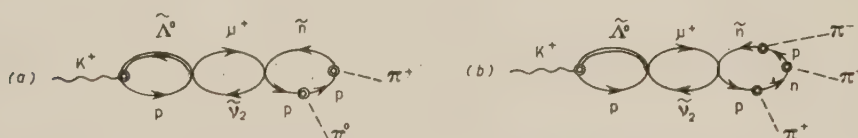
Fig. 2. – Typical Feynman diagrams for the processes:
(a) $K^+ \to \pi^+ + \pi^0$;   (b) $K^+ \to \pi^+ + \pi^+ + \pi^-$.

$$(4.1) \qquad f^2 G^3 \mathcal{M}_{\pi 2}(P, p) \Phi_{K^+}(P) \varphi_{\pi^0}^*(p) \varphi_{\pi^+}^*(P - p),$$

([8]) S. LOKANATHAN and J. STEINBERGER: *Bull. Am. Phys. Soc.*, **29**, 25 (1954); *Phys. Rev.*, **98**, 240 (A) (1955); H. FRIEDMAN and J. RAINWATER: *Phys. Rev.*, **81**, 644 (1951).

where P_μ and p_μ mean respectively the energy-momentum four vector of the K-meson and of the π^0-meson. According to the usual perturbation calculation the non-zero value of $\mathcal{M}_{\pi 2}$ is a diverging scalar quantity obtained from the interference terms between the parity conserving and parity non-conserving terms of the virtual neutrino interactions (with parity violation). In order to obtain the decay life consistent with the known experimental results from (4.1), we must use the cut-off momentum for the virtual lepton pair much larger than that for the baryon pairs. However it may be not necessarily unnatural to use this large cut-off momentum for the lepton pair, because the leptons have no strong interactions.

The discussion along similar lines can also be applied to the $K_{\pi 3}$ decay. Thus, the τ and Θ decay modes can be derived from a single kind of K-meson, for example, with odd parity and zero spin.
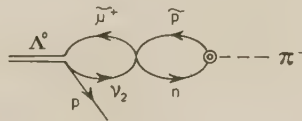

Fig. 3. – One type of Feynman diagrams for the decay: $\Lambda^0 \to p + \pi^-$.

Next we consider the hyperon decay without accompanying neutrino, for example $\Lambda^0 \to p + \pi^-$ (Fig. 3). If we assume the parity assignment for the stronglys corresponding to the odd parity of the K-meson, we get the transition matrix element for the decay $\Lambda^0 \to p + \pi^-$ as follows:

$$(4.2) \qquad \sum f_j^2 G \mathcal{M}_\mu(P, p)\, \psi_p(p) \gamma_5^{(j)} \gamma_\mu \Psi_{\Lambda^0}(P) \varphi_{\pi^-}^*(P - p) \,,$$

where the non-zero $\mathcal{M}_\mu$ is a vector quantity, and $\gamma_5^{(j)} = 1$ $(j=0)$ or γ_5 $(j=1)$.

5. – Conclusions.

The content of the present paper can be summarized as follows:

A) To forbid the unwanted processes such as (1.4), (1.5) and (3.2) on the one hand and to allow the wanted process (3.1) on the other, we have introduced two kinds of neutrinos—the right circularly polarized neutrino and the left circularly polarized neutrino—in the normal particle state.

B) The neutrino has been assumed to be the true origin of all the weak interactions (not only of the lepton interactions but also of the weak interactions between the stronglys). As a result of this assumption, we can derive both the τ and Θ decay modes of K-particles from a single kind of K-meson,

for example, with odd parity and zero spin, but the decay life times obtained from the present interaction model are too long to be compared with the experimental values unless we use a cut-off momentum for the muon-neutrino loop much larger than that for the baryon loops.

<div align="center">APPENDIX</div>

Relation between the mass zero neutrino and the photon field. ([9])

To describe the free photon field, we employ a sixteen component wave function $\varphi_{\alpha\beta}$ ($\alpha, \beta = 1, 2, 3, 4$), which transforms under Lorentz-transformations as the direct product of two Dirac spinors with zero mass and satisfies the following equation:

(A-I) ([10])
$$\left(\beta_\mu \frac{\partial}{\partial x_\mu} + \Gamma\right)\varphi = 0 ,$$

where β_μ and Γ are 16×16 matrices obeying the commutation relation:

(A-1)
$$\beta_\mu \beta_\nu \beta_\varrho + \beta_\varrho \beta_\nu \beta_\mu = \delta_{\mu\nu}\beta_\varrho + \delta_{\varrho\nu}\beta_\mu$$

(A-2)
$$\Gamma^2 = \Gamma$$

(A-3)
$$\Gamma\beta_\mu + \beta_\mu\Gamma = \beta_\mu .$$

For the β_μ and Γ, we use a special reducible representation such as

(A-4)
$$\beta_\mu = \tfrac{1}{2}(\gamma_\mu^{(1)} \times 1^{(2)} + 1^{(1)} \times \gamma_\mu^{(2)}) ,$$

(A-5)
$$\Gamma = \tfrac{1}{2}(1^{(1)} \times 1^{(2)} + \gamma_5^{(1)} \times \gamma_5^{(2)}) ,$$

or

(A-5')
$$\Gamma = \tfrac{1}{2}(1^{(1)} \times 1^{(2)} - \gamma_5^{(1)} \times \gamma_5^{(2)}) .$$

We call the Γ given by (A-5) as Γ_+, the Γ given by (A-5') as Γ_-. The Γ_+ and Γ_- are respectively the projection operators in the linear manifold $\{\varphi\}$

([9]) S. GOTÔ: *Reports of Tokyo Gakugei University* (1952), p. 35.
([10]) H. CHANDRA: *Proc. Roy. Soc.*, A **186**, 502 (1946). He proposed to use the equation (A-I) as the photon equation by employing the irreducible representation of β_μ and Γ.

such as

$$\Gamma_+ + \Gamma_- = 1 \, ,$$

(A-7) $$\Gamma_+ \cdot \Gamma_- = 0 \, .$$

The self charge conjugate condition

(A-8) $$\varphi' = C\overline{\varphi} = \varphi$$

has to be imposed to the equation (A-I) in order to be able to describe the photon field. In (A-8) C is given in terms of the charge conjugation matrix, C, of the mass zero Dirac field by

(A-9) $$C = C^{(1)} \times C^{(2)}$$

and φ is defined by

(A-10) $$\overline{\varphi} = \varphi^\dagger \gamma_4^{(1)} \times \gamma_4^{(2)}$$

From the equation (A-I) we obtain

(A-II) $$\beta_\mu \frac{\partial}{\partial x_\mu} (\Gamma\varphi) = 0 \, ,$$

which indicates that $\Gamma\varphi$ is a solution of the Duffin-Kemmer equation with zero rest mass.

A gauge transformation corresponding to that of the prevalent theory is given by

(A-III) $$\varphi \to \varphi + (1 - \Gamma)\chi \, ,$$

where χ is an arbitrary solution of the equation (A-III). In order to eliminate the longitudinal waves, φ is to be chosen in such a way that it satisfies in addition to (A-I) the equation

(A-IV) $$\frac{\partial}{\partial x_\mu} (\beta_\mu \beta_\nu \varphi) = \frac{\partial}{\partial x_\nu} \varphi \, .$$

We shall demonstrate that the Maxwell equations are deduced from the equations (A-I) and (A-II). In the first place we notice that

(A-11) $$C^{-1}\varphi = C_{\alpha\beta}^{-1}\varphi_{\alpha\beta}$$

is a scalar as it was used by A. KLEIN in his meson theory [11]. By operating

---

[11] A. KLEIN: *Phys. Rev.*, **82**, 639 (1951).

$\gamma_A^\top C^{-1}$ to the equation (A-I) and (A-II) from the left we can easily derive

(A-12)
$$\frac{1}{2}(\gamma_\mu^- \gamma_A^\top - \gamma_A^\top \gamma_\mu^\top) C^{-1} \frac{\partial}{\partial x_\mu} \varphi - \gamma_A^\top C^{-1} \Gamma \varphi = 0 \ .$$

and

(A-13)
$$\frac{1}{2}(\gamma_\mu^\top \gamma_A^- - \gamma_A^\top \gamma_\mu^-) O^{-1} \frac{\partial}{\partial x_\mu} (\Gamma \varphi) = 0 \ ,$$

where γ_A indicates any one of the set:

$$\left(1, \ \gamma_\mu, \ \sigma_{\mu\nu} = \frac{i}{2}(\gamma_\mu \gamma_\nu - \gamma_\mu \gamma_\nu), \ \gamma_5 \gamma_\mu, \ \gamma_5 \right) \ .$$

If we take $\gamma_A = \gamma_\nu^\top$ in (A-13), we deduce

(A-14)
$$\frac{\partial}{\partial x_\mu} F_{\mu\nu} = 0 \ .$$

with the abbreviation of

(A-15)
$$F_{\mu\nu} = - F_{\nu\mu} = - \sigma_{\mu\nu}^\top C^{-1} \Gamma \varphi \ .$$

Further we put $\gamma_A = \sigma_{\lambda\nu}$ in the equation (A-12), from which results

(A-16)
$$F_{\mu\lambda} = \frac{\partial A_\lambda}{\partial x_\nu} - \frac{\partial A_\nu}{\partial x_\lambda} \ ,$$

where

(A-17)
$$A_\nu = \gamma_\nu^\top C^{-1} \varphi \ .$$

The equations (A-14) and (A-16) are the Maxwell equations.

Now, the subsidiary condition (A-IV) gives the usual one

(A-18)
$$\frac{\partial A_\mu}{\partial x_\mu} = 0.$$

In the following we shall give a revised relation between the circular polarized neutrino and photon. We are concerned with the linear manifold defined by

(A-19)
$$\gamma_\mu \frac{\partial \psi}{\partial x_\mu} = 0$$

and

(A-20a)
$$\gamma_5 \psi = - \psi$$

and with the other one for which

(A-20b) $\gamma_5 \psi = \psi$

holds. As is well known both manifolds correspond physically to right and left circular polarization. These two manifolds can also be written by using the ψ defined by (A-19) as follows:

(A-21a) $\psi_v = P_r \psi \qquad \left(P_\gamma = \dfrac{1 - \gamma_5}{2} \right),$

(A-12b) $\psi_. = P_. \psi \qquad \left(P_l = \dfrac{1 + \gamma_5}{2} \right).$

If we define

(A-22a) $\Gamma_r = P_r^{(1)} \times P_r^{(2)},$

(A-22b) $\Gamma_l = P_l^{(1)} \times P_l^{(2)},$

we get the right circularly polarized state $\Gamma_r \varphi$ and the left circularly polarized state $\Gamma_l \varphi$ in the manifold φ. We obtain the following relation:

(A-23) $\Gamma_r = \tfrac{1}{2}(\Gamma_+ - \beta_.)$

(A-23) $\Gamma_l = \tfrac{1}{2}(\Gamma_- + \beta)$

(A-25) $\Gamma_- = P_r^{(1)} \times P_l^{(2)} + P_l^{(1)} \times P_r^{(2)},$

where $\beta_.$ is given by

(A-26) $\beta_. = \tfrac{1}{2}(1^{(1)} \times \gamma_5^{(2)} + \gamma_5^{(1)} \times 1^{(2)}).$

From (A-23) and (A-24) we get

(A-27) $\Gamma_+ = \Gamma_r + \Gamma_l$

and

(A-28) $\Gamma_\gamma \cdot \Gamma_l = 0$

by making use of the relation

(A-29) $\Gamma_+ = \beta_5^2.$

If we divide A_μ defined by the equation (A-17) into two parts:

(A-30) $A_\mu = A_\mu^{(s)} + A_\mu^{(p)}$

(A-31a) $A_\mu^{(s)} = \gamma_\mu \, C^{-1} \Gamma_+ \varphi$

(A-31b) $A_\mu^{(p)} = \gamma_\mu^\top C^{-1} \Gamma_- \varphi,$

we obtain

(A-32) $$A_\mu^{(s)} = A_\mu^{(r)} + A_\mu^{(l)}$$

(A-33a) $$A_\mu^{(r)} = \gamma_\mu^\top C^{-1} \Gamma_\gamma \varphi$$

(A-33b) $$A_\mu^{(l)} = \gamma_\mu^\top C^{-1} \Gamma_l \varphi \,,$$

where $A_\mu^{(r)}$ and $A_\mu^{(l)}$ correspond to the right and left circularly polarized photons. Similarly $A_\mu^{(p)}$ is composed of two independent polarized states whose polarization is not circular.

Note added in proof:

This paper was written before we knew the many new experimental results of the β- and the π-μ-e decays, for instance, those reported at the *Seventh Rochester Conference* (1957). The asymmetry of the emitted positron from ^{58}Co, the new experimental values of the Michel parameter etc. require some modifications of the present model. Discussions on these points will be soon published elsewhere on a new standpoint where both the isospin and the strangeness are not assigned for the lepton and a new quantum number J ($J_3 = Q$, charge) appears as a very useful concept characterizing the lepton.

RIASSUNTO (*)

LEE e YANG sono riusciti ad attribuire la non conservazione della parità nelle interazioni deboli alla natura singolare del neutrino di massa zero — una teoria che attribuisce al neutrino a due componenti rotazione di verso determinato. Nel presente lavoro introduciamo due specie di neutrini — quello polarizzato circolarmente a destra e quello polarizzato circolarmente a sinistra nel loro stato normale — onde render proibiti i processi non desiderati, quali $\mu^\pm \to e^\pm + e^+ + e^-$ e $\mu^- + p \to p + e^-$ che nella formulazione originale di Lee e Yang non sono proibiti e discutiamo la possibilità di risolvere il cosiddetto dilemma τ-Θ in virtù dell'effetto del neutrino virtuale.

Spin-orbit Coupling and Tensor Forces (*).

B. Jancovici

Laboratoire de Physique de l'École Normale Supérieure - Université de Paris

Résumé. — Nous avons cherché si on peut expliquer les forces spin-orbite dans les noyaux complexes comme un effet du 2ᵉ ordre des forces tensorielles. Suivant les méthodes de Brueckner, nous calculons d'abord une amplitude de réaction modifiée, pour les collisions de deux nucléons au sein de la matière nucléaire. Nous utilisons la deuxième approximation de Born, et nous tenons compte du principe d'exclusion dans les états intermédiaires. Nous obtenons ensuite le potentiel spin-orbite moyen auquel est soumis un nucléon en sommant sur toutes ses collisions l'amplitude de réaction. Le potentiel spin-orbite ainsi obtenu est d'un ordre de grandeur trop faible et peut même avoir le mauvais signe. Nous discutons quelques implications de ces résultats.

1. – Introduction.

The only non-central forces which are known with certainty to exist in the two-body nuclear problem (e.g. from the quadrupole moment of the deuteron) are the tensor forces. For the sake of simplicity, it may be asked if these forces are sufficient to account for the spin-orbit coupling which explains the shell model and the high energy nucleon-nucleus polarization experiments.

In the case of light nuclei, some evidence has been given that this is indeed the case (¹). We here treat the problem for heavy nuclei, using an approach

---

(¹) E. P. Wigner and A. M. Feingold: *Phys. Rev.*, **79**, 221 (1950); A. M. Feingold: *Phys. Rev.*, **101**, 258 (1956); **105**, 944 (1957); D. H. Lyons: *Phys. Rev.*, **105**, 936 (1957).

in the spirit of Brueckner's model [2]. A preliminary account of this work has already been given [3]. Independent results obtained by L. S. KISSLINGER are in disagreement with ours [4].

We derive the spin-orbit effective potential from the reaction matrix for two-body collisions [5,6]. This reaction matrix will actually be a « modified » reaction matrix, which means that it is defined for the two-body collisions inside the nuclear matter and that it takes into account the presence of other nucleons, through the use of the exclusion principle in the intermediate states (statistical correlations). The modified reaction matrix has a spin-linear part

$$(1) \qquad [\alpha + \beta(\boldsymbol{\tau}_i \cdot \boldsymbol{\tau}_j)](\boldsymbol{\sigma}_i + \boldsymbol{\sigma}_j) \cdot (\boldsymbol{k}_i' \boldsymbol{k}_j' \,|\, A \,|\, \boldsymbol{k}_i \boldsymbol{k}_j)$$

for the collision of two particles i and j having initial and final momenta $\boldsymbol{k}_i$, $\boldsymbol{k}_j$ and $\boldsymbol{k}_i'$, $\boldsymbol{k}_j'$, respectively. $\boldsymbol{\tau}$ and $\boldsymbol{\sigma}$ are the isotopic spin and spin operators.

We here assume that the effective potential in which the i-th nucleon moves is obtained by summing (1) on all two-body collisions with other nucleons j. This assumption will be discussed in Sect. 7. A spin-orbit potential may emerge (Sect. 2) from such a calculation only in a nucleus of non-uniform density: the spin-orbit potential is a surface effect [7]. However, it is convenient to compute (1) from the two-body forces in a medium of uniform density (Sect. 3). Therefore, we use the Thomas-Fermi approximation: the density $\varrho(r)$ is varying, but, in the neighbourhood of each point, the nuclear structure may be approximated by a Fermi-gas with a local Fermi momentum

$$(2) \qquad f(r) = \left[\frac{3\pi^2}{2}\,\varrho(r)\right]^{\frac{1}{3}}.$$

2. - From the modified reaction amplitude to the spin-orbit potential.

The average spin-dependent potential $\boldsymbol{\sigma}_i \cdot \boldsymbol{V}_i$ in which the i-th nucleon moves is obtained by adding the reaction amplitudes (1) for the collisions with all the other nucleons j. Thus, in momentum space, a matrix element of $\boldsymbol{V}_i$

[2] H. A. BETHE: Phys. Rev., **103**, 1353 (1956).

[3] B. JANCOVICI: Phys. Rev., **107**, 631 (1957); Thèse (Paris, 1957).

[4] L. S. KISSLINGER: Phys. Rev., **104**, 1077 (1956). See note [9] in ref. [3].

[5] S. FERNBACH, W. HECKROTTE and J. V. LEPORE: Phys. Rev., **97**, 1059 (1955).

[6] J. S. BELL and T. H. R. SKYRME: Phil. Mag., **1**, 1055 (1956).

[7] E. FERMI: quoted by R. M. STERNHEIMER.

reads:

(3)
$$\begin{cases} (\boldsymbol{k}_i' \,|\, \boldsymbol{V}_i \,|\, \boldsymbol{k}_i) = 4 \sum_{\varPsi_j} (2\pi)^{-6} \int \mathrm{d}^3 k_j' \int \mathrm{d}^3 k_j \,, \\[2mm] \varPsi_j^*(\boldsymbol{k}_j') \left[\alpha(\boldsymbol{k}_i' \boldsymbol{k}_j' \,|\, \boldsymbol{A} \,|\, \boldsymbol{k}_i \boldsymbol{k}_j) - (\tfrac{1}{2})(\alpha + 3\beta)(\boldsymbol{k}_j' \boldsymbol{k}_i' \,|\, \boldsymbol{A} \,|\, \boldsymbol{k}_i \boldsymbol{k}_j) \right] \varPsi_j(\boldsymbol{k}_j) \,, \end{cases}$$

where the $\varPsi_j(\boldsymbol{k}_j)$ are the Fourier transforms of the one-particle orbital states $\varPsi_j(\boldsymbol{r}_j)$:

(4)
$$\varPsi(\boldsymbol{k}) = \int \mathrm{d}^3 r \exp\left[-i\boldsymbol{k}\cdot\boldsymbol{r}\right]\varPsi(\boldsymbol{r}) \,.$$

Eq. (3) can be brought, with some approximations, to the form of a usual spin-orbit potential ([5,6]). In our model, we assume a varying spherically symmetrical nuclear density.

(5)
$$4 \sum_{\varPsi_j} \varPsi_i^*(\boldsymbol{r}_j)\,\varPsi_j(\boldsymbol{r}_j) = \varrho(r_j) \,,$$

while around each point we describe the correlations by those of a « local » Fermi gas of « local » Fermi momentum f:

(6)
$$4 \sum_{\varPsi_j} \varPsi_i^*(\boldsymbol{r}_j')\varPsi_j(\boldsymbol{r}_j) = \varrho(r_j')[3/4\pi\ ^3(r_j')] \int\limits_{\varkappa<f} \exp[-i\boldsymbol{k}\cdot(\boldsymbol{r}_j' - \boldsymbol{r}_j)]\,\mathrm{d}^3\varkappa \,.$$

In such a model, using (6) and the momentum conservation:

(7)
$$(\boldsymbol{k}_i'\boldsymbol{k}_j' \,|\, \boldsymbol{A} \,|\, \boldsymbol{k}_i \boldsymbol{k}_j) = (2\pi)^3\,\delta(\boldsymbol{k}_i' + \boldsymbol{k}_j' - \boldsymbol{k}_i - \boldsymbol{k}_j)(\boldsymbol{k}_j' \,|\, \tilde{\boldsymbol{A}} \,|\, \boldsymbol{k}_i \boldsymbol{k}_j) \,,$$

we may bring (3) to the form:

(8)
$$\boldsymbol{k}_i' \,|\, \boldsymbol{V}_i \,|\, \boldsymbol{k}_i) = \int \mathrm{d}^3 g \int \mathrm{d}^3 r_j' \exp\left[i\boldsymbol{g}\cdot\boldsymbol{r}_j'\right]\varrho(r_j')\,\delta(\boldsymbol{k}_i' - \boldsymbol{k}_i + \boldsymbol{g})[3/4\pi f^3(r_j')]\cdot$$
$$\cdot \int\limits_{k_j<f} \mathrm{d}^3 k_j [\alpha(\boldsymbol{k}_j + \boldsymbol{g} \,|\, \tilde{\boldsymbol{A}} \,|\, \boldsymbol{k}_i, \, \boldsymbol{k}_j) - (\tfrac{1}{2})(\alpha + 3\beta)(\boldsymbol{k}_i - \boldsymbol{g} \,|\, \tilde{\boldsymbol{A}} \,|\, \boldsymbol{k}_i \boldsymbol{k}_j)] \,.$$

The last integral in the expression (8) is a pseudovector depending only on $\boldsymbol{k}_i$ and $\boldsymbol{g}$ (after this last integration has been performed). We may expand this expression in successive powers of $\boldsymbol{g}$, which would make successive derivatives of the density ϱ appear in (8). We keep only the linear term in $\boldsymbol{g}$. This means that we assume the spin-orbit effects to depend mostly on the first derivative of the density. Or, from another point of view, this approximation means

that we only consider small angle (direct and exchange) scatterings of the i-th nucleon in the nuclear matter. This first non-vanishing term of the expansion must be of the form:

$$(9) \qquad (3/4\pi f^3) \int_{k_j < f} \mathrm{d}^3 k_j (\boldsymbol{k}_j + \boldsymbol{g} \,|\, \tilde{A} \,|\, \boldsymbol{k}_i, \, \boldsymbol{k}_j) = \boldsymbol{g} \times \boldsymbol{k}_i \, E_0(k_i, f) + \dots ,$$

$$(10) \qquad (3/4\pi f^3) \int_{k_j < f} \mathrm{d}^3 k_j (\boldsymbol{k}_i - \boldsymbol{g} \,|\, \tilde{A} \,|\, \boldsymbol{k}_i, \, \boldsymbol{k}_j) = \boldsymbol{g} \times \boldsymbol{k}_i \, E_1(k_i, f) + \dots .$$

Using (9) and (10) in (8), and changing the integration variable $\boldsymbol{r}'_j$ into $\boldsymbol{r}_i$, we obtain the familiar expression

$$(11) \qquad (\boldsymbol{k}'_i \,|\, \boldsymbol{V}_i \,|\, \boldsymbol{k}_i) = \int \mathrm{d}^3 r_i \exp\left[-i\boldsymbol{k}'_i \cdot \boldsymbol{r}_i + i\boldsymbol{k}_i \cdot \boldsymbol{r}_i\right] a(k_i, \,\, (r_i)) \frac{1}{r_i} \frac{\partial \varrho}{\partial r_i} (\boldsymbol{r}_i \times \boldsymbol{k}_i) ,$$

where

$$(12) \qquad a(k_i, f(r_i)) = a_0 + a_1 = i\left[\alpha E_0(k_i, f) - (\tfrac{1}{2})(\alpha + 3\beta) E_1(k_i, f)\right] .$$

Thus the energy of the i-th nucleon is the same as if it were submitted to an effective spin-orbit force [8]

$$(13) \qquad a(k_i, f(r_i)) \frac{1}{r_i} \frac{\partial \varrho}{\partial r_i} (\boldsymbol{l}_i \cdot \boldsymbol{\sigma}_i) .$$

In addition to $\boldsymbol{l}_i$, there is a velocity dependence in a because of k_i. However, if i is the « last » bound nucleon, k_i is peaked around f and we will just take $k_i = f(r_i)$. If i is a scattered high energy nucleon, $\hbar^2 k_i^2 / 2M$ must be taken as its kinetic energy inside the potential well.

3. – The calculation of the modified reaction amplitude.

Our task is now to obtain the modified reaction amplitudes (9) and (10) from the interaction between particles i and j, assuming that these particles are part of a locally uniform Fermi gas of Fermi momentum f. The reaction

---

[8] The a coefficient depends on both k_i and (through f) r_i. This could lead to some difficulties, since these two variables do not commute. Actually, we can consider them now as classical variables in the same approximation as the Thomas-Fermi approximation; in the latter, a momentum (e.g. the Fermi momentum) is defined at each point, which is also only a classical concept.

matrix θ_{ij} at energy E is given by the integral equation

$$(14) \qquad \theta_{ij} = v_{ij} + v_{ij} \frac{Q}{E - H} \theta_{ij} ,$$

where Q is the projector outside the states which are already occupied by other nucleons and H is the « model » hamiltonian for the average potential.

Here, we just use for (14) the second Born approximation, which gives the first non-vanishing spin-linear result in the case where the spin-dependent part of v_{ij} is a tensor force. In this second order Born approximation, the reaction amplitude is

$$(15) \qquad (2\pi)^{-3} (2M/\hbar^2) \int_{q_i > f} d^3 q_i \int_{q_j > f} d^3 q_j (\boldsymbol{k}_i' \boldsymbol{k}_j' | v_{ij} | \boldsymbol{q}_i \boldsymbol{q}_j) \frac{1}{k_i^2 + k_j^2 - q_i^2 - q_j^2} (\boldsymbol{q}_i \boldsymbol{q}_j | v_{ij} | \boldsymbol{k}_i \boldsymbol{k}_j).$$

The momenta $\boldsymbol{q}_i \boldsymbol{q}_j$ of the intermediate state must be outside the Fermi sphere. We assume that v_{ij} has a tensor part

$$(16) \qquad v_{ij} = [1 - \chi + \chi(\boldsymbol{\tau}_i \cdot \boldsymbol{\tau}_j)] u(r_{ij}) S_{ij}(\boldsymbol{r}_{ij}) + \dots ,$$

where

$$(17) \qquad S_{ij}(\boldsymbol{r}_{ij}) = \frac{3}{r_{ij}^2} (\boldsymbol{\sigma}_i \cdot \boldsymbol{r}_{ij})(\boldsymbol{\sigma}_j \cdot \boldsymbol{r}_{ij}) - (\boldsymbol{\sigma}_i \cdot \boldsymbol{\sigma}_j) ,$$

and we are only interested in the part of (15) which is linear in the spins. By inserting (16) into (15), it is readily found that this part is (1) where

$$(18) \qquad \alpha = 1 - 2\chi + 4\chi^2 , \qquad \beta = 2\chi - 4\chi^2 ,$$

and

$$(19) \qquad \boldsymbol{k}_j' | \tilde{\boldsymbol{A}} | \boldsymbol{k}_i \boldsymbol{k}_j) = i(9M/16\pi^2 \hbar^2) \int_{\Omega(K)} d^3 q (\boldsymbol{k}' - \boldsymbol{q}) \times (\boldsymbol{k} - \boldsymbol{q}) \cdot$$

$$\cdot \frac{(\boldsymbol{k}' - \boldsymbol{q}) \cdot (\boldsymbol{k} - \boldsymbol{q})}{k^2 - q^2} \frac{w(| \boldsymbol{k}' - \boldsymbol{q} |) w(| \boldsymbol{k} - \boldsymbol{q} |)}{| \boldsymbol{k}' - \boldsymbol{q} |^2 | \boldsymbol{k} - \boldsymbol{q} |^2} ,$$

where we have inserted the relative momenta:

$$(20) \qquad \boldsymbol{k} = \boldsymbol{k}_i - \boldsymbol{k}_j , \qquad \boldsymbol{k}' = \boldsymbol{k}_i' - \boldsymbol{k}_j' , \qquad \boldsymbol{q} = \boldsymbol{q}_i - \boldsymbol{q}_j , \qquad \boldsymbol{K} = \boldsymbol{k}_i + \boldsymbol{k}_j ,$$

and

$$(21) \qquad w(k) = \int_0^\infty j_2(kr) u(r) r^2 \, dr ,$$

(j_2 is a spherical Bessel function ([9])). The domain of integration over q, Ω, is defined by the conditions

$$(22) \qquad q_i, q_j > f, \quad \text{i.e.} \quad |q \pm (\tfrac{1}{2})K| > f.$$

We only need (19) for $k_j' = k_j + g$ and $k_j' = k_i - g$. We just keep the first term in an expansion in powers of g:

$$(23) \qquad (k_j + g \,|\, \widetilde{A} \,|\, k_i,\, k_j) = i(9M/16\pi^2\hbar^2)\int_{\Omega} \mathrm{d}^3q\, \frac{g \times (g - k)}{k^2 \quad q^2}\left[\frac{w(|q - k|)}{|q - k|}\right]^2 + \dots,$$

and

$$(24) \qquad (k_i - g \,|\, A \,|\, k_i,\, k_j) = i(9M/16\pi^2\hbar^2)\int_{\Omega} \mathrm{d}^3q\, \frac{w(q - k)}{|q - k|^2} \cdot$$

$$\cdot \left\{ g \times (q - k)\,\frac{w(|q + k|)}{|q + k|^2} - \frac{2(k \times q)[g \cdot (q - k)]}{k^2 - q^2}\,\frac{w(|q + k|)}{|q + k|^2} + \right.$$

$$\left. + 2(k \times q)\left[g \cdot (q + k)\,\frac{1}{|q + k|}\,\frac{\partial}{\partial |q + k|}\,\frac{w(|q + k|)}{|q + k|^2}\right]\right\} + \dots.$$

We need only the integrated values (9) and (10), the tensorial nature of which we know in advance, so that one may readily show that:

$$(25) \qquad E_0(k_i, f) = i\,\frac{9M}{16\pi^2\hbar^2}\,\frac{3}{4\pi f^3}\,\frac{1}{k_i^2}\int_{k_j < f}\mathrm{d}^3k_j \int_{\Omega}\mathrm{d}^3q\,\frac{k_i \cdot (q - k)}{k^2 - q^2}\left[\frac{w(|q - k|)}{|q - k|}\right]^2,$$

and

$$(26) \qquad E_1(k_i, f) = i\,\frac{9M}{16\pi^2\hbar^2}\,\frac{3}{4\pi f^3}\,\frac{1}{k_i^2}\int_{k_j < f}\mathrm{d}^3k_j \int_{\Omega}\mathrm{d}^3q\,\frac{w(|q - k|)}{|q - k|^2} \cdot$$

$$\cdot \left\{\left[-\,k_i \cdot k + \frac{(k_i \cdot k)q^2 - (k_i \cdot q)(k \cdot q)}{k^2 - q^2}\right]\frac{w(|q + k|)}{|q + k|^2} + \right.$$

$$+ \left[(k_i \cdot q)(k \cdot q) - (k_i \cdot k)q^2 + k^2(k_i \cdot q) - (k_i \cdot k)(k \cdot q)\right] \cdot$$

$$\left. \cdot \frac{1}{|q + k|}\,\frac{\partial}{\partial |q + k|}\,\frac{w(|q + k|)}{|q + k|^2}\right\} \cdot$$

In Appendix I, we give a method for computing by a one-variable numerical integration the integral (25), for any tensor force, the Bessel transform (21)

([9]) P. M. MORSE and H. FESHBACH: *Methods of Theoretical Physics* (New York, 1953).

of which is known. (25) is given by the integral

$$(27) \qquad E_0(k_i, f) = - i \, 36 (M/\hbar^2) V_0^2 f^{-1} \int_0^\infty \Phi_{k_i}(x) \left[w \left(\frac{2f}{\mu} x \right) \right]^2 dx ,$$

where $\Phi_{k_i}(x)$ is a universal function $1/\mu$ is the range of the tensor force. For the last bound nucleon, $k_i = f$, and

$$(28) \quad \begin{cases} \Phi_f(x) = \dfrac{3}{8} (1 - x^2)^2 \operatorname{Log} \dfrac{x+1}{x-1} + \\[2mm] \qquad + 2x(x+1)^2(x-2) \operatorname{Log} 2 + \dfrac{1}{4} x(-2x^3 - 3x^2 + 12x + 13) , \quad \text{if } x < 1, \\[3mm] \Phi_f(x) = 2x(x-1)^2(x+2) \operatorname{Log}(x-1) + 2x(x+1)^2(x-2) \operatorname{Log}(x+1) + \\[2mm] \qquad + 4x^2(-x^2 + 3) \operatorname{Log} x + 2x^2 + 3 , \qquad\qquad\qquad \text{if } x > 1. \end{cases}$$
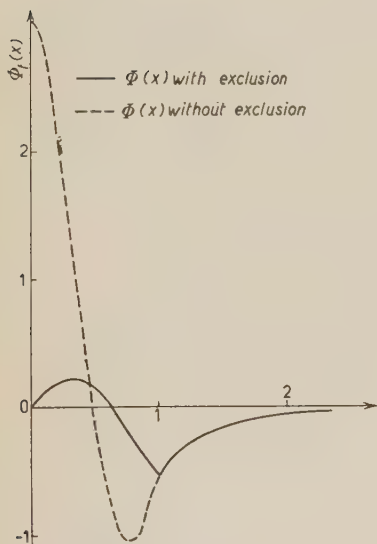
Fig. 1. – The functions $\Phi_f(x)$ for a bound nucleon.

$\Phi_f(x)$ is plotted on Fig. 1. One sees that it changes sign when x increases, so that the magnitude and sign of (1) depend in a sensitive way on the region where (21) is peaked, that is, on the shape of the tensor force and on the ratio f/μ.

In Appendix II, we give a method for computing the integral (26) for $k_i = f$ by a one-variable integration, in the special case of a tensor force

$$(29) \qquad u(r) = V_0 \, \mu^2 r^2 \exp\left[-\tfrac{1}{2} \mu^2 r^2 \right].$$

It is found that

$$(30) \qquad E_1(f, f) = - i \, 54\pi \, \frac{M V_0^2 f^3}{\hbar^2 \mu^{10}} \int_0^\infty N(y) \, dy ,$$

where

$$N(y) = \exp\left[- (2f^2/\mu^2) y \right] \Big\{ (1-y)^{\frac{3}{2}} \left(- (466/315) y^2 - (272/315) y + (176/105) \right) +$$

$$+ y^4 - (118/105) y^3 - (272/315) y^2 + (1136/315) y - (176/105) +$$

$$+ ((16/35) y^4 - (16/15) y^3)(1/\sqrt{y}) \operatorname{tgh}^{-1} \sqrt{y} + (- (8/15) y + (8/35)) \cdot$$

$$\cdot \operatorname{Log}(1 - y) + (f^2/\mu^2) [(1 - y)^{\frac{5}{2}} (- (944/945) y^2 - (1541/945) y + (211/135)) +$$

$$+ (4/45) y^6 - (17/15) y^5 + 3y^4 - (14/9) y^3 - (62/15) y^2 + (529/105) y -$$

$$- (211/135)] \Big\}, \qquad\qquad\qquad \text{if } y < 1.$$

$$N(y) = \exp\left[-(2f^2/\mu^2)y\right]\left\{(512/735)K^7 + ((832/525)y - (1448/525))K^5 +\right.$$

$$+ ((8/315)y^2 - (230/63)y + (334/105))K^3 + (y-1)(-(26/35)y^2 + (2/7)y -$$

$$- (22/105))K + (y-1)^2((13/35)y^2 + (4/21)y - (8/35))(2/\sqrt{y-1})\cdot$$

$$\cdot\ (\mathrm{tg}^{-1}\sqrt{2}/\sqrt{y-1} - 1 - \mathrm{tg}^{-1}(1/\sqrt{y-1})) - (512/735)Q^7 +$$

$$+ ((576/175)y + (8/25))Q^5 - Q^4 + (-(1352/315)y^2 + (4/45)y)Q^3 +$$

$$+ ((2/3)y + (8/15))Q^2 + (-(92/105)y^3 + (4/15)y^2)Q - (44/245)k^7 +$$

$$+ ((124/175)y - (64/75))k^5 + k^4 + (-(16/105)y^2 + (16/45)y)k^3 +$$

$$+ (-2y + (8/15))k^2 + (-(16/35)y^3 + (16/15)y^2)k + (16/21)q^7 +$$

$$+ (-4y + (16/15))q^5 + ((52/9)y^2 - (28/9)y)q^3 + ((4/3)y^3 - (4/3)y^2)q -$$

$$- (16/245)y^7 + (124/175)y^6 - (1508/525)y^5 + (1123/315)y^4 + (8/7)y^3 -$$

$$- (100/63)y^2 + (4034/1575)y - (1628/1225) - (2/\sqrt{y})\left[(-(8/35)y^4 +\right.$$

$$+ (8/15)y^3)\,\mathrm{tgh}^{-1}(1/\sqrt{y}) + (-(46/105)y^4 + (2/15)y^3)\,\mathrm{tgh}^{-1}(\sqrt{y}/(1+\sqrt{y-1})) +$$

$$+ ((2/3)y^4 - (2/3)y^3)\,\mathrm{tgh}^{-1}\sqrt{y}/(2y-1) + (-(8/35)y^4 + (8/15)y^3)\cdot$$

$$\cdot\ \mathrm{tgh}^{-1}\sqrt{2} - y] + (-(8/15)y + (8/35))\,\mathrm{Log}\,(y(y-1)^{3}/2) + (f^2/\mu^2)\cdot$$

$$\cdot\ [-(16/63)K^9 + (-(16/15)y + (128/105))K^7 + (-(16/15)y^2 + (52/15)y -$$

$$- (28/15))K^5 + (y-1)((4/9)y^2 + (16/9)y - (8/9))K^3 - (4/3)(y-1)^3K +$$

$$+ (16/63)Q^9 + (-(128/105)y - (8/105))Q^7 + (4/9)Q^6 + (8/5)y^2Q^5 -$$

$$- (4/3)yQ^4 + ((4/3)y^2 - (16/15)y + (16/35))Q^2 - (8/189)k^9 +$$

$$+ ((32/105)y - (16/35))k^7 + (4/9)k^6 + (-(8/15)y^2 + (16/15)y)k^5 -$$

$$- (4/3)yk^4 + ((4/3)y^2 - (16/15)y + (16/35))k^2 - (8/27)q^9 +$$

$$+ ((32/31)y - (8/21))q^7 + (-(32/15)y^2 + (16/15)y)q^5 + (8/189)y^9 -$$

$$- (32/105)y^8 + (104/105)y^7 - (68/45)y^6 + (4/3)y^5 - (4/3)y^4 +$$

$$+ (88/45)y^3 - (496/105)y^2 + (64/15)y - (416/315)]\Big\}\,,$$

where

$$K = \sqrt{1 - y + 2\sqrt{y-1}}\,, \quad k = \sqrt{2y - y^2}\,, \quad q = \sqrt{2y-1}\,, \quad Q = 1 + \sqrt{y-1}$$

$$\text{if } 1 < y < 2.$$

$$N(y) = \exp\left[-(2f^2/\mu^2)y\right]\left\{P(y, \sqrt{2y-1}) - P(y, \sqrt{2y})\right\},$$

where

$$(31) \qquad P(y, q) = (16/21)q^7 + (-4y + (15/16))q^5 - ((52/9)y^2 - (28/9)y)q^3 +$$
$$+ ((4/3)y^3 - (4/3)y^2)q + (-(4/3)y^4 + (4/3)y^3)(1/\sqrt{y})\,\mathrm{tgh}^{-1}(\sqrt{y}/q) +$$
$$+ (f^2/\mu^2)[-(8/27)q^9 + ((32/21)y - (8/21))q^7 +$$
$$+ (-(32/15)y^2 + (16/15)y)q^5], \qquad\qquad \text{if } y > 2.$$

4. – Experimental and calculated results.

For a bound nucleon, (13) is the well-known spin-orbit potential which is responsible for the shell-model. The analysis of low-lying energy levels may determine an average value $\bar{a}$ through the nuclear surface for a $[f(r_i), f(r_i)]$. This determination cannot be very precise, because of various uncertainties; however ^{15}O and ^{17}N are fairly accounted for by $\bar{a} \sim 70$ MeV $(10^{-13}$ cm$)^5$ (^{6}). The nuclei around ^{208}Pb indicate $\bar{a} \sim 57$ (^{10}). $\bar{a}$ must be positive to account for the « inversed doublet » structure.

We have computed the direct term a_0 of (12), through (27), for some potentials, the Bessel transforms (21) of which are easy to obtain. These potentials are, together with their Bessel transforms:

$$(32a) \qquad \begin{cases} u(r) = V_0 \exp[-\mu_r], \\[2mm] w(k) = V_0 \left[\dfrac{3}{k^3} \,\mathrm{tg}^{-1}\dfrac{k}{\mu} - \mu \,\dfrac{5k^2 + 3\mu^2}{k^2(k^2+\mu^2)^2} \right]. \end{cases}$$

$$(32b) \qquad \begin{cases} u(r) = V_0 \dfrac{\exp[-\mu r]}{\mu r}, \\[2mm] w(k) = V_0 \left[-\dfrac{3}{k^3} \,\mathrm{tg}^{-1}\dfrac{k}{\mu} + \dfrac{2k^2 + 3\mu^2}{\mu k^2(k^2 + \mu^2)} \right]. \end{cases}$$

$$(32c) \qquad \begin{cases} u(r) = V_0 \left(\dfrac{1}{\mu r} + \dfrac{3}{\mu^2 r^2} + \dfrac{3}{\mu^3 r^3} \right) \exp[-\mu r], \;(^{11}) \\[2mm] w(k) = V_0 \dfrac{k^2}{\mu^3(k^2 + \mu^2)}. \end{cases}$$

$$(32d) \qquad \begin{cases} u(r) = V_0 \mu^2 r^2 \exp[-\tfrac{1}{2}\mu^2 r^2], \\[2mm] w(k) = V_0 \sqrt{\dfrac{\pi}{2}} \dfrac{k^2}{\mu^5} \exp\left[-\dfrac{1}{2}\dfrac{k^2}{\mu^2}\right]. \end{cases}$$

(^{10}) R. J. BLIN-STOYLE: *Phil. Mag.*, **46**, 973 (1955).
(^{11}) Such a singular potential is fed into the second Born approximation only for indicative purposes.

The exchange dependence is as indicated in (16). The computed values of a_0 for these different potentials are listed in Table I. The parameters of the potentials were first taken from classical potentials ([12,13,14]) for (32 a, b, c), and for (32d) we tried approximately to reproduce Gartenhaus' potential ([15]). The results obtained in such a way are of the wrong sign. It is easy to see from (27) that a_0 can be positive only for not too singular forces with a long range, since only such forces will contain mostly low momenta, and thus appreciable contribution to the integral in (27) will come mostly from the region where Φ_f is positive. Accordingly, we tried to increase the range $1/\mu$, decreasing at the same time V_0 by a factor estimated from Feshbach's and Schwinger's calculations ([16]). The results are also listed in Table I. It is seen that a_0 may become positive, but remains too small by an order of magnitude.

TABLE I.

Potentials	$1/\mu$ $(10^{-13}$ cm)	V_0 (MeV)		Bound nucleon				300 MeV nucleon	
				a_0 in units of MeV$(10^{-13}$cm$)^5$		a_1 in units of MeV $(10^{-13}$ cm$)^5$		a_0 in units of MeV $(10^{-13}$ cm$)^5$	
				with exclusion	without exclusion	with exclusion	without exclusion	with exclusion	without exclusion
(a) exponential	0.75	50.8	0.875	-4	-18	—	—	$19-i27$	$28-i30$
	0.984	22.6	»	5	19	—	—	$15-i16$	$28-i18$
(b) YUKAWA	1.529	8.11	1.29	<1	-13	—	—	$7-i9$	$13-i10$
	2.362	2.39	»	3	29	—	—	$6-i5$	$14-i6$
	2.756	1.61	»	40	380	—	—	—	—
(d) Mesic	1.40	1.13	1	-9	-12	—	7	$-4-i7$	$-3-i8$
	$+\infty$	—	»	<0	0	—	>0	—	—
(e) GARTENHAUS	0.557	46.2	1	-26	-50	-5.7	20	$6-i14$	$8-i15$
	0.788	17	»	-13	-29	-92	17	—	—

a_0 is the calculated direct part of the spin-orbit interaction coefficient.
a_1 is the calculated exchange part.
The experimental value is $a = a_0 + a_1 = +70$ MeV $(10^{-13}$ cm$)^5$.

([12]) R. JASTROW: *Phys. Rev.*, **81**, 165 (1951).
([13]) H. H. HALL and J. L. POWELL: *Phys. Rev.*, **90**, 912 (1953).
([14]) A. MARTIN and L. VERLET: *Nuovo Cimento*, **12**, 483 (1954).
([15]) S. GARTENHAUS: *Phys. Rev.*, **100**, 900 (1955).
([16]) H. FESHBACH and J. SCHWINGER: *Phys. Rev.*, **84**, 194 (1951).

In all calculations, the local Fermi momentum was taken as $f = 1.27 \cdot 10^{-13}$ cm through the whole nuclear surface, a value which would rather correspond to the inside of the nucleus. If the Thomas-Fermi approximation is valid, f should actually be smaller through the nuclear surface, and this would lead to still algebraically smaller values of a_0.

Other models for the nuclear surface do not appreciably change the results. A tentative description of the surface by the model of an infinite potential barrier was made ([17]). We also tried to take into account possible higher momenta in nuclear matter ([18]). All these attempts do not change the above result that the computed a_0 is algebraically too small.

It might be interesting to estimate the importance of the Pauli principle inasmuch as it is possible to consider exclusion effects as being less important on the nuclear surface. a_0 was also computed without taking into account the exclusion effects in the intermediate states, i.e. extending the integrations to all values of $\boldsymbol{q}_i$, $\boldsymbol{q}_j$, $\boldsymbol{q}$ (27) is still valid, but $\Phi_f(x)$ is now given by the second expression of (28) for all values of x. The results are listed in Table I It is seen that a_0 increases, but that a_0 cannot attain proper values for a reasonable range $1/\mu$.

The exchange term a_1 was computed only for the potential (32d), with and without exclusion. The results are listed on Table I. Again, proper values are not obtained.

5. – Explicit calculation of the non-modified reaction amplitude.

The failure of obtaining proper values for a may be understood from another point of view, in the special case where exclusion effects are not taken into account.

In this case, it is possible to have an explicit expression for the forward and backward reaction amplitudes, in second Born approximation, at least for the potentials (32c, d) and for

$$(32e) \quad \begin{cases} u(r) = V_0 \left(1 + \dfrac{1}{\mu r} \right) \exp\left[-\mu r \right], \\[2mm] w(k) = V_0 \dfrac{2k^2}{\mu(k^2 + \mu^2)^2}. \end{cases}$$

Without exclusion effects, the reaction amplitude depends only on the

---

([17]) W. J. SWIATECKI: *Proc. Phys. Soc.*, A **64**, 226 (1951).

([18]) G. F. CHEW and M. L. GOLDBERGER: *Phys. Rev.*, **77**, 470 (1950); K. A. BRUECK-NER, R. J. EDEN and N. C. FRANCIS: *Phys. Rev.*, **98**, 1445 (1955).

relative momenta, and is of the form

$$(33) \qquad (\boldsymbol{k}'_i, \boldsymbol{k}'_j \,|\, A \,|\, \boldsymbol{k}_i, \boldsymbol{k}_j) = i(2\pi^3)\,\delta(\boldsymbol{k}'_i + \boldsymbol{k}'_j - \boldsymbol{k}_i - \boldsymbol{k}_j)(\boldsymbol{k}' \times \boldsymbol{k})D\,.$$

From (23) and (24), it is found that, for forward scattering

$$(34) \qquad D = D_0(k) = \frac{18}{\pi}\frac{M}{\hbar^2}\frac{1}{k^2}\,P\int \mathrm{d}^3q\,\frac{k^2 - \boldsymbol{k}\cdot\boldsymbol{q}}{k^2 - q^2}\left|\frac{w(|\boldsymbol{q} - \boldsymbol{k}|)}{|\boldsymbol{q} - \boldsymbol{k}|}\right|^2,$$

while, for backward scattering

$$(35) \qquad D = D_1(k) = \frac{18}{\pi}\frac{M}{\hbar^2}\frac{1}{k^2}\,P\int \mathrm{d}^3q\,\frac{w(|\boldsymbol{q} - \boldsymbol{k}|)}{|\boldsymbol{q} - \boldsymbol{k}|^2}\cdot$$

$$\cdot\left\{\left[-k^2 + \frac{k^2q^2 - (\boldsymbol{k}\cdot\boldsymbol{q})^2}{k^2 - q^2}\right]\frac{w(|\boldsymbol{q} + \boldsymbol{k}|)}{|\boldsymbol{q} + \boldsymbol{k}|^2} + \frac{(\boldsymbol{k}\cdot\boldsymbol{q})^2 - k^2q^2}{|\boldsymbol{q} + \boldsymbol{k}|}\frac{\partial}{\partial|\boldsymbol{q} + \boldsymbol{k}|}\frac{w(|\boldsymbol{q} + \boldsymbol{k}|)}{|\boldsymbol{q} + \boldsymbol{k}|^2}\right\}.$$

For potentials ($32c$, d, e), (34) and (35) provide the respective forward and backward amplitudes:

$$(36c) \qquad D_0(k) = 12\pi\,\frac{MV_0^2}{\hbar^2\mu^7}\left[-\frac{3\mu^2(3k^2 + \mu^2)}{k^2(4k^2 + \mu^2)} + \frac{3\mu^3}{2k^3}\,\mathrm{tg}^{-1}\frac{2k}{\mu}\right],$$

$$(37c) \qquad D_1(k) = 12\pi\,\frac{MV_0^2}{\hbar^2\mu^7}\left[-\frac{3\mu^2}{4k^2} + \frac{3\mu^3(4k^2 + \mu^2)}{8k^3(2k^2 + \mu^2)}\,\mathrm{tg}^{-1}\frac{2k}{\mu}\right].$$

$$(36d) \qquad D_0(k) = 6\pi\sqrt{\pi}\,\frac{MV_0^2}{\hbar^2\mu^7}\cdot$$

$$\cdot\left[-\left(\frac{3\mu^3}{2k^3} + 6\frac{\mu}{k} + 12\frac{k}{\mu}\right)\frac{\sqrt{\pi}}{2i}\,\mathrm{Erf}\left(i\frac{2k}{\mu}\right)\exp\left[-\frac{4k^2}{\mu^2}\right] + \frac{3\mu^2}{k^2} + 3\right],$$

$$(37d) \qquad D_1(k) = 6\pi\sqrt{\pi}\,\frac{MV_0^2}{\hbar^2\mu^7}\cdot$$

$$\cdot\left[-1 - 2\frac{k^2}{\mu^2} + \frac{4k^3}{\mu^3}\exp\left[-\frac{k^2}{\mu^2}\right]\frac{\sqrt{\pi}}{2i}\,\mathrm{Erf}\left(i\frac{k}{\mu}\right)\right]\exp\left[-\frac{k^2}{\mu^2}\right].$$

$$(36e) \qquad D_0(k) = \frac{6\pi MV_0^2}{\hbar^2\mu^7}\frac{-1 - 24(k^2/\mu^2) + 48(k^4/\mu^4)}{[1 + 4(k^2/\mu^2)]^3},$$

$$(37e) \qquad D_1(k) = \frac{6\pi MV_0^2}{\hbar^2\mu^7}\left[\frac{3\mu^8}{2k^2(k^2 + \mu^2)(2k^2 + \mu^2)^2} - \frac{3\mu^5(8k^4 + 4k^2\mu^2 + \mu^4)}{2k^3(2k^2 + \mu^2)^3}\cdot\right.$$

$$\left.\cdot\left(\mathrm{tg}^{-1}\frac{2k}{\mu} - \mathrm{tg}^{-1}\frac{k}{\mu}\right)\right].$$

These amplitudes are plotted on Fig. 2. a_0 and a_1 are respectively obtained by summing (36) and (37) on all collision, with the results:

$$(38) \qquad a_0(f, f) = [(1 - \chi)^2 + 3\chi^2]\frac{6}{f^3}\int_0^f dk\, k^3 (f^2 - k^2)\, D_0(k)\,,$$

$$(39) \qquad a_1(f, f) = \left(\frac{1}{2} + 2\chi - 4\chi^2\right)\frac{6}{f^3}\int_0^f dk\, k^3 (f^2 - k^2)\, D_1(k)\,.$$

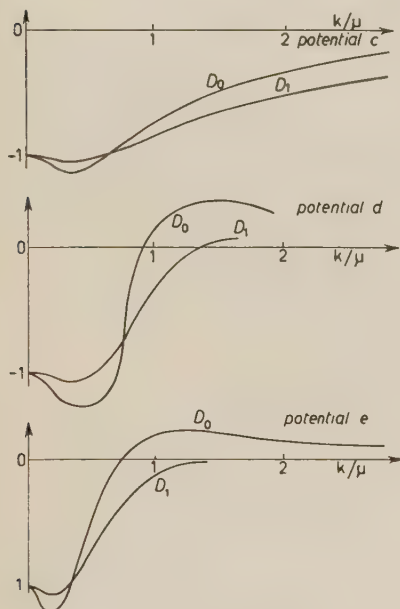These expressions may be used to check the corresponding results, without exclusion, in Table I.

From a qualitative point of view, it is interesting to note that the contributions of the right sign (i.e. positive) to a_0 come only from the high values of k in (38), for which D_0 may become positive if the tensor potential $u(r)$ is not too singular (Fig. 2). The low values of k always make D_0 negative (this last result may be shown to be independent of the potential). The small net result comes from cancellation between the two regions.

The sign of a_1 is determined in (39) by the exchange character of the tensor potential. However, its magnitude was shown to be always too small, for reasonable potentials.

Fig. 2. – The reaction amplitudes D_0 and D_1 as functions of k/μ. c(D_0 and D_1 are in units of $12\pi M V_0^2/\hbar^2\mu^7$; d) D_0 and D_1 are in units of $6\pi\sqrt{\pi}M V_0^2/\hbar^2\mu^7$; e) D_0 and D_1 are in units of $6\pi M V_0^2/\hbar^2\mu^7$.

6. – **High energies** (300 MeV).

The strong polarization observed in the high scattering of nucleons by nuclei may be accounted for by a spin-orbit potential (13) [19] where a has an average value of the same order of magnitude as in shell-model problems. Values of a in the literature [20] are around 40 MeV $(10^{-13}$ cm$)^5$.

[19] E. FERMI: *Nuovo Cimento.* **11**, 407 (1954).

[20] W. HECKROTTE and J. V. LEPORE: *Phys. Rev.*, **94**, 500 (1954); **95**, 1109 (1954); G. A. SNOW, R. M. STERNHEIMER and C. N. YANG: *Phys. Rev.*, **94**, 1073 (1954); B. J. MALENKA: *Phys. Rev.*, **95**, 522 (1954); R. M. STERNHEIMER: *Phys. Rev.*, **95**, 597 (1954); **97**, 1314 (1955); **100**, 886 (1955).

Our calculations of the direct term can be readily extended to higher energies. (The exchange term is not expected to be important). To describe a scattering problem, we use the scattering amplitude rather than the reaction amplitude, by inserting a small imaginary part into the energy denominator of (14). The actual calculations was performed for $k_i = 3f$; this corresponds to about 300 MeV for the incident nucleon. (27) is still valid but $\Phi(x)$ now reads:

$$
\begin{aligned}
\Phi_{3f}(x) = & \left(-4 + \frac{8}{9}\right) \operatorname{Log} 2 + \left(-\frac{2}{27}x^4 + \frac{10}{9}x^2 - \frac{52}{27}x + \frac{8}{9}\right) \operatorname{Log}(1-x) + \\
& + \left(\frac{2}{27}x^4 - \frac{10}{9}x^2 - \frac{56}{27}x - \frac{8}{9}\right) \operatorname{Log}(x+2) + \\
& + \left(-\frac{1}{27}x^4 + x^2 + 2x\right) \operatorname{Log}(x+3) + \left(\frac{1}{27}x^4 - x^2 + 2x\right) \operatorname{Log}(3-x) + \\
& + \frac{1}{9}x^2 + \frac{16}{9}x + i\pi\left(\frac{1}{27}x^4 - \frac{1}{9}x^2 - \frac{2}{27}x\right), \qquad \text{if } 0 < x < 1.
\end{aligned}
$$

$$
\begin{aligned}
\Phi_{3f}(x) = & \left(-\frac{2}{27}x^4 + \frac{10}{9}x^2 + 2x + \frac{8}{9}\right) \operatorname{Log}\frac{x+1}{x+2} + \\
& + \left(\frac{5}{216}x^4 - \frac{7}{36}x^2 + \frac{5}{24} + \frac{7}{27x^2} - \frac{2}{9x^4}\right) \operatorname{Log}\frac{(2-x)(x+1)}{(x+2)(x-1)} + \\
& + \frac{2}{27}x \operatorname{Log}\frac{(x-1)(2-x)}{4x^2} - \frac{1}{36}x^3 + \frac{1}{9}x^2 + \frac{79}{108}x + \frac{5}{6} + \frac{1}{54x} + \frac{2}{9x^3} + \\
& + i\pi\left(-\frac{5}{216}x^4 + \frac{7}{36}x^2 - \frac{2}{27}x - \frac{5}{24} - \frac{7}{27x^2} + \frac{2}{9x^4}\right), \qquad \text{if } 1 < x < 2.
\end{aligned}
$$

$$
\begin{aligned}
\Phi_{3f}(x) = & \left(-\frac{2}{27}x^4 + \frac{10}{9}x^2 + 2x + \frac{8}{9}\right) \operatorname{Log}\frac{x+1}{x+2} + \\
& + \left(-\frac{2}{27}x^4 + \frac{10}{9}x^2 - 2x + \frac{8}{9}\right) \operatorname{Log}\frac{x-1}{x-2} - \\
& - \frac{2}{27}x \operatorname{Log}\frac{(x+1)(x+2)}{(x-1)(x-2)} + \frac{2}{9}x^2 + \frac{5}{3}, \qquad \text{if } x > 2.
\end{aligned}
$$

(40)

$\operatorname{Re}\Phi_{3f}(x)$ and $(1/\pi)\operatorname{Im}\Phi_{3f}(x)$ are plotted on Fig. 3.

We also compute a_0 neglecting the exclusion principle in the intermediate states. In that case, $\operatorname{Re}\Phi(x)$ is the third expression (40) for all values of x, and

$$
\begin{aligned}
& \operatorname{Im}\Phi_{3f}(x) = \pi\left(-\frac{4}{27}x\right), \qquad && \text{if } x < 1. \\
& \operatorname{Im}\Phi_{3f}(x) = \pi\left(-\frac{2}{27}x^4 + \frac{10}{9}x^2 - \frac{56}{27}x + \frac{8}{9}\right), \qquad && \text{if } 1 < x > 2. \\
& \operatorname{Im}\Phi_{3f}(x) = 0, \qquad && \text{if } x > 2.
\end{aligned}
$$

(41)

The results for a_0 are listed on Table I for the previously considered potentials.

It is interesting to see that the Pauli principle is still so important at 300 MeV, at least for the real part of a_0, except for the singular potential (32c). This looks quite general, and can be understood easily, because, for regular potentials, mostly small momentum transfers occur in (21), and the small transfers are still forbidden by the exclusion principle, whatever the incident nucleon energy is.
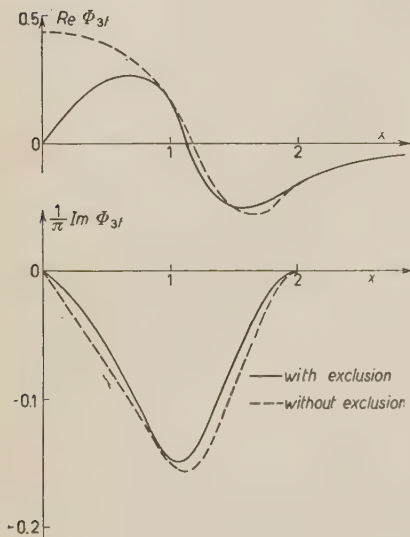
The sign of a_0 is correct, for regular potentials, but its magnitude is too small. This is in agreement with the commonly accepted idea that regular tensor forces do not provide enough polarization at high energy. Insertion of singular forces (the Born approximation being no longer used) could probably lead to higher polarizations.

a_0 is complex. It may be noted that the real and imaginary parts are of opposite signs and of the same order of magnitude. Such a complex spin-orbit potential has been proposed [21] to explain the scattering from carbon, in the small-angle region where there is interference with the Coulomb scattering.

Fig. 3. – The function $\Phi_{3f}(x)$ for an incident 300 MeV nucleon.

7. – Discussion and conclusions.

In principle, the failure of tensor forces to account for the shell-model spin-orbit coupling is a strong indication for the existence of elementary mutual spin-orbit forces in the two-body interaction. However, our computation involves several assumptions, some of which will be now discussed.

7'1. *The Born approximation.* – It was shown in Sect. 5 that, in the case where the exclusion effects are neglected, the negative value or smallness of a_0 come from the behaviour of $D_0(k)$ for small k. This behaviour was estimated

[21] W. HECKROTTE: *Phys. Rev.*, **101**, 1406 (1956).

by computations from the second Born approximation while the actual $D_0(k)$ could be different. Actually, $D_0(k)$ ought to have a pole at low energy, since there is a bound state for the deuteron [6], and our approximation does not reproduce this pole.

However, in the case where exclusion effects are taken into account the Born approximation was claimed to be much more justified [2], at least in the case of regular forces. It is still possible that singular tensor forces would alter the results. Of course, in the second Born approximation, we showed that for the singular tensor forces (32c), things are rather worse, but for such a force, the Born approximation is certainly bad. Thus, our results, at best, are restricted to smooth tensor forces, and, if singularities, hard cores, etc., could play a part even at low energy, this could change our results.

7˙2. *The many-particle terms.* – In the spirit of Brueckner's theory, we have computed only these terms of a perturbation series, which are contained in the two-body reaction amplitude (14). Up to the second order in the inter-action, these terms are the only ones which occur, only if momentum is con-served in two-body collisions. This is indeed the case in the approximation of infinite nuclear matter, and the assumption of momentum-conservation has some consistency with a Thomas-Fermi approximation.

However, in the nuclear surface, there could occur terms that do not con-serve momentum. In the second order perturbation theory, these terms are for instance 3-particle groups, like $v_{12}v_{13}$. Such terms have been previously considered in light nuclei by FEINGOLD *et al.* [1]. FEINGOLD could show that, in this case, the most important part of the vector forces are indeed such 3-body effective forces. The question therefore remains open to know if, in heavier nuclei, contrarily to the spirit of Brueckner's model, such 3-particle terms are important.

7˙3. *Elementary spin-orbit forces.* – With the above restrictions, our cal-culations indicate that tensor forces cannot account for the spin-orbit coupling. Therefore, these results rather strengthen the idea of elementary mutual spin-orbit forces in the two-body interaction. From such forces, an average $\boldsymbol{l} \cdot \boldsymbol{s}$ effect can of course be easily derived [22]. The point of not assuming ele-mentary spin orbit forces from the beginning was for simplicity, since tensor forces are anyhow known to exist, and also because the field theory does not account for a spin-orbit two-body interaction. On another hand, there is

[22] J. HUGUES and K. J. LECOUTEUR: *Proc. Phys. Soc.*, A **63**, 1212 (1950); I. TALMI: *Helv. Phys. Acta*, **25**, 185 (1952); J. P. ELLIOTT and A. M. LANE: *Phys. Rev.*, **96**, 1160 (1954).

growing evidence from two-body scattering and polarization experiments that
two-body spin-orbit forces do exist ([23]).

<p style="text-align:center">* * *</p>

I am indebted to Dr. L. VERLET for helpful discussions.

<p style="text-align:center">APPENDIX I</p>

The direct term.

To compute (25), we make the change of variable

(A.1) $$z = q - k.$$

Then

(A.2) $$E_0(k, f) = -i \frac{9M}{16\pi^2\hbar^2} \frac{3}{4\pi f^3} \frac{1}{k_i^2} \int_{|z+k_i|>f} \mathrm{d}^3z \int_{\substack{k_j<f \\ |k_j-z|>f}} \mathrm{d}^3k_j \frac{z \cdot k}{z^2 + (k_i - k_j).z} \left[\frac{w(z)}{z}\right]^2.$$

We first perform the integration with respect to k_j. The cases $z < 2f$ and $z > 2f$
must be distinguished. The integration on angles of z is then performed. The
final integration on z is the numerical integral (27) where $x = z/2f$.

<p style="text-align:center">APPENDIX II</p>

The exchange term.

The calculation is too long to be given here. We just indicate the method.
To compute (25), in the special case (29), we make use of the same kinds of
methods as Euler ([24]). We choose as variables q, k. The domain of integration Ω

([23]) P. S. SIGNELL and R. E. MARSHAK: *Phys. Rev.*, **106**, 832 (1957).

([24]) H. EULER: *Zeits. f. Phys.*, **105**, 553 (1937).

in q is of revolution around $\boldsymbol{K} = \boldsymbol{k}_i - \boldsymbol{k}$. We first integrate over polar angles of $\boldsymbol{q}$, $\boldsymbol{K}$ being the polar axis. Then, $\boldsymbol{k}$ is defined by k and K, and we perform the integration over the polar angles of $\boldsymbol{k}$, i. e. over K. Of course, many regions appear because of the limits. We are left with an integral over q and k. The further change of variable

$$k^2 - q^2 = 2\,x, \qquad k^2 + q^2 = 2y \,,$$

is done. The integration over x can still be performed analytically, and we are left with the numerical integration (30) over y.

RIASSUNTO (*)

Abbiamo indagato se si possano spiegare le forze spin-orbita nei nuclei complessi come un effetto del second'ordine delle forze tensoriali. Secondo i metodi di Brueckner calcoliamo dapprima un'ampiezza di reazione modificata per le collisioni di due nucleoni entro la materia nucleare, usando la seconda approssimazione di Born e tenendo conto del principio d'esclusione negli stati intermedi. Otteniamo in seguito il potenziale spin-orbita medio al quale è soggetto un nucleone sommando su tutte le sue collisioni l'ampiezza di reazione. Il potenziale spin-orbita così ottenuto risulta di ordine di grandezza troppo piccolo e può anche essere dotato del segno sbagliato. Discutiamo qualche conseguenza di tali risultati.

(*) Traduzione a cura della Redazione.

On the Calculation of Fluctuations and Correlations
by the Gibbs Method.

I. P. Terletskij

Department of Physics – Moscow State University.

Summary. — The exact relations for the calculation of mean square deviations and correlation functions determined both by the fluctuation and the Brown movement theories have been obtained by the Gibbs method of statistichal mechanics.

The formulae used in the fluctuation and Brown movement theories for the calculation of mean square deviations and correlation functions are usually obtained as approximate relations of thermodynamical statistics or Markov's processes theory which are valid only with some limitations of the deviation magnitude or of the kind of dissipative forces. It is known, however, that many of these formulae can be obtained as exact relations of Gibbs statistical mechanics, ([1-4]).

It is easy to show that practically all formulae used in the fluctuation and Brown movement theories for the calculation of mean square deviations and correlation functions can be obtained as exact relations of Gibbs classical statistical mechanics. It is the purpose of this paper to derive these exact relations.

1. – The calculation of quantities depending only on co-ordinates.

Let us consider the system described by canonical variables $x_1, x_2, ..., x_{6N}$ (briefly x), where $x_1, ..., x_{3N}$ are co-ordinates and $x_{3N+1}, ..., x_{6N}$ are momenta.

([1]) J. W. Gibbs: *Elementary Principles in Statistical Mechanics.*
([2]) V. V. Vladimirskij: *Žu. Eksper. Teor. Fiz.*, **12**, 199 (1942).
([3]) V. V. Vladimirskij and I. P. Terletskij: *Žu. Eksper. Teor. Fiz.*, **15**, 258 (1945).
([4]) I. P. Terletskij: *Dynamical and Statistical Laws of Physics* (Moscow, 1949) (in Russian).

Let us suppose $q_1(x)$, $q_2(x)$, ..., $q_n(x)$ to be generalized co-ordinates which are functions only of the co-ordinates x_1, ..., x_{3N}. If additional constant forces a_1, a_2, ..., a_n act in the direction of the co-ordinates q_1, q_2, ..., q_n, we can write the Hamiltonian function in the form

$$(1) \qquad H(X, a) = H_0(X) + \sum_k a_k q_k(x)$$

and the probability density for a system being in thermodynamical equilibrium in the form

$$(2) \qquad W(X) = \exp\left[\frac{\Psi(\Theta, a) - H_0(X) - \sum_k a_k q_k(x)}{\Theta}\right].$$

The value Ψ is determined by the normalizing equation:

$$(3) \qquad \int_{(x)} \exp\left[\frac{\Psi(\Theta, a) - H_0(X) - \sum_k a_k q_k(x)}{\Theta}\right] dx = 1 .$$

Differentiating with respect to a_k, we obtain from (3)

$$(4) \qquad q_k = \frac{\partial \Psi}{\partial a_k} .$$

After double differentiation of (3) with respect to a_i and a_k, we can write

$$(5) \qquad \overline{(q_i - \overline{q}_i)(q_k - \overline{q}_k)} = -\Theta \frac{\partial \overline{q}_i}{\partial a_k} = -\Theta \frac{\partial \overline{q}_k}{\partial a_i} .$$

Differentiating with respect to a_i, a_k and a_l, we obtain from (3)

$$(6) \qquad \overline{(q_i - \overline{q}_i)(q_k - \overline{q}_k)(q_l - \overline{q})} = \Theta^2 \frac{\partial^2 \overline{q}_i}{\partial a_k \partial a_l} = \Theta^2 \frac{\partial^2 \overline{q}_k}{\partial a_l \partial a_i} = \Theta^2 \frac{\partial^2 \overline{q}_l}{\partial a_i \partial a_k} .$$

The further differentiation gives us the higher order correlation functions; however, these formulae have more complicated form than (5) and (6).

The expression of the mean square deviation such as

$$(7) \qquad \overline{(q_k - \overline{q}_k)^2} = -\Theta \frac{\partial \overline{q}_k}{\partial a_k}$$

is a particular case of formula (5).

In distinction from corresponding expressions obtained by the methods of thermodynamical statistics, the formulae (5)-(7) are the exact relations of statistical mechanics which are valid for any system being in the state of thermodynamical equilibrium.

2. – The correlations of quantities depending both on co-ordinates and velocities.

The considered method of the calculation of the correlation functions depending only on the co-ordinates can be extended to the following case: one of the quantities $F(x)$ is an arbitrary function both of co-ordinates and velocities and another quantity is either the generalized co-ordinate $Q(x)$ (which depends only on co-ordinates), or the corresponding generalized velocity $\dot{Q} = \mathrm{d}Q/\mathrm{d}t$.

Let us suppose, as in the previous case, $- a$ to be an additional constant force in the direction of the co-ordinate Q. Then we can write the mean value of an arbitrary quantity $F(x, a)$ in the form

$$(8) \qquad \overline{F} = \int_{(x)} F(x, a) \exp\left[\frac{\Psi(a, \Theta) - H_0(x, a) - aQ(x)}{\Theta}\right] \mathrm{d}x \ .$$

Differentiating, we obtain from (8)

$$(9) \quad \frac{\partial \overline{F}}{\partial a} = \frac{\overline{\partial F}}{\partial a} + \frac{1}{\Theta}\int_{(x)} F(x, a)\left[\frac{\partial \Psi}{\partial a} - Q(x)\right]\exp\left[\frac{\Psi - H_0((x) - aQ(x)}{\Theta}\right]\mathrm{d}x \ .$$

According to (4) we obtain from the previous expression:

$$(10) \qquad \overline{(F - \overline{F})(Q - \overline{Q})} = -\ \Theta\left[\frac{\partial \overline{F}}{\partial a} - \frac{\overline{\partial F}}{\partial a}\right] \ .$$

Since $F(x)$ is an arbitrary function, formula (10) can be also written in the form:

$$(11) \qquad \overline{(\dot{F} - \overline{\dot{F}})(Q - \overline{Q})} = -\ \Theta\left[\frac{\partial \overline{\dot{F}}}{\partial a} - \frac{\overline{\partial \dot{F}}}{\partial a}\right] \ .$$

But $\partial W/\partial t = [HW] = 0$ for any equilibrium distribution, and hence,

$$(12) \qquad \overline{\dot{F}} = \int_{(x)} [HF]W\mathrm{d}x = -\int_{(x)} F[HW]\mathrm{d}x = 0 \ .$$

for the arbitrary function $F(x)$.

We also obtain from this expression

$$(13) \qquad \frac{\mathrm{d}}{\mathrm{d}t}\,(\overline{QF}) = \overline{\dot{F}Q} + \overline{F\dot{Q}} = 0 \,.$$

According to (11), (12) and (13), we obtain:

$$(14) \qquad \overline{F\dot{Q}} = -\,\Theta\,\frac{\overline{\partial \dot{F}}}{\partial a} \,.$$

The formula (10) permits to calculate the correlation function for quantities F depending on all canonical variables and quantities Q which depend on co-ordinates, and the formula (14) can be used for the calculation of the mean values of any function of the velocity $\dot{Q}$.

The formulae (10) and (11) are the exact relations of statistical mechanics as well as the formulae (5)-(7).

3. – The calculation of time correlations.

Let us consider a non-equilibrium ensemble obtained from an equilibrium one by introducing at the initial instant an additional constant force α which acts in the direction of the generalized co-ordinate $Q(x)$. If we indicate the canonical variables of the ensemble particles at the moment $t = 0$ as x^0, and the canonical variables of those at the moment t as x^t, according to Liouville's theorem we can write the probability density at the moment t as

$$(15) \qquad W(x^t, t) = \exp\left[\frac{(\Psi - H_0\{x^0(x^t, t)\}}{\Theta}\right],$$

where $H_0(x)$ is the Hamiltonian function of the initial equilibrium system, $x^0(x^t, t)$ are the initial values of the canonical variables expressed by the values of those at the moment t, Ψ is determined by normalizing the equation.

Since after applying the additional force we can write the Hamiltonian function in the form $H_0(x) - \alpha Q(x)$, the relation (15) can be written in the form

$$(16) \qquad W(x^t, t) = \exp\left[\frac{\Psi - H_0(x^t) + \alpha Q(x^t) - \alpha Q\{x^0(x^t, t)\}}{\Theta}\right],$$

because $H_0(x^0) - \alpha Q(x^0) = H_0(x^t) - \alpha Q(x^t)$ according to the energy conservation.

We can write the mean value of the arbitrary quantity $F(x, \alpha)$ for the

non-equilibrium ensemble (16) at the moment t in the form

$$(17) \qquad \overline{F^t}^\alpha = \int\limits_{(x^t)} F(x^t, \alpha) \exp\left[\frac{\Psi - H_0(x^t) + \alpha Q(x^t) - \alpha Q\{x^0(x^t, t)\}}{\Theta}\right] \mathrm{d}\dot{x}^t .$$

Differentiating with respect to α and supposing $\alpha = 0$, we obtain

$$\left[\frac{\partial \overline{F^t}^\alpha}{\partial \alpha}\right]_{\lambda=0} = \int\limits_{(x^t)} \left\{\frac{\partial F(x^t, \alpha)}{\partial \alpha} + \frac{F(x^t, \alpha)}{\Theta}\left[Q(x^t) - Q\{x^0(x^t, t)\}\right]\right\} \exp\left[\frac{\Psi - H_0(x^t)}{\Theta}\right] \mathrm{d}x^t$$

or

$$(18) \qquad \left[\frac{\partial \overline{F^t}^\alpha}{\partial \alpha}\right]_{\alpha=0} = \frac{\partial \overline{F}}{\partial \alpha} + \frac{1}{\Theta}\overline{F^t(Q^t - Q^0)} .$$

Thus, to calculate the time correlation of the quantity F and of the generalized coordinate Q we must determine the mean value of quantity $F(x, \alpha)$ in the nonequilibrium process obtained by applying the additional force α which acts in the direction of the co-ordinate Q.

This quantity $\overline{F^t}^\alpha$ is the macroscopical mean value of F in the considered non-equilibrium process and can be determined empirically.

Let us suppose $Q = q_i$, $F = q_k$ to be generalized co-ordinates; α_i and α_k to be additional constant forces introduced at the initial instant and acting in the directions q_i and q_k. Obviously

$$(19) \qquad \overline{q_i^t q_k^0} = \overline{q_i^{t+\tau} q_k^\tau}$$

and, according to the reversibility of the equations of mechanics,

$$(20) \qquad \overline{q_i^t q_k^0} = \overline{q_i^{-t} q_k^0} = \overline{q_i^0 q_k^t} .$$

If q_i does not depend on α_m, according to (18), (19), (20)

$$(21) \qquad \overline{(q_i^t - q_i^0)(q_k^t - q_k^0)} = 2\Theta\left[\frac{\partial \overline{q_i^t}^\alpha}{\partial \alpha_k}\right]_{\alpha=0} = 2\Theta\left[\frac{\partial \overline{q_k^t}^\alpha}{\partial \alpha_i}\right]_{\alpha=0} .$$

The latter equation can be considered as a special form of Onsager's reciprocity equations ([5]).

The relation determining the time dependence of the mean square deviation of co-ordinate Q

$$(22) \qquad \overline{(Q^t - Q^0)^2} = 2\Theta\left[\frac{\partial \overline{Q^t}^\lambda}{\partial \alpha}\right]_{\alpha=0}$$

([5]) L. Onsager: *Phys. Rev.*, **37**, 405 (1931); **38**, 2265 (1931).

is obtained from the formula (21) in the particular case:

$$q_i = q_k = Q , \qquad \alpha_i = \alpha_k = \alpha .$$

The main problem of the Brown movement theory is solved by the help of the relation (22) in trivial manner, if we know the macroscopic equation of motion for co-ordinate Q.

We can also obtain the relation which permits the determination of time correlation of quantities depending on velocity from the formula (18).

Obviously,

$$(23) \qquad \frac{\mathrm{d}}{\mathrm{d}\tau} \overline{\dot{F}^{\tau+t}\dot{Q}^{\tau}} = \overline{\dot{F}^t\dot{Q}^0} + \overline{\dot{F}^t\ddot{Q}^0} = 0 .$$

By taking into consideration (14), (23) and that the function $F(x)$ is arbitrary, we can write the formula (18) in the form:

$$(24) \qquad \Theta \left| \frac{\partial \overline{\dot{\tilde{F}}^t}^\alpha}{\partial \alpha} \right|_{\alpha=0} = \overline{\dot{F}^t\dot{Q}^0} .$$

The obtained formulae (18), (21), (22) and (24) express *exact* relations of statistical mechanics which permit to reduce the calculation of time correlations in the general Brown movement theory to the determination of time dependence of macroscopically measured mean values in non-equilibrium processes caused by the introduction of constant forces. The movement equations for macroscopic mean values can be of any kind, including non-linear or functional equations (e.g. taking into consideration post-action forces ([3])). The formulae (18)-(24) are applicable in all these cases. Thus, the exact method of the time correlation calculation considered above is more general than the method of the Brown movement theory, usually used, such as the Einstein-Fokke-Planck equation method or the Langevin-Ornstein method.

RIASSUNTO (*)

Le relazioni esatte per il calcolo degli scarti quadratici medi e delle funzioni di correlazione determinati dalle teorie della fluttuazione e del moto Browniano sono state ottenute col metodo di Gibbs della meccanica statistica.

A New Measurement Technique for Use in the Region of the Blob-Density Maximum in Nuclear Emulsions.

B. J. O'BRIEN

The F.B.S. Falkiner Nuclear Research and Adolph Basser Computing Laboratories, School of Physics (*), The University of Sydney - Sydney, N.S.W.

Summary. — The blob density (N_b) is insensitive to changes in ionization in the region of its maximum value. However the density (N_s) of isolated grains, i.e. blobs which are single grains, has been found to be useful in this region, and thus the combined techniques of measuring N_b and N_s provide a simple and rapid method of track measurement over the complete range of ionization. An approximate theoretical expression for the variation of N_s with the probability of development is presented. This expression is tested by measurements on tracks of relativistic cosmic rays over a wide range of charge, and an application of the technique to cosmic-ray studies described. The variation of N_s with the residual range of protons in two emulsions with plateau grain densities of 8 and 20 grains per 100 μm is compared with the corresponding variation of N_b. Possible sources of error in measured values of N_s are found to be similar to those of N_b.

The measurement of blob density is one of the methods of track identification in frequent use in nuclear-emulsion work at the present time. This technique is more objective and applicable to a greater range of ionization than is grain counting, it is more rapid than many other methods and it is capable of giving high statistical accuracy from only short track lengths. It can be supplemented ([1,2]) by measurement of the density of « long » gaps, but

---

([1]) C. CASTAGNOLI, G. CORTINI and A. MANFREDINI: *Nuovo Cimento*, **2**, 301 (1955).
([2]) P. H. FOWLER and D. H. PERKINS: *Phil. Mag.*, **46**, 587 (1955).

this latter method generally requires alignment of the track, and it suffers from the disadvantages introduced by the use of filar eyepieces with hairlines of finite thickness.

The blob density increases with the rate of energy loss until it reaches a maximum and then it decreases. In G5 emulsions of normal minimum grain density ($\sim$ 25 grains per 100 μm) this maximum occurs at blob densities around 60 per 100 μm corresponding to about six to ten times the minimum rate of energy loss. Consequently in this turnover region the blob density is insensitive to changes of ionization.

Since the blob density is otherwise useful over the complete range of ionization extending from $Z = 1$ up to tracks of relativistic iron nuclei in G5 emulsions of normal sensitivity ([3]) it would be advantageous to have a comparable technique which is useful in the region of the maximum in blob density.

A very simple technique which is always sensitive to ionization changes in this turnover region is the counting of single, isolated grains along the track, i.e. only those blobs are counted which are single grains.

The range of usefulness of N_s has been studied by counting tracks of fast heavy nuclei from α-particles to iron in a stack of G5 emulsion with plateau grain density of 8 grains per 100 μm. N_s was used to estimate the relative proportions of light ($3 \leqslant Z < 5$) and medium ($6 \leqslant Z \leqslant 9$) nuclei in a sample of 86 heavy-primary tracks.

To make a reliable estimate of this proportion a measured track parameter should have a spread in measured values for boron and carbon nuclei which is less than the separation between the average values for these nuclei. With blob-density measurements in this stack this requirement was not fulfilled. However, the measured distribution in N_s showed resolved peaks for boron and carbon, and confirmed further the value of the light-to-medium ratio reported elsewhere ([4]).

It is convenient to invoke one of the models of track formation in consideration of this technique. The Herz-Davis ([5]) model gives good fit for the along-the-track characteristics of the tracks of heavy primaries found in our stack, and this model is used in the following.

The emulsion is considered to have an ordered line of AgBr crystals with a lattice spacing α along the line of each track. It is then assumed that a fraction p of the AgBr crystals which are traversed by the particle are de-

([3]) M. KOSHIBA, G. SCHULTZ and M. SCHEIN (1957). Reported at Varenna Conference, 1957, by Professor SCHEIN.

([4]) B. J. O'BRIEN, A. J. HERZ and J. H. NOON (1957). Reported at Varenna Conference 1957, by Dr. A. J. HERZ.

([5]) A. J. HERZ and G. DAVIS: *Aust. Journ. Phys.*, **8**, 129 (1955).

veloped and grow to a uniform grain diameter $\alpha\gamma$. The different along-the-track characteristics can then be expressed in terms of α, γ, p and T, where T is the number of AgBr crystals in the measurements interval, and p is the probability of development.

Measurements ([6]) have shown that along-the-track characteristics of tracks in the scanning sheet of one of our emulsion stacks can be described by the Herz-Davis model with values,

$$\alpha = 0.34\ \mu\mathrm{m}\,, \qquad \gamma = 1.5\,.$$

Thus in this case the integral part (Γ) of the growth factor of the crystal is 1.

It is possible to obtain a good fit also with $\alpha = 0.2\ \mu\mathrm{m}$ and $\gamma = 2.5$, so that $\Gamma = 2$. However, for simplicity we restrict some of our discussion to the case of $\Gamma = 1$. Then the blob density is given ([5]) by

$$(1) \qquad N_b = Tp(1-p)^\Gamma$$

and this has a maximum at $p = 0.5$ for $\Gamma = 1$ as shown in Fig. 1.

Similarly an expression may be derived for the density of isolated grains. This will be simply

$$(2) \qquad N_s = Tp(1-p)^{2\Gamma}$$

and this is shown also in Fig. 1 with $\Gamma = 1$.

It is seen that N_b and N_s are very useful complementary methods since one is changing where the other has its maximum and is consequently insensitive to ionization variations. A further simple expression governs the value of $(N_b - N_s)$.

Fig. 1. – Variation of blob density N_b and isolated-grain density N_s with the probability of development p, predicted using the Herz-Davis model with $\alpha = 0.34\ \mu\mathrm{m}$, $\gamma = 1.5$.

Equation (2) was tested in the following manner. The integral gap lengths of 39 relativistic nuclei were measured and used to estimate to about 6% accuracy the value of p of each track in a G5 emulsion with plateau grain density of 8 grains per 100 μm. The density of isolated grains of each track was found from measurement of about 1 mm track length, and the resultant value of N_s compared with that pre-
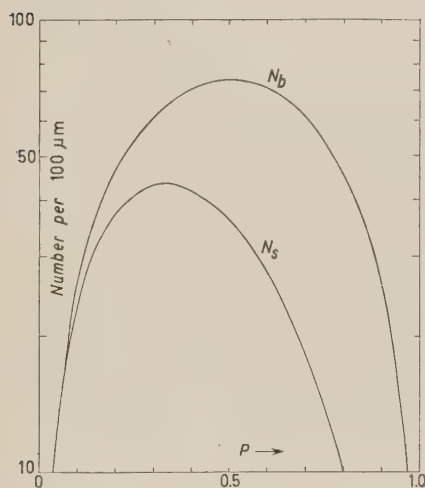
([5]) B. J. O'BRIEN: *Nuovo Cimento* **7**, 147 (1958).

dicted from equation (2). The results are shown in Fig. 2, together with the theoretical and measured blob densities.

It is seen from Fig. 2 that Equation (2) gives an underestimate of N_s, although it follows closely the shape of the experimental curve of N_s versus p. This may be due to failure of the Herz-Davis model (see also CASTAGNOLI et al [1], where the experimental and theoretical gap-length distributions differ sligthly) or to the observer occasionally counting a small blob of two over-lapping grains as a single grain, or to both these sources of error.
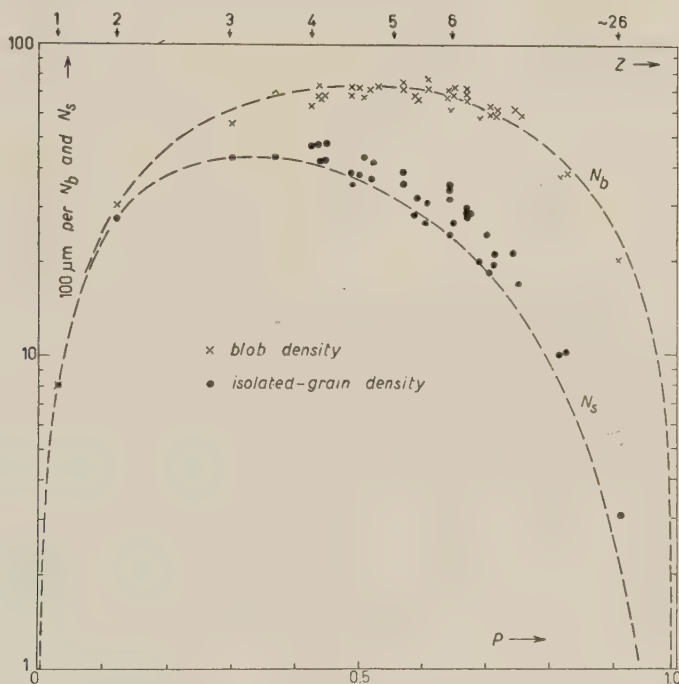
Fig. 2. – Theoretical curves and experimentally-measured values of N_s and N_b versus p for tracks of relativistic heavy nuclei of charge Z.

We have also measured N_s and N_b as a function of residual range of ten stopping protons in two G5 stacks with plateau grain densities of 8 and 20 grains per 100 μm respectively, and the results are shown in Fig. 3. It is apparent from this figure also that N_s is useful in the region where N_b is insensitive to changes of ionization.

It might be expected that the subjective error in N_s would be large be-cause of the uncertainties in the judgment of what constitutes a single grain. However in our emulsions where the distribution in grain diameter is narrow the subjective error has been measured for tracks of different densities as

Fig. 3. – Variation of N_s and N_b with residual range of protons in two 5G stacks with plateau grain densities of 8 and 20 grains per 100 μm respectively. ――― plateau 8 grains/100 μm; ----- plateau 20 grains/100 μm.

$\sim 3\%$, which is comparable with the subjective error in blob counts ([6]). It is probable that the subjective error will be larger in emulsions where the grain-diameter distribution has a wider spread. An initial period in which the observer establishes his judgment criteria is necessary, again as with blob counting. The quality of the illumination is, of course, as important with this technique as it is with blob counting.

The intrinsic variations in the value of N_s for any one track, which arise because of the statistical process of track formation, will be dep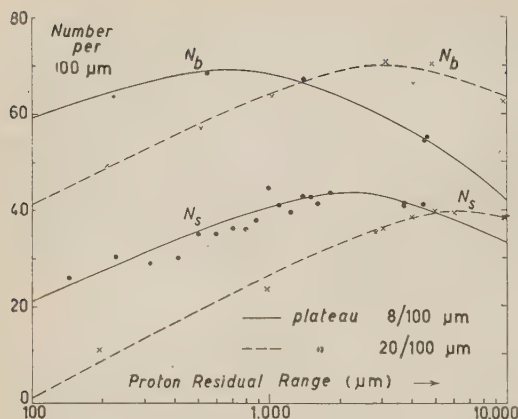endent on p, as are the corresponding variations in N_b ([6,7]). For very light tracks where $N_s \sim N_b$ the errors will be closely Poissonian, and for medium tracks with $p \sim 0.5$ the errors will be less than Poissonian. For example, the standard deviation of N_s along a beryllium track ($p \sim 0.4$) was measured as ~ 0.8 Poissonian. With very heavy tracks, where an important proportion of the gaps may result ([2]) from the absence of AgBr crystals, it is possible that such emulsion flaws may influence the intrinsic variations in N_s. However in our emulsion where N_b for the heaviest track was ~ 20 per 100 μm, the intrinsic errors in both N_b and N_s of this track were approximately Poissonian.

Although the counting of isolated grains can be regarded as a separate identification technique in its own right, it is considered here solely as a complementary technique to blob counting. For this reason no comparison is given here of the efficacy of this method with those of techniques other than blob counting. However it is shown in the theoretical curves of Fig. 1, the heavy-nuclei measurements in Fig. 2 and the proton measurements in Fig. 3 that the density of isolated grains is changing in the region of the maximum in blob density where the latter parameter is insensitive to changes in ionization.

Using the combined and similar techniques of blob and isolated-grain counting, one thus has a rapid and simple method of track measurement over the complete range of ionization.

([7]) J. M. BLATT: *Aust. Journ. Phys.*, **8**, 248 (1955).

* * *

RIASSUNTO (*)

La densità di blob (N_b) è insensibile alle variazioni di ionizzazione nella regione del suo valor massimo. Tuttavia la densità (N_s) dei granuli isolati, cioè dei blob consistenti di unico granulo, si è rivelata utile in tale regione, di modo che le misure combinate di N_b e N_s forniscono un metodo semplice e rapido per la misura delle tracce sull'intero range di ionizzazione. Si dà un'espressione teorica approssimata per la variazione di N_s con la probabilità di sviluppo. Si è saggiata tale espressione con misure di tracce di raggi cosmici relativistici su una vasta gamma di cariche e si descrive una applicazione di questa tecnica allo studio dei raggi cosmici. La variazione di N_s col range residuo dei protoni in due emulsioni con densità massima rispettivamente di 8 e 20 granuli per 100 μs si confronta con la corrispondente variazione di N_b. Le possibili fonti di errore nelle misure dei valori di N_s si trovano essere simili a quelle degli errori di N_b.

(*) *Traduzione a cura della Redazione.*

The Stimulated Decay of the Lambda Hyperon - I.

F. Ferrari and L. Fonda

Istituto Nazionale di Fisica Nucleare - Sezione di Padova
Istituto di Fisica dell' Università - Padova
Istituto Nazionale di Fisica Nucleare - Sottosezione di Trieste
Istituto di Fisica dell' Università - Trieste

Summary. — In order to interpret a recent experimental result regarding the stimulated decay of Λ-hyperons bound in hyperfragments, a model has been considered in which the decay of the Λ-hyperon may also occur when in the virtual Σ-state. The consequences of the non-conservation of parity are also considered.

1. – Introduction.

As is well known, the hypothesis of the decay of the bound Λ and the subsequent re-absorption of the decay pion is insufficient to explain the observed ratio of mesonic to non-mesonic decays in hyperfragments: instead it has proved necessary to invoke the hypothesis of the stimulation of the hyperon decay by the nucleons of the hyperfragment. Recently an experimental work [1] has shown that it is possible to separate the events into those stimulated by protons and those stimulated by neutrons. Although the statistics so far available is not large, it seems rather probable that the ratio « R » of neutron to proton stimulations is greater than one. In the present work we examine the theoretical consequences of this result.

It should be pointed out immediately that in what follows we will consider the possibility that the Λ can also live as a virtual Σ state when in the

---

[1] M. Baldo-Ceolin, C. Dilworth, W. F. Fry, W. D. B. Greening, H. Huzita, S. Limentani and A. E. Sichirollo: *Stimulated Decay of the Λ Hyperon in Light Hyperfragments*, in *Nuovo Cimento*, **7**, 328 (1958).

presence of nucleons, and that decay can take place when the hyperon finds itself in this virtual state, giving rise to schemes of the type shown in Fig. 1 in addition to those already described by RUDERMAN and KARPLUS ([2]) (see Fig. 2). Further, we will consider the effects connected with the non-conservation of parity in these processes.
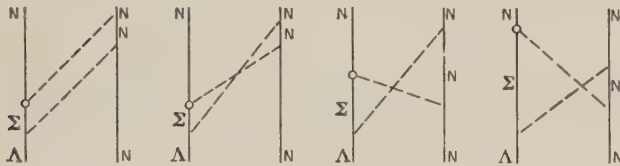
Fig. 1.
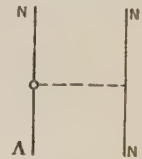
Fig. 2.

We will start from the interaction hamiltonian density

(1)
$$H_I = H_{pn} + H_{\Sigma\Lambda} + H_{dec.\,\Lambda} + H_{dec.\,\Sigma} \,,$$

where

$$H_{pn} = g_{np}\left[p^*(\boldsymbol{\sigma}\boldsymbol{\nabla})\pi^0 p - n^*(\boldsymbol{\sigma}\boldsymbol{\nabla})\pi^0 n + \right.$$
$$\left. + \sqrt{2}\left(p^*(\boldsymbol{\sigma}\boldsymbol{\nabla})\pi^+ n + n^*(\boldsymbol{\sigma}\boldsymbol{\nabla})\pi^- p \right) \right] ,$$

$$H_{\Sigma\Lambda} = g_{\Sigma\Lambda}[\Sigma^{0*}(\boldsymbol{\sigma}\boldsymbol{\nabla})\pi^0\Lambda + \Sigma^{+*}(\boldsymbol{\sigma}\boldsymbol{\nabla})\pi^+\Lambda +$$
$$+ \Sigma^{-*}(\boldsymbol{\sigma}\boldsymbol{\nabla})\pi^-\Lambda + \text{herm. conj.}] .$$

$$H_{dec.\,\Lambda} = \lambda^+[\sqrt{2}\, p^*(\boldsymbol{\sigma}\boldsymbol{\nabla})\pi^+\Lambda - n^*(\boldsymbol{\sigma}\boldsymbol{\nabla})\pi^0\Lambda + \text{herm. conj.}] +$$
$$+ \lambda^-[\sqrt{2}\, p^*\pi^+\Lambda - n^*\pi^0\Lambda + \text{herm. conj.}] .$$

$$H_{dec.\,\Sigma} = (\eta_1^+ + \eta_2^+)\, n^*(\boldsymbol{\sigma}\boldsymbol{\nabla})\,\pi^+\Sigma^- - \eta_2^+\sqrt{2}\, p^*(\boldsymbol{\sigma}\boldsymbol{\nabla})\pi^0\Sigma^+ +$$
$$+ (\eta_1^+ - \eta_2^+)n^*(\boldsymbol{\sigma}\boldsymbol{\nabla})\pi^-\Sigma^+ + \eta_1^+ n^*(\boldsymbol{\sigma}\boldsymbol{\nabla})\pi^0\Sigma^0 +$$
$$+ \sqrt{2}\eta_2^+ p^*(\boldsymbol{\sigma}\boldsymbol{\nabla})\pi^+\Sigma^0 +$$
$$+ (\eta_1^- + \eta_2^-)n^*\pi^+\Sigma^- - \eta_2^-\sqrt{2}p^*\pi^0\Sigma^+ +$$
$$+ (\eta_1^- - \eta_2^-)n^*\pi^-\Sigma^+ + \eta_1^- n^*\pi_0\Sigma^0 +$$
$$+ \sqrt{2}\eta_2^- p^*\pi^+\Sigma^0 + \text{herm. conj.}$$

The terms H_{pn} and $H_{\Sigma\Lambda}$ represent the strong pion-nucleon and pion-hyperon

---

([2]) M. RUDERMAN and R. KARPLUS: *Phys. Rev.*, **102**, 247 (1956).

interactions respectively, $H_{\text{dec. }\Lambda}$ and $H_{\text{dec. }\Sigma}$ are the weak interactions which describe the decay processes of the Λ and Σ into pions and nucleons. It is to be noted that the decay hamiltonians have been chosen in such a way that they behave as the component of an isospinor, in order to satisfy charge conservation and the rules $\Delta U = \pm 1$ and $\Delta I = \pm \frac{1}{2}$ ([3]). Further, it is assumed that the parity of the Λ and Σ hyperons is the same ([4]).

The following symbols have been used:

g_{np} and $g_{\Sigma\Lambda}$ coupling constants with the pion field for nucleons and hyperons respectively;

λ^+ and λ^- coupling constants for the decay of the Λ when its parity is equal to or different from that of the nucleon;

η_1^+, η_2^+ and η_1^-, η_2^- coupling constants for the decay of the Σ when its parity is equal to or different from that of the nucleon.

Using the interaction hamiltonian density (1) in connection with the non-relativistic perturbation method, we shall now calculate the ratio

$$(2) \qquad R = \frac{W(\Lambda \text{n} \to \text{nn})}{W(\Lambda \text{p} \to \text{np})} ,$$

where W is the total rate for non-mesonic decay.

Owing to the approximate nature of the experimental results, we shall restrict ourselves to the two cases:

     i) The decay process occurs when the hyperon is in the Λ state.

     ii) The decay process occurs when the hyperon is in the virtual Σ state.

If the pion-hyperon interaction exists, and if its strength is of the same order of magnitude as that of the pion-nucleon interaction ([4]) (i.e. if $g_{\Lambda\Sigma} \simeq g_{\text{np}}$) then it can be shown that the fourth-order process ii) is dominant over the second-order process i).

2. – The direct decay of the Λ.

In this case, the interaction hamiltonian density (1) which describes the stimulated decay process reduces to

$$(3) \qquad H_{\text{I}}^{\Lambda} = H_{\text{pn}} + H_{\text{dec.}} .$$

([3]) B. D'ESPAGNAT and J. PRENTKI: *Nuovo Cimento*, **3**, 1045 (1956); R. GATTO: *Nuovo Cimento*, **2**, 318 (1956); G. TAKEDA: *Phys. Rev.*, **101**, 1547 (1956); G. WENTZEL: *Phys. Rev.*, **101**, 1214 (1956).

([4]) M. GELL-MANN: *Phys. Rev.*, **106**, 1296 (1957); F. FERRARI and L. FONDA: *Nuovo Cimento*, **6**, 1027 (1957).

The relative diagrams are of the type shown in Fig. 2. The total rate for non-mesonic decay is given by:

$$(4) \qquad W = \frac{2\pi}{\hbar} \frac{1}{4} \sum_{if} \left| \left\langle f \left| H_I^\Lambda \frac{1}{a} H_I^\Lambda \right| i \right\rangle \right|^2 \varrho_f ,$$

where $|i\rangle$ and $|f\rangle$ specify the initial and final energy-momentum states; $a = E - H_0$ and E is the energy of the initial and final states; ϱ_f is the final state density.

If we now consider that parity may not be conserved in the decay of the hyperons, as some experimental results seem to indicate [5], the ratio « R» becomes:

$$(5) \qquad R = \frac{\varrho_n}{\varrho_p} \left[1 - \frac{8(\lambda^-)^2}{(\lambda^+)^2 k^2 + 9(\lambda^-)^2} \right] ,$$

where ϱ_p and ϱ_n are the proton and neutron density and k is the momentum of the final-state nucleons in their center of mass system. The initial nucleon and the Λ hyperon are assumed at rest and uncorrelated.

It is to be remarked that in Eq. (5) the interference terms do not appear after summing over the initial and final spin states. Consequently it results that if parity is conserved the ratio « R » is equal to unity when the parity of the Λ is the same as that of the nucleon, and $\frac{1}{9}$ when it is different. On the other hand, if parity is not conserved, « R » lies between these two values (*).

3. – The decay of the Λ hyperon while in the virtual Σ state.

We will now consider the possibility that the Λ hyperon can exist as a virtual Σ and that it can decay while in this state. The terms of the inter-

---

[5] L. W. ALVAREZ, H. BRADNER, P. FALK-VAIRANT, J. D. GROW, A. H. ROSENFELD, F. T. SOLMITZ and R. D. TRIPP: *Nuovo Cimento*, **5**, 1026 (1957); F. CERULUS: *Nuovo Cimento*, **5**, 1685 (1957); J. SCHNEPS, W. F. FRY and N. S. SWAMI: *Phys. Rev.*, **106**, 1062 (1957); C. CEOLIN: *Nuovo Cimento*, **6**, 1006 (1957) (we are indebted to Dr. C. CEOLIN for many discussions); B. T. FELD: *Nuovo Cimento*, **6**, 650 (1957).

(*) These considerations are not substantially changed if one takes into account also the fourth order matrix element symbolically represented by the graph of Fig. 3.
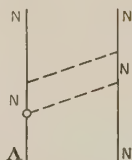

Fig. 3.

The ratio R is 1 again if the parity of the Λ and nucleon is the same, and parity is conserved. Is always < 1 if parity is not conserved.

action hamiltonian density (1) giving a contribution are:

$$(6) \qquad H_{\mathrm{I}}^{\Sigma} = H_{\mathrm{pn}} + H_{\Sigma\Lambda} + H_{\mathrm{dec.\,\Sigma}} \,.$$

The relative processes are described by diagrams of the type given in Fig. 1. The total rate for non-mesonic decay reads:

$$(7) \qquad W = \frac{2\pi}{\hbar} \frac{1}{4} \sum_{if} \left| \left\langle f \left| H_{\mathrm{I}}^{\Sigma} \frac{1}{a} H_{\mathrm{I}}^{\Sigma} \frac{1}{a} H_{\mathrm{I}}^{\Sigma} \frac{1}{a} H_{\mathrm{I}}^{\Sigma} \right| i \right\rangle \right|^2 \varrho_f \,,$$

where the symbols are as defined above. The calculations have been carried out in static approximation, eliminating those matrix elements which give rise to diagrams with bare barions in the intermediate states: in fact this can be justified in non-adiabatic approximation when the recoil of the barions is taken into account ([6]). In the most general case we have ([*]):

$$(8) \qquad R = \frac{W_{\Lambda n}^{+} + W_{\Lambda n}^{-}}{W_{\Lambda p}^{+} + W_{\Lambda p}^{-}} \,,$$

where:

$$W_{\Lambda p}^{-} = \frac{2\pi}{\hbar} \frac{1}{4} \sum_{if} |[(\eta_1^- - 2\eta_2^-)I_1 - (\eta_1^- + 2\eta_2^-)I_2]|^2 \varrho_f \,,$$

$$W_{\Lambda n}^{-} = \frac{2\pi}{\hbar} \frac{1}{4} \sum_{if} |[(\eta_1^- + \tfrac{2}{3}\eta_2^-)I_1 - (\eta_1^- - \tfrac{2}{3}\eta_2^-)I_2|^2 \varrho_f \,,$$

([6]) D. LICHTENBERG and M. ROSS: *Phys. Rev.*, **107**, 1714 (1957); N. DALLAPORTA and F. FERRARI: *Nuovo Cimento*, **5**, 111 (1957).

([*]) The interaction hamiltonian considered takes into account only those therms which give rise to the decay processes of second and fourth order. Thus we have not considered those interactions which give rise to scattering processes (see Fig. 4) and to electromagnetic decay of the Σ^0 into $\Lambda + \gamma$ (see Fig. 5). Since in all these cases the
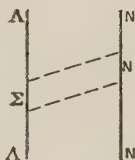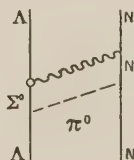

Fig. 4.   Fig. 5.

final states are identical to the initial ones, nothing is observed. Therefore we can neglect all those processes which give rise to a continuous virtual scattering of the hyperon inside the nucleus, and which have no influence on the only observable decay processes.

and

$$I_1 = -\frac{3ig_{np}^2 g_{\Sigma\Lambda}}{2V(2\pi)^3}\int d^3p\, v_{pn}(p)\,v_{pn}(\boldsymbol{p}-\boldsymbol{k})\,v_{\Sigma\Lambda}(\boldsymbol{p}-\boldsymbol{k})\cdot$$

$$\cdot\frac{[u_N^*(k)(\boldsymbol{\sigma p})(\boldsymbol{\sigma}\cdot\boldsymbol{p}-\boldsymbol{k})u_N(0)][u_N^*(-k)(\boldsymbol{\sigma}\cdot\boldsymbol{p}-\boldsymbol{k})u_\Lambda(0)]}{\omega_p^2\omega_{p-k}^2(\omega_p+\omega_{p-k})} ,$$

$$I_2 = -\frac{3ig_{pn}^2 g_{\Lambda\Sigma}}{2V(2\pi)^3}\int d^3p\, v_{pn}(p)\,v_{pn}(\boldsymbol{p}-\boldsymbol{k})\,v_{\Sigma\Lambda}(p)\cdot$$

$$\frac{[u_N^*(k)(\boldsymbol{\sigma p})(\boldsymbol{\sigma}\cdot\boldsymbol{p}-\boldsymbol{k})u_N(0)][u_N^*(-k)(\boldsymbol{\sigma p})u_\Lambda(0)]}{\omega_p\omega_{p-k}(\omega_p+\omega_{p-k})}\left[\frac{1}{\omega_p\omega_{p-k}}+\frac{1}{\omega_{p-k}^2}+\frac{1}{\omega_p^2}\right] .$$

Furthermore

$$W_{\Lambda n}^+ = \frac{2\pi}{\hbar}\frac{1}{4}\sum_{if}\left|\frac{g_{np}^2 g_{\Sigma\Lambda}}{V(2\pi)^3}\int d^3p\, v_{pn}(p)\,v_{pn}(\boldsymbol{p}-\boldsymbol{k})\left\{\frac{v_{\Sigma\Lambda}(\boldsymbol{p}-\boldsymbol{k})\,v_{\Sigma\,\text{dec.}}(p)}{\omega_p^2\omega_{p-k}^2(\omega_p+\omega_{p-k})}\cdot\right.\right.$$

$$\cdot\left[\left(\frac{3}{2}\eta_1^+ + \eta_2^+\right)[u_N^*(k)(\boldsymbol{\sigma p})(\boldsymbol{\sigma}\cdot\boldsymbol{p}-\boldsymbol{k})u_N(0)][u_N^*(-k)(\boldsymbol{\sigma p})(\boldsymbol{\sigma}\cdot\boldsymbol{p}-\boldsymbol{k})u_\Lambda(0)]+\right.$$

$$\left.+\left(\frac{3}{2}\eta_1^+ - \eta_2^+\right)[u_N^*(k)(\boldsymbol{\sigma}\cdot\boldsymbol{p}-\boldsymbol{k})(\boldsymbol{\sigma p})u_N(0)][u_N^*(-k)(\boldsymbol{\sigma p})(\boldsymbol{\sigma}\cdot\boldsymbol{p}-\boldsymbol{k})u_\Lambda(0)]\right]+$$

$$+\frac{(\frac{3}{2}\eta_1^+ - \eta_2^+)}{\omega_p^3\omega_{p-k}(\omega_p+\omega_{p-k})}\cdot$$

$$\cdot\left[v_{\Sigma\Lambda}(p)\,v_{\Sigma\text{dec.}}(\boldsymbol{p}-\boldsymbol{k})[u_N^*(k)(\boldsymbol{\sigma p})(\boldsymbol{\sigma}\cdot\boldsymbol{p}-\boldsymbol{k})u_N(0)][u_N^*(-k)(\boldsymbol{\sigma}\cdot\boldsymbol{p}-\boldsymbol{k})(\boldsymbol{\sigma p})u_\Lambda(0)]+\right.$$

$$\left.\left.+v_{\Sigma\Lambda}(\boldsymbol{p}-\boldsymbol{k})\,v_{\Sigma\text{dec.}}(p)[u_N^*(k)(\boldsymbol{\sigma}\cdot\boldsymbol{p}-\boldsymbol{k})(\boldsymbol{\sigma p})u_N(0)][u_N^*(-k)(\boldsymbol{\sigma p})(\boldsymbol{\sigma}\cdot\boldsymbol{p}-\boldsymbol{k})u_\Lambda(0)]\right\}\right|^2\varrho_f ,$$

$$W_{\Lambda p}^+ = \frac{\varrho_p}{\varrho_n}\,W_{\Lambda n}^+ ,$$

where the u_i are the normalized spinors describing the barions, V is the normalization volume and $v(q)$ is the cut-off function for the PS-PV interaction.

From these expressions (*) it results that if parity is conserved the ratio « R » is equal to unity when the parity of the Σ is the same as that of the nucleons,

---

(*) The integration of the above eqs., has been performed by using the following approximation:

$$\omega_{p-k} = \frac{\omega_{p-k} + \omega_{p+k}}{2} .$$

Furthermore, we have supposed that the form factor for the weak interactions $v_{\Sigma\text{dec}} \sim 1$ for the region of interest in the integration.

and lies between 0.06 and 1.9 when it is different. The behaviour of the ratio $W_{\Lambda p}^-/W_{\Lambda n}^-$ for the last case is plotted in Fig. 6 as a function of η_1^-/η_2^- .
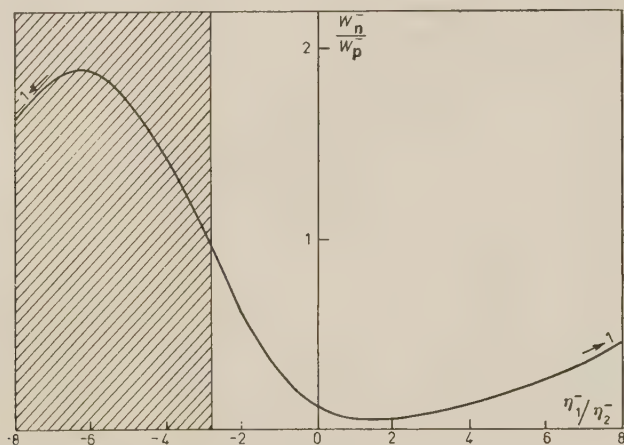
Fig. 6.

On the other hand, if parity is not conserved, and the quantity η_1^-/η_2^- is negative and smaller than $\sim - 2.8$, the ratio «R» is always greater than 1. In this connection it should be noted that if an attempt is made to calculate the ratio of the mean life-times for the positive and negative Σ hyperons, and the branching ratio $f = (\Sigma^+ \to p + \pi^0)/(\Sigma^+ \to n + \pi^+)$ by means of the inter-action density (1), one finds agreement with experiment only if one makes the additional assumption that parity is not conserved in the decay process ([6]). As a consequence, at least in Born approximation ([3]), one obtains that η_1^-/η_2^- and η_1^+/η_2^+ are negative.

4. – Comparison with experiment.

Recently a provisional experimental value for «R» of 1.4 has been reported ([1]). This seems to indicate that the non-mesonic decay of Λ hy-perons in light hyperfragments is stimulated by neutrons more frequently than by protons. Unfortunately, owing to the small statistics, this result can only be taken as indicative. Therefore, we shall discuss the following three cases:

i) Should the experimental value of «R» be clearly greater than unity, this would be an indication that the stimulated decay of the Λ hyperon in-volves the virtual Σ state. Further, it would result that either the parity is *not* conserved during decay, or, if it *is* conserved, that the Σ has parity op-posite to that of the nucleon.

This conclusion could be altered by some effects connected with the structure of the core of the hyperfragment. Such effects might be due to the neutrons being sensibly more external than the protons, even in the lighter nuclei, thus favouring the Λ-neutron interaction. An approximate calculation on this line has been done assuming gaussian density for the nucleons in the nucleus [7], and a neutron distributions r.m.s. radius 10% greater than that for the proton. Using the following expression for the Λ wave function:

$$\psi(r) = C\,\frac{1}{r}\left(\exp\left[-r/r_0\right] - \exp\left[-\alpha r/r_0\right]\right),$$

where r_0 has been fixed through the binding energy of the Λ in the hyperfragment considered, the results show that such an effect would not be appreciable. Furthermore, this effect could only be apparent in those hyperfragments having $Z > 3$: it would therefore be interesting to determine « R » for the helium hyperfragments alone.

ii) If experiments should give a value for « R » very close to unity, this could be considered either as an indication that the parity is conserved during decay or, if the parity is not conserved, that the decay process takes place in the virtual Σ state.

iii) Should the experimental value of « R » be much less than one, this would be evidence that parity is not conserved in the decay of the hyperon.

We would like to point out that if the stimulated decay of the hyperon occurs principally in the virtual Σ state, certain conclusions may be drawn regarding the mesonic to non-mesonic decay ratio for hyperfragments. In fact it may be shown that in this case also the mesonic decay will depend on the density of the nucleons, and consequently the mesonic to non-mesonic ratio will tend to saturation with increasing atomic number.

* * *

[7] R. HOFSTÄDTER et al.: *Proceedings Sixth Annual Rochester Conference*, 1956.

RIASSUNTO

Per interpretare un recente risultato sperimentale riguardante il decadimento degli iperoni Λ legati in iperframmenti è stato preso in esame un modello nel quale il decadimento dell'iperone Λ può accadere anche nello stato Σ virtuale. Si considerano anche le conseguenze della non conservazione della parità.

Stimulated Decay of the Λ Hyperon in Light Hyperfragments (*).

M. Baldo-Ceolin, C. Dilworth, W. F. Fry (+), W. D. B. Greening,

H. Huzita (×), S. Limentani and A. E. Sichirollo

Istituto Nazionale di Fisica Nucleare - Sezione di Milano
Istituto Nazionale di Fisica Nucleare - Sezione di Padova
Istituto di Fisica dell' Università - Padova

Summary. — From a group of double stars which were produced by 4.5 GeV negative pions, a selection has been made of those events with linking tracks longer than 20 μm and which appeared to represent the non-mesonic decays, mainly, of $_\Lambda$He, $_\Lambda$Li, and $_\Lambda$Be hyperfragments. A total of 31 hyperfragments satisfied these criteria. From a study of the energy distribution of the charged particles from these disintegrations, it has been found possible to separate the decays into those where the hyperon was stimulated into decaying by a neutron, from those caused by a proton. The ratio of neutron to proton stimulation is found to be about 1.4. This value may give some indications about the parity of the Λ hyperon and the possible transition $\Lambda \rightarrow \Sigma + \pi$.

1. – Introduction.

Shortly after the discovery of the first examples of hyperfragments [1], it became clear that not only can a Λ hyperon which is bound in nuclear fragment, decay with the emission of a pion, but that also the decay can occur without

---

(1) M. Danysz and J. Pniewski: *Phil. Mag.*, **44**, 348 (1953).

pion emission, the so-called non-mesonic decay mode. Subsequent studies [2] have shown that the non-mesonic to mesonic ratio increases rapidly with increasing atomic number and the non-mesonic mode quickly becomes the predominant decay mode. For example, in Li this ratio [2] is about 15. It has been pointed out by several authors [3-5] that many factors may enter into the non-mesonic to mesonic ratio; for example the spin of the Λ hyperon, the binding energy of the Λ hyperon, as well as the structure of the core nucleus. PRIMAKOFF and CHESTON [3] and FOWLER [6] have shown that to explain the rapid increase in the non-mesonic to mesonic ratio with increasing atomic number, it is necessary to postulate that in the non-mesonic disintegrations, i.e. $\Lambda + \mathcal{N} \rightarrow \mathcal{N} + \mathcal{N} + 180$ MeV the Λ hyperon is stimulated into decay as opposed to the absorption of the real pion from the mesonic decay of the Λ hyperon.

Aside from the variation of the non-mesonic to mesonic ratio with atomic number, little is known about the Λ hyperon-stimulation process. It seemed reasonable that some information might be obtained from a study of the non-mesonic decays in the lightest hyperfragments by considering the energy distribution and the frequency of the energetic nucleons, for in the lightest hyperfragments the total number of nucleons is small and there is a good possibility that fast nucleons from the stimulated decay process would escape without interacting with the remaining nucleons.

2. – Procedure.

A 600 μm pellicle stack which was exposed to 4.5 GeV negative pions from the Berkeley Bevatron accelerator, has been systematically scanned for events which can be interpreted as hyperfragment decays. In fact there are several types of events which, under certain circumstances, can be mistaken as hyperfragment decays; for example, the capture of slow negative particles such as pions, K⁻ mesons and Σ⁻ hyperons, and collisions in flight of nuclear particles. If the track is at least 20 μm long, it may be possible, under favorable circumstances, to confirm by profile measurements that the connection track was

[2] W. F. FRY, J. SCHNEPS and M. S. SWAMI: *Phys. Rev.*, **99**, 1561 (1955); **101**, 1526 (1956); **106**, 1062 (1957).

[3] W. CHESTON and H. PRIMAKOFF: *Phys. Rev.*, **92**, 1537 (1953); H. PRIMAKOFF: *Nuovo Cimento*, **3**, 1394 (1956).

[4] M. RUDERMAN and R. KARPLUS: *Phys. Rev.*, **102**, 247 (1956).

[5] R. H. DALITZ: *Proceedings Sixth Annual Rochester Conference*, p. v-40 (New York, 1956).

[6] T. K. FOWLER: *Phys. Rev.*, **102**, 844 (1956).

produced by a nuclear fragment coming to rest rather than by a singly charged particle. Many of the double stars which have a connecting track shorter than 20 μm are probably hyperfragment decays, but it is also possible that an appreciable number are not hyperfragments. Because of this uncertainty, is was decided to include in this study only those double stars which have a connecting track longer than 20 μm. Profile measurements have been made on all of those cases where the connecting track appeared to have been produced by a fragment, was longer than 20 μm and had dip $< 30°$. In each of these cases, the profile measurements were consistent with the fragment assumption. In two cases, rejected by visual observations as fragments not at rest, the profile measurement confirmed the observation. In addition to the above selection, only those events which appeared to be non-mesonic decays at rest of $_\Lambda$He, $_\Lambda$Li and $_\Lambda$Be were chosen for this study.

In order to select the hyperfragments of $_\Lambda$He, $_\Lambda$Li and $_\Lambda$Be it was necessary to base, in most cases, the estimate of the charge of the hyperfragment on the total charge of the disintegration products, since in most cases the length of the hyperfragment track was not generally sufficient for a charge determination. The charge of the fragment is assumed to be equal to the total charge of the disintegration star. In some cases one or more of the tracks from the disintegration stars were short and therefore the charge could not be determined.

Where the secondary stars in those events contain very short tracks which could be due to the recoil of a heavier nucleus, the nature of the hyperfragment track itself was taken into consideration before the event was accepted as a light hyperfragment. There will still be a bias towards an underestimation of the total charge and therefore an inclusion of some fragments of charge greater than 4. However, in this preliminary study, a small contamination of fragments of charge greater than 4 would not seem to be important since, of necessity, the results are an average over several light nuclei of different charge and atomic weight.

3. – Results.

Of all the possible hyperfragments 176 were shorter than 20 μm. The bulk of these double stars may be fragments but undoubtedly other processes may be included and therefore these events have been rejected in this work. Of those longer than 20 μm, 31 events satisfied our selection criteria, while 8 had $Z > 4$.

The energies of the secondary particles were determined by range whenever this was possible: in the other cases it was based on the ionization of the track. The general features of the hyperfragments are summarized in Table I.

TABLE I.

Events	Range of HF in μm	Probable charge of HF	Stimulation by p or by n	No. of tracks	Probable Identity	Kinetic energy in MeV	K.E. of charged particles in MeV	Total energy of charged particles minus K.E. of fast proton
Pd$_1$	21	2 or 3	P	1 2	P P.D.T.α	85 .6	86	.6
Pd$_2$	96	2 or 3	P	1 2	P P.D.T.α	67 .7	68	.7
Mi$_1$	131	2	P	1 2	P P.D.T.	90 4	94	4
Mi$_2$	210	2	P	1 2	P P	9 140	149	9
Mi$_3$	185	2 or 3	P	1 2	P P.D.T.α	105 5.2	110	5.2
Mi$_4$	197	3	P	1 2 3	P P.D.T. P.D.T.	55 1 6	62	7
Pd$_3$	48	3 or 4	P	1 2 3	P P.D.T.α P.D.T.	92 2.5 9.5	104	12
Pd$_4$	45	3	P	1 2 3	P P. P.	86 6.1 26.5	118.6	32.6
Pd$_5$	150	3	P	1 2 3	P P.D. P.D.	41.5 8.5 5.5	55.5	14
Pd$_6$	22	4	P	1 2 3 4	P P.D.T. P.D.T. P.D.T.	32 .8 1 3.5	37	5
Mi$_5$	240	3	P	1 2	P α	41 2	43	2
Pd$_7$	190	2	P	1 2	P P	34 20	54	20
Mi$_6$	99	2	P	1 2	P.D.T. P	3.8 75	79	3.8
Mi$_7$	397	2	N	1 2	P P.D.T.	28 4	32	
Mi$_8$	55	3	N	1 2	P α	26.5 3.5	30	
Mi$_9$	161	2 or 3	N	1 2	P.D.T.α P.D.T.	1.2 7	8.2	

TABLE I (continued).

Events	Range of HF in μm	Prob- able charge of HF	Stimul- ation by p or by n	No. of tracks	Probable Identity	Kinetic energy in MeV	K.E. of charged particles in MeV	Total energy of charged particles minus K.E. of fast proton
Pd_8	69	2	N	1 2	P.D.T. P.D.T.	8.2 9	17	
Pd_3	56	2	N	1 2	P P	11 11	22	
Pd_{10}	81	2	N	1 2	P P	16.8 17.5	34.3	
Pd_{11}	113	2	N	1 2	P P	16.3 12	28.3	
Pd_{12}	62	2 or 3	N	1 2	P.D.T. P.D.T.α	1.3 1	2.3	
Pd_{13}	66	3	N	1 2	P.D.T. α	8.6 9.2	17.8	
Pd_{14}	41	3	N	1 2	P.D.T. α	.7 5.1	5.8	
Pd_{15}	302	2	N	1 2	P.D.T. P.D.T.	4.4 1.4	5.8	
Pd_{16}	53	3	N	1 2 3	P.D.T. P.D.T. P.D.T.	1.5 2.6 2.7	6.8	
Pd_{17}	214	3 or 4	N	1 2 3	P.D.T. P.D.T. P.D.T.α	9.5 3.2 0.4	13	
Pd_{18}	73	3 or 4	N	1 2 3	P.D.T. P.D.T. P.D.T.	2.1 2.8 1.9	6.8	
Pd_{19}	172	4	N	1 2 3 4	P.D.T. P.D.T. P.D.T. P.D.T.	2.7 .5 .5 .7	4.4	
Pd_{20}	152	2	N	1 2	P.D.T. P	3.2 16	19.2	
Pd_{21}	480	2 or 3	N	1 2	P.T.α P	18α 15	33	
Mi_{10}	184	3 or 4	N	1 2 3	P.D.T. P.D.T.α P.D.T.	5.1 .4 1.2	6.8	

In Fig. 1 is shown the energy distribution of all of the charged particles from the hyperfragment disintegrations. The distribution appears to consist of a group of tracks of quite low energy and a group of fast protons with a relatively wide energy spread.
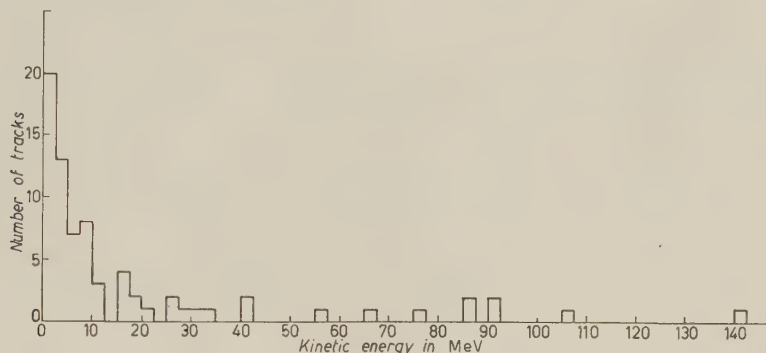
Fig. 1.

The low energy is interpreted as due to the break-up of the residual nucleus following the emission of the two fast nucleons from the stimulation process. In many of the hyperfragments of He, Li and Be the residual nucleus, after removing two neutrons or a neutron and a proton, is unstable against break-up and therefore one might expect such a group of low energy particles.

The fast protons, on the other hand, are attributed to the initial stimulation process by protons. One would expect that a large fraction of the fast protons from the stimulated decay of the Λ hyperon would escape from the nucleus in the light hyperfragments, for the number of nucleons is small and the nuclear cross-section is not high at these energies.

If the stimulated decay of the Λ hyperon were caused by a free proton, the energy of the proton would be one half of the Q of the stimulation process, namely 88 MeV. However, if the stimulation is by a proton bound in a nucleus, the expected energy distribution of the fast protons would be broad due to the vector sum of the Fermi momentum of the Λ hyperon and the proton. The expected average energy of the protons would be somewhat less than one half of the Q of the stimulation process, minus the binding energy of the Λ hyperon and of the stimulating nucleon. The spread in the energy distribution of the fast proton can be attributed to a Fermi momentum of the Λ hyperon and nucleon of about 130 MeV/c. The mean kinetic energy of the fast proton is 73 MeV. The mean kinetic energy and the spread in the energy distribution of fast protons are therefore consistent with the assumption that a major portion of these protons are due to the stimulation of the Λ hyperon by a single proton.

With the small number of particles available, it is not easy to determine the line of separation between the low and high energy protons; those with energy between 20 and 30 MeV be considered as border-line events.

Those protons having energies greater than 30 MeV have been considered as « fast » protons produced directly by the stimulation process. This cut-off has been suggested by the following considerations: the mean energy of the nucleons in the nucleus is $\frac{1}{2}Q = 88$ MeV, while outside the nucleus this must be diminished by about 10 MeV in order to take account of the binding energy. Assuming that the distribution of the « fast » protons is symmetrical about the mean, we obtain this lower limit for their energy. It is possible that also some of the slower protons come directly from the stimulation process, though on the other hand some particles having energies of $20 \div 30$ MeV might be expected to come from the break-up of unstable nuclei having excitation energies of say 20 MeV. In any case it seems reasonable to suppose that the ratio of stimulations by neutrons to those of protons is not altered appreciably by the choice of the energy of separation.

Since the number of fragments is small, it is possible that some of the events with fast protons as well as those examples with fast neutrons, could come from a stimulation process involving more than one nucleon. However, it would be expected that the one-nucleon process would predominate in the stimulation since all of the conservations laws can be satisfied in the one-nucleon process. One could hope to estimate the percentage of two nucleon stimulations by a study of non-mesonic hyperfragment decays which have two fast protons, taking into account the probability of the interaction of a fast neutron to give the second fast proton. To date, no such event has been reported in the literature and it therefore seems likely that the two nucleon stimulation is relatively unimportant. We shall assume in the subsequent discussion that all of the stimulated decays were caused by one nucleon.
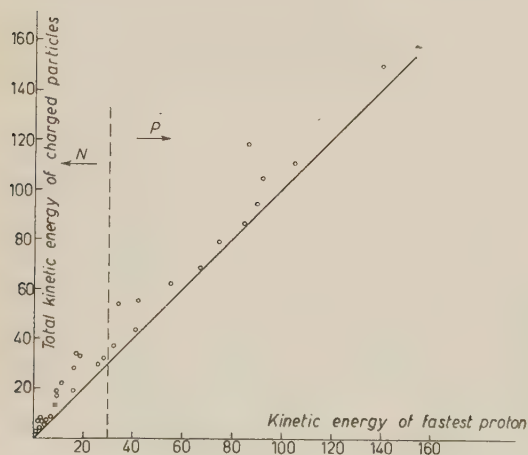
In order to investigate the possibility that a reasonable fraction of the fast nucleons from the primary stimulation process interact with the nucleons before escaping, a plot has been made of the total energy of the charged particles from the decays *vs.* the energy of the fastest proton. This plot is shown in Fig. 2.

Fig. 2.

From conservation of energy, it is impossible that an event lie to the right of the 45° line. As can be seen, nearly all the events lie reasonably close to the 45° line. The mean vertical displacement from the 45° line is 9 MeV, and the maximum displacement is 33 MeV. This would indicate that the fast nucleons (neutrons as well as protons) did not transfer a large fraction of their energy before escaping.

In order to estimate the ratio of stars with fast protons to the number with only slow nucleons, it is necessary to evaluate the difference in the probability of finding and recognizing the two classes of events.

One might expect to have a bias against the recognition of events containing only slow nucleons owing to the possible confusion of two prong events with collisions of singly charged particles and one prong events with a scattering of the fragment. The existence of such a bias should lead to a higher total number of tracks per star or a higher mean energy per track for the slow particles from the neutron induced decays as compared to the proton events.

TABLE II.

No. of tracks per decay		Mean energy per track of slow nucleons	
Stars with fast proton	Stars without fast proton	Stars with fast proton	Stars without fast proton
$\frac{32}{13} = 2.5$	$\frac{42}{18} = 2.3$	5.1	7.1

Table II shows that in our small sample there is no significant evidence for such a bias, and we can therefore make no correction although we believe some bias should exists. For this reason, the neutron to proton stimulation ratio given below is probably lower than the true value.

The average energy of the fast protons, their energy distribution and the small amount of nuclear excitation would suggest that the events can be separated into two classes, i.e. those with a fast proton which result from the hyperon stimulation by a proton, and the stars without fast protons caused by the stimulation by a neutron leading to two fast neutrons which are not observed. Of the 31 hyperfragments, there are 13 events with fast protons and 18 events with only charged particles giving a ratio of neutron stimulated to proton stimulated events of 1.4.

4. – Results and discussion.

Our results show that to the two basic parameters which have been used to obtain information on the Λ^0 hyperon interaction in nuclear matter, namely the binding energy and the non-mesonic to mesonic decay ratio, there can be added the parameter, neutron to proton stimulation ratio.

If we assume that the non-mesonic decay occurs through a process of the type suggested by RUDERMAN and KARPLUS, and that the stimulated bound Λ's decay with the same branching ratio as the free Λ's, then the expected value for the ratio

$$R = \frac{\text{stimulation by neutrons}}{\text{stimulation by protons}}$$

is unity or $\frac{1}{9}$ according to whether one considers that hyperons and nucleons have the same or different parity. If parity is not conserved, this ratio will lie between 0.1 and 1.0.

It has however been suggested by FERRARI and FONDA ([7]) that the stimulation may occur by a virtual process involving a Σ hyperon and a pion with subsequent emission and absorption of a second pion, and consequently the neutron to proton ratio is greater or equal to unity. It might be expected that the process involving the Σ hyperon may be as important, or perhaps more important than the single virtual pion reaction because the binding of a Λ-hyperon in a hyperfragment can only result from virtual processes involving more than one pion, or processes such as the virtual Σ hyperon, as has been calculated by LICHTENBERG and ROSS ([8]) and by DALLAPORTA and FERRARI ([9]).

In order to determine the relative strength of the interaction giving rise to stimulation by neutrons and protons, it may be necessary to consider the structure of the nuclear core of the hyperfragments. In some nuclei it may be possible that the overlap of the wave function of the Λ hyperon with the protons is not the same as with neutrons. For this reason it would be interesting to see if the ratio R varies with the A and Z of the hyperfragment. Unfortunately it is not possible to investigate this variation using the small amount of data available at this time.

([7]) F. FERRARI and L. FONDA: *The Stimulated decay of Bound Λ-Hyperons*, appearing in this issue.

([8]) D. LICHTENBERG and M. ROSS: *Phys. Rev.*, **103**, 1131 (1956).

([9]) N. DALLAPORTA and F. FERRARI: *Nuovo Cimento*, **5**, 111 (1956).

* * *

RIASSUNTO (*)

Da un gruppo di stelle doppie prodotte da pioni negativi di 4.5 GeV sono stati scelti gli eventi con tracce di collegamento maggiori di 20 μm che apparivano rappresentare decadimenti non mesonici, principalmente iperframmenti di $_\Lambda$He, $_\Lambda$Li e $_\Lambda$Be. Un totale di 31 iperframmenti soddisfaceva a tali esigenze. Da uno studio della distribuzione dell'energia delle particelle cariche derivanti da tali disintegrazioni è risultato possibile separare i decadimenti in cui l'iperone era stimolato a decadere da un neutrone da quelli causati da un protone. Il rapporto della stimolazione neutronica alla protonica risulta essere circa 1.4. Questo valore è atto a dare qualche indicazione sulla parità dell'iperone Λ e sulla possibile transizione $\Lambda \to \Sigma + \pi$.

(*) *Traduzione a cura della Redazione.*

Nucleon-Nucleon Scattering at High Energy (*).

M. GOURDIN

Laboratoire de Physique, École Normale Supérieure, Université de Paris

Summary. — The nucleon-nucleon scattering and polarization experiments cannot be explained by a simple local potential. This method gives good results in the low energy domain. But between 0 and 300 MeV, for example, it is well known that the Schrödinger equation is inadequate. It is necessary, at high energies, to use a completely covariant formulation for two body systems—the Bethe and Salpeter equation ([1,2])—in order to take into account relativistic corrections. With an analytical continuation of the scattering amplitude for the imaginary values of relative time (or relative energy), we can generalize the method of partial waves to a four dimensional euclidian problem. It is shown that, in the simplified case of spinless particles (Klein-Gordon particles), the physical phase shifts corresponding to a given value of the orbital angular momentum are easily obtained. For the more realistic case of spin $\frac{1}{2}$ particles (Dirac particles) it is possible to calculate the differential cross-section. Explicit solutions are obtained with an approximate method of resolution for the integral equations. Further, one can determine the value of the coupling constant that gives the correct experimental neutron-proton singlet scattering length, in the case of the « ladder approximation ». The ^1S phase shift, calculated for various values of the energy, exhibits a change of sign in the energy region of 140 MeV. This result is in agreement with the experiments and the « hard core » theory of Lévy ([3-6]).

([1]) H. A. BETHE and E. E. SALPETER: *Phys. Rev.*, **84**, 1232 (1951).
([2]) H. GELL-MANN and F. LOW: *Phys. Rev.*, **48**, 350 (1951).
([3]) M. M. LÉVY: *Phys. Rev.*, **86**, 806 (1952).
([4]) M. M. LÉVY: *Phys. Rev.*, **88**, 72 (1952).
([5]) M. M. LÉVY: *Phys. Rev.*, **88**, 725 (1952).
([6]) R. JASTROW: *Phys. Rev.*, **81**, 165 (1951).

1. – Bethe and Salpeter equation.   Wick's transformation.

The Bethe and Salpeter equation is an inhomogeneous integral equation for the scattering amplitude $\psi(1, 2)$ of two fermions in pseudoscalar inter-action with π pseudoscalar mesons:

$$(1.1) \qquad \psi(1, 2) = \psi_0(1, 2) + \frac{1}{4} \int S_F^{(1)}(1, 3) S_F^{(2)}(2, 4) G(3, 4; 5, 6) \psi(5, 6) \, d3 \ d4 \, d5 \, d6 \,,$$

The kernel $G(3, 4; 5, 6)$ is an infinite sum of irreducible graphs defined in a manner similar to that used by DYSON ([7-11]).   For the lowest order in the coupling constant g, we have only one fundamental graph corresponding to the exchange of a virtual meson during a small time interval:

$$G^{(1)}(3, 4; 5, 6) = g^2 \gamma_5^{(1)} \gamma_5^{(2)} \Delta_F(3, 4) \, \delta(5\text{-}3) \, \delta(6\text{-}4) \,.$$

The Bethe and Salpeter equation includes an infinite number of reducible « ladder type » graphs which are the iteration of this process.   This summation is the so-called « ladder approximation » ([12-14]).
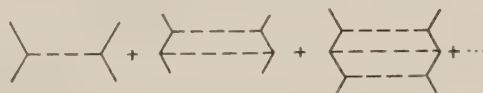
Fig. 1. – Reducible graphs included in $G^{(1)}$. (Solid lines denote nucleons and broken lines mesons).

The S_F and Δ_F functions, which appear in (1.1) and $G^{(1)}$, are defined as in DYSON ([11]).

It is convenient to insert energy-momentum variables.   The Fourier transform $\chi(p_1, p_2)$ of the amplitude $\psi(1, 2)$ satisfies a new integral equation:

$$(1.2) \qquad \chi(p_1, p_2) = \chi_0(p_1, p_2) + F_1(p_1) F_2(p_2) \int V(p_1, p_2; \, p_1', p_2') \chi(p_1', p_2') \, dp_1' \, dp_2' \,,$$

where V contains the Fourier transform of the kernel G.   The one particle propagators $F_1(p_1)$ and $F_2(p_2)$, if one neglects radiative corrections, reduce to:

[7] R. P. FEYNMAN: *Phys. Rev.*, **76**, 749 (1949).

[8] R. P. FEYNMAN: *Phys. Rev.*, **76**, 769 (1949).

[9] R. P. FEYNMAN: *Phys. Rev.*, **80**, 440 (1950).

[10] F. J. DYSON: *Phys. Rev.*, **75**, 486 (1949).

[11] F. J. DYSON: *Phys. Rev.*, **75**, 1736 (1949).

[12] Y. NAMBU: *Prog. Theor. Phys.*, **5**, 614 (1950).

[13] J. SCHWINGER: *Proc. Nat. Acad. Sci.*, **37**, 452 (1951).

[14] J. SCHWINGER: *Proc. Nat. Acad. Sci.*, **37**, 455 (1951).

$F(p) = -i(p^2 + {}^2M^2 - i\varepsilon)^{-1}$ for spinless particles of mass M, and

$F(p) = -i(i\gamma p + M - i\varepsilon)^{-1} = -i(i\gamma p - M)(p^2 + M^2 - i\varepsilon)^{-1}$ for spin $\frac{1}{2}$ particles.

The mass M is assumed to have an infinitesimal negative imaginary part $-i\varepsilon$, so that the integration paths, in the complex plane of the variable p_0, are perfectly defined.

We cannot define, in a relativistic theory, the co-ordinate X of the center of mass; but the total momentum P, namely the momentum of the center of mass motion, can be unambiguously defined. With an arbitrary para-meter λ, we shall denote « absolute » and « relative » co-ordinates by:

$$x = x_1 - x_2 , \qquad x_1 = X + (1 - \lambda)x ,$$
$$X = \lambda x_1 + (1 - \lambda)x_2 , \qquad x_2 = X - \lambda x .$$

We have for the conjugate momenta:

$$P = p_1 + p_2 , \qquad p_1 = \lambda P + p ,$$
$$p = (1 - \lambda)p_1 - \lambda p_2 , \qquad p_2 = (1 - \lambda)P - p .$$

To make the transition to the non-relativistic limit easier, we choose: $\lambda = M_1/(M_1 + M_2)$. In the present particular case fo two identical particles, we obtain the value $\lambda = \frac{1}{2}$.

If the interaction kernel G is a function of the relative space-time co-ordinates x and x' and of the difference of the two absolute co-ordinates $(X - X')$, it is easy to prove that the wave functions χ and ψ can take the particular forms:

$$\chi(p_1, p_2) = \varphi(P)(2\pi)^4\,\delta(P - K) \quad \text{and} \quad \psi(x_1, x_2) = \varphi(x)\exp[iKX] ,$$

where K is an arbitrary constant four-dimensional vector.

With these changes of variables and functions, Eq. (1.2) reduces to:

$$(1.3) \qquad \varphi(p) = \varphi_0(p) + F_1\left(\frac{P}{2} + p\right) F_2\left(\frac{P}{2} - p\right) \int W(p, p'; P)\varphi(p')\,\mathrm{d}p' .$$

The fourth component of the vectors x or p is purely imaginary and the absence of a positive definite norm for this vectors is a mathematical diffi-culty. In addition, the physical significance of a relative time (or a relative energy) of two particles is not entirely clear. These questions and other ones more directly related to the Bethe and Salpeter equation led WICK ([15]) to

([15]) G. G. WICK: Phys. Rev., 96, 1124 (1954).

express some boundary conditions at $t = \pm \infty$ that are equivalent to stability requirements. For the bound-state case, this condition implies that the wave function φ can be analytically continued to purely imaginary values of the « relative time » (or the relative energy). A rotation of $\pi/2$ of the integration path in the complex plane of the variable x_0 (or p_0) allows to consider a new equation with $x_4 = ix_0$ (or $p_4 = ip_0$) purely real. The use of an imaginary time has no physical meaning; on the other hand, it has mathematically several advantages. The new four-dimensional space becomes euclidian.

For a scattering problem, KEMMER and SALAM ([16]) show that the analytical continuation of the wave function φ is still possible. Nevertheless several difficulties appear owing to the distribution of the poles in the complex plane of the variable p_0. Using the notations:

$$P = (0, 0, 0, iE), \quad E = 2E_k, \quad E_k = \sqrt{k^2 + M^2}, \quad E_p = \sqrt{|\boldsymbol{p}|^2 + M^2}$$

we have the two possible situations illustrated by Fig. 2 for the poles of $F_1(p)$

$$a) \ E_p > E_k \ \text{or} \ |\boldsymbol{p}| > k, \qquad b) \ E_p < E_k \ \text{or} \ |\boldsymbol{p}| < k$$
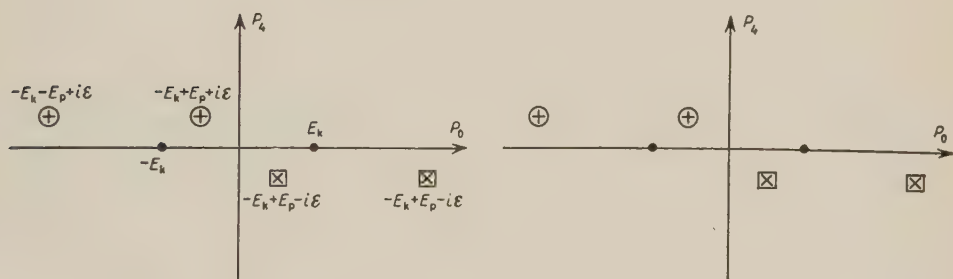
Fig. 2. – The complex plane of the variable p_0. The poles of F_1 and F_2.

and $F_2(p)$. It is easy to see that, in the case $b)$ the two paths p_4 and p_0 are not equivalent for the partition of poles. In order to solve this difficulty we carry out an analytical continuation of the wave function for the imaginary values of p_0 and P_0, i.e. of the energies of each particle. The consideration of a total energy P_0, purely imaginary, is a simple mathematical trick, without physical significance, that permits, in all cases, the correct choice of the poles. After integration over p_0, the momentum P_0 takes its physical real value: E.

([16]) N. KEMMER and A. SALAM: Proc. Roy. Soc., A 230, 266 (1955).

2. – Klein-Gordon particles.

The case of spin 0 particles, in scalar interaction with scalar mesons, corresponds to Δ_F functions for the one-particle propagators. The Bethe and Salpeter equation can be written, after Wick's transformation:

$$(2.1) \quad \Phi(\mathbf{p}) = (2\pi)^4\,\delta_4(\mathbf{p} - \mathbf{k}) + \frac{\alpha}{(p^2 + M^2 + (P^2/4))^2 - p_4^2 P^2} \int W(\mathbf{p}, \mathbf{p}')\,\Phi(\mathbf{p}')\,\mathrm{d}\mathbf{p}' \ .$$

We use the notation $\mathbf{p}$ for the four-dimensional vector, setting:

$$\mathbf{p \cdot p} = p^2 = p_1^2 + p_2^2 + p_3^2 + p_4^2 \ .$$

We shall begin to separate Φ, using spherical variables θ, φ, β, and to reduce the problem to an infinite set of one-dimensional coupled integral equations.

2'1. *Integration over angular variables.* – We perform the expansion of the wave function in hyperspherical harmonics (see Appendix I):

$$(2.2) \qquad \Phi(p) = \sum_{n=0}^{\infty}\ \sum_{l=n}^{\infty}\ \sum_{m=-l}^{m=+l} A(p;\,l,\,m,\,n)\mathcal{Y}_{ln}^m(\Omega_p) \ .$$

This development is inserted into the integral equation (2.1) and we multiply both sides by $\mathcal{Y}_{ln}^{m*}(\Omega_p)$. The integration over the angles Ω_p is performed by using the properties of orthonormalization of the hyperspherical harmonics. Next, we assume that the interaction kernel $N(\mathbf{p}, \mathbf{p}')$ depends only on p, p' and Θ the angle between $\mathbf{p}$ and $\mathbf{p}'$ (Lorentz invariance). Under this assumption, it is easy to develop N in Gegenbauer polynomials of $\cos\Theta$, and by application of the addition theorem (Appendix I), we obtain:

$$(2.3) \qquad N(\mathbf{p}, \mathbf{p}') = \sum_{\lambda\mu\nu} \Delta_\nu(p, p')\,\mathcal{Y}_{\lambda\nu}^\mu(\Omega_p)\,\mathcal{Y}_{\lambda\nu}^{\mu*}(\Omega_{p'}) \ .$$

If one inserts this expression into (2.1), one finds after integration over $\theta_{p'}$ and $\varphi_{p'}$ a set of integral equations:

$$(2.4) \qquad A(p;\,l,\,m,\,n) = A_0 + \alpha \sum_{n'=1}^{\infty} E(p;\,l,\,n,\,n') \int_0^\infty A(p';\,l,\,m,\,n')\Delta_n(p, p')p'^3\,\mathrm{d}p' \ ,$$

where

$$(2.5) \qquad E(p;\,l,\,n,\,n') = \int_0^\pi \frac{\mathcal{C}_l^n(\beta)\,\mathcal{C}_l^{n'}(\beta)}{(p^2 + M^2 + (P^2/4)) - p^2 P^2 \cos^2\beta}\,\sin^2\beta\,\mathrm{d}\beta \ .$$

The functions $\mathcal{C}_l^n(\beta)$ are the part of the hyperspherical harmonics related to the Gegenbauer polynomials. The first part A_0 corresponding to the incident wave is calculated in Appendix II:

$$(2.6) \qquad A_0(p; l, m, n) = (2\pi)^4 \frac{\delta(p-k)}{k^3} \, \mathcal{Y}_{ln}^{m*}(\Omega_k) \,.$$

At this stage, we can notice two well-known results:

    1) m is a good quantum number, equal to zero: the problem has a cylindrical symmetry.

    2) l, the orbital angular momentum, is a constant of motion, and

    3) $(-1)^n = (-1)^{n'} = (-1)^l$: the conservation of the parity of n can be pointed out with the help of the symmetry properties of the Gegenbauer polynomials [17]. It will be more convenient to use, instead of n and n': q and q':

$$n = l + 2q \qquad \text{and} \qquad n' = l + 2q' \,,$$

We shall now consider the integration over the β angle (2.5). The integrand is a function of $\cos^2 \beta$ and therefore of the angle $\psi = 2\beta$. We can develop the numerator in a Fourier series of ψ

$$(2.7) \qquad \mathcal{C}_l^{l+2q}(\beta) \, \mathcal{C}_l^{l+2q'}(\beta) \sin^2 \beta = \sum_{-\infty}^{+\infty} c_m(l; q, q') \exp[im\psi] \,.$$

Furthermore, applying Poisson's formula to Eq. (2.5) (P_0 is purely imaginary), we perform the integration over β. When P_0 takes its physical value, $2E_k$, two poles appear $p = \pm k$. With the change of function:

$$E(p; l, q, q') = \frac{1}{p^2 - k^2} \, H(p; l, q, q') \,,$$

we obtain for H the following result:

$$(2.8) \qquad H(p; l, q, q') = \frac{\pi}{[(p^2 - k^2)^2 + 4p^2 E_k^2]^{\frac{1}{2}}} \sum_{-\infty}^{+\infty} c_m(l; q, q') h^{|m|} \,,$$

where

$$h = \frac{p^2 - k^2 - [(p^2 - k^2)^2 + 4p^2 E_k^2]^{\frac{1}{2}}}{p^2 + k^2 + [(p^2 - k^2)^2 + 4p^2 E_k^2]^{\frac{1}{2}}} \,.$$

The poles $p = \pm k$ are true poles and it is easy to compute the value of H at this point:

$$(2.9) \qquad H(k; l, q, q') = \frac{\pi}{2kE_k} \, \mathcal{C}_l^{l+2q}(\pi/2) \, \mathcal{C}_l^{l+2q'}(\pi/2) \,.$$

---

[17] W. MAGNUS and F. OBERHETTINGER: *Formeln und Sätze für die speziellen Funktionen der Mathematischen Physik.*

We now can write the infinite set of coupled integral equations for the radial functions $A(p; l, q)$:

$$(2.10) \quad A(p; l, q) = (2\pi)^4 \frac{\delta(p - k)}{k^3} \sqrt{\frac{2l + 1}{4\pi}}\, \mathcal{C}_l^{l+2q}(\pi/2) +$$

$$+ \frac{\alpha}{p^2 - k^2} \sum_{q'=0}^{\infty} H(p; l, q, q') \int_0^\infty \Delta_{l+2q'}(p, p') A(p'; l, q') p'^3 \,\mathrm{d}p'\,.$$

In general, Eq. (2.10) cannot be exactly solved. It is necessary to use approximate methods. This problem will be treated later. For the moment, we attempt to define physical quantities, such as phase shifts and scattering differential cross-sections, from the wave $A(p)$.

2'2. *Definition of phase-shifts.* – In a similar manner, one can consider an expansion of the wave function $\Phi(\mathbf{p})$—written in the configuration space—in hyperspherical harmonics, with the radial fnctions $A(r; l, q)$. The correlation between $A(r)$ and $A(p)$ is given in Appendix III. Applying the transformation:

$$A(r; l, q) = \frac{(-1)^q i^l}{(2\pi)^2} \int_0^\infty A(p; l, q) \frac{J_{2q+l+1}(pr)}{pr}\, p^3 \,\mathrm{d}p\,,$$

—where $J_{2q+l+1}(pr)$ is the regular Bessel function—to the integral equation, we can separate the right hand side of Eq. (2.10) into two parts: the first one, corresponding to the incident wave is immediately calculated:

$$A_0(r; l, q) = (-1)^q i^l (2\pi)^2 \sqrt{\frac{2l + 1}{4\pi}}\, \mathcal{C}_l^{l+2q}(\pi/2) \frac{J_{2q+l+1}(kr)}{kr}\,.$$

For the second part, we are only interested in its asymptotic behaviour for large values of r. If one puts:

$$(2.11) \qquad B(p; l, q) = \int_0^\infty \Delta_{l+2q}(p, p') A(p'; l, q) p'^3 \,\mathrm{d}p'\,,$$

one may perform integrals of the following type:

$$\text{P.V.} \int_0^\infty \frac{p^3}{p^2 - k^2} H(p; l, q, q') B(p; l, q') \frac{J_{l+2q'+1}(pr)}{pr}\, p\,\mathrm{d}\,.$$

The main contribution to the asymptotic form comes from the pole $p = k$ [18]

---

[18] M. M. Lévy: *Phys. Rev.*, **94**, 460 (1955).

and we can write:

$$H(k; l, q, q') B(k; l, q') \text{ P.V.} \int_0^\infty \frac{p^3}{p^2 - k^2} \frac{J_{l+2q'+1}(pr)}{pr} \, dp \; .$$

The last integral is performed in Appendix IV and $A(r; l, q)$ takes the asymmetric form:

$$(2.12) \quad A(r; l, q) \simeq (-1)^q i^l (2\pi)^2 \sqrt{\frac{2l+1}{4\pi}} \, \mathcal{C}_l^{l+2q} \left(\frac{\pi}{2}\right) \left\{ \frac{J_{l+2q+1}(kr)}{kr} - \text{tg} \, \delta_l \, \frac{N_{l+2q+1}(kr)}{kr} \right\},$$

N_{l+2q+1} are the irregular Bessel functions and δ_l is a pseudo-phase shift, unconnected with the parameter q. It is the same for all radial functions related to a given angular momentum l,

$$(2.13) \qquad \text{tg} \, \delta_l = \alpha \, \frac{k}{16\pi E_k} \frac{1}{[4\pi(2l+1)]^{\frac{1}{2}}} \sum_{q'} \mathcal{C}_l^{l+2q'} \left(\frac{\pi}{2}\right) B(k; l, q') \; .$$

WICK has pointed out that the wave function $\varphi(x)$ goes to zero when the time t goes to ∞ in any direction, in both the lower and upper half planes of the variable x_0, and especially along the imaginary t axis (i.e. for x_t real). The fact that the phase shift δ_l does not depend on q seems to be a consequence of this asymptotic behaviour of $\varphi(\mathbf{x})$.

In the foregoing discussion we have considered spinless particles with scalar interaction. It is clear that the conclusions must necessarily remain valid for Dirac particles.

Finally, with the aim of defining physical quantities, we must consider the wave corresponding to a given value of l, by summation on q of the partial wave (see Appendix V). We obtain:

$$(2.14) \qquad A_l(r) \simeq i^l [4\pi(2l+1)]^{\frac{1}{2}} \{j_l(kR) - \text{tg} \, \delta_l n_l(kR)\},$$

where $R = r \sin \beta_r$.

When the times of the two particles are equalled, the variables R and r are the same. Eq. (2.14) proves that δ_l is the true phase-shift associated with the partial wave $A_l(r)$.

Since δ_l has a simple physical interpretation, we must again consider the integral equation (2.10) in order to get approximate methods of resolution.

2·3. *Approximate method and variational principle.* – In order to consider the infinite set of coupled equations corresponding to a value of l, we use infinite matrices. The columns and rows are denoted by q and q'. Summations have been replaced by products of matrices. Eq. (2.10) with the notation

(2.11) can be written:

$$(2.15) \qquad A(p) = \frac{\delta(p-k)}{k^3} D + \frac{x}{p^2 - k^2} H(p) B(p) .$$

And the phase-shift (21.3) takes the form:

$$(2.16) \qquad \mathrm{tg}\, \delta_l = x \frac{k}{8E_k(2l+1)(2\pi)^5} D^r B(k) ,$$

where D^r is the transposed matrix of D.

We note of course that, in case of the first Born approximation, we obtain

$$\mathrm{tg}\, \delta_l^B = x \frac{k}{8E_k(2l+1)(2\pi)^5} D^r \Delta(k, k) D .$$

2·3.1. First method: approximate kernel. – By analogy with a method used by LÉVY [19] and MARTIN [20] for meson-nucleon scattering, we replace the kernel $\Delta(p, p')$ by an approximate form:

$$\Delta(p, k) \Delta^{-1}(k, k) \Delta(k, p')$$

but, in our case, the validity of such a treatment is more difficult to justify. The substitution is an identity when p or p takes its initial value k. We assume that, in the integral (2.11), the most important contributions are due to the small transfers of moments.

The integral equation becomes an exacty soluble equation with the solution $A_1(p)$. Carrying out the transformation indicated above, we find:

$$A_1(p) = \frac{\delta(p-k)}{k^3} D + \frac{x}{p^2 - k^2} H(p) \Delta(p, k)[1 - x M(k)]^{-1} D ,$$

where $M(k)$ is the following integral:

$$\Delta(k, k) M(k) = \mathrm{P.V.} \int_0^\infty \frac{\Delta(k, p) H(p) \Delta(p, k)}{p^2 - k^2} p^3 \, \mathrm{d}p .$$

It is possible to define successive iterations $A_n(p)$ and consequently, a series of approximate phase shifts δ_n. But the calculations are very difficult

[19] M. M. LÉVY: *Phys. Rev.*, **98**, 1470 (1955).
[20] A. MARTIN: *Nuovo Cimento*, **4**, 369 (1956).

(multiple integrals) and we shall only consider the first iteration δ_2 as compared with the results given by a variational principle.

2˙3.2. Second method: variational principle. – Following KOHN [21] we formulate a variational principle for the integral equation (2.15). Calling now $\varphi(p)$ an infinite square matrix, we investigate the functional:

$$(2.17) \qquad J = \int_0^\infty A^T(p)\varphi(p)[(p^2 - k^2)A(p) - \alpha H(p)B(p)]p^3\,\mathrm{d}p\;.$$

Let us now first evaluate J for the correct wave function $A(p)$. Because of the presence of a δ function, the value of J is not zero. We find:

$$J = \alpha B^T(k)H(k)\varphi(k)D\;.$$

Next, we calculate the first variation of J; the variation of A may be written as:

$$\delta A(p) = \frac{\alpha}{p^2 - k^2}\,H(p)\,\delta B(p)$$

and we obtain:

$$\delta J = 2\alpha D^T\,\delta B(k)$$

with the particular choice of $\varphi(p)$:

$$\varphi(p)H(p) = H(p)\varphi(p) = 1\;.$$

The combination $J - 2\alpha D^T B(k)$ is related to δ_l:

$$(2.18) \qquad J - 2\alpha D^T B(k) = -\alpha D^T B(k) = -\frac{8E_k}{k}(2l+1)(2\pi)^5\,\mathrm{tg}\,\delta_l\;.$$

This equality provides a stationary expression for $\mathrm{tg}\,\delta$.

We use as trial function a linear combination of the type:

$$a(p) = \lambda\frac{\delta(p-k)}{k^3}D + \frac{\alpha}{p^2 - k^2}H(p)\sum_{i=1}^n \mu_i b_i(p)$$

[21] W. KOHN: *Phys. Rev.*, **84**, 495 (1951).

and perform the calculation of J. Eq. (2.18) becomes:

$$\lambda^2(\operatorname{tg} \delta_l - \operatorname{tg} \delta_l^B) - \frac{\alpha^2 k}{8 E_k (2l+1)(2\pi)^5} \cdot$$
$$\cdot D^T \Delta(k, k) \Big[2\lambda \sum_i \mu_i I_i(k) - \sum_{ij} \mu_i \mu_j (K_{ij} - \alpha L_{ij}) \Big] D = 0 \ ,$$

where I, K and L are various integrals involving the b_i functions. This equation is stationary with respect to variations of the parameters λ and μ_i. This condition leads to a system of $(n+1)$ homogeneous linear equations with $(n+1)$ variables. The determinant of the coefficient must vanish and we have the expression of $\operatorname{tg} \delta_l$.

With one parameter μ and the first Born approximation as trial function, we obtain

$$(2.19) \qquad \operatorname{tg} \delta_l = \operatorname{tg} \delta_l^B + \frac{\alpha^2 k}{8 E_k (2l+1)(2\pi)^5} \frac{\big(D^T \Delta(k, k) M(k) D\big)^2}{D^T \Delta(k, k) [M(k) - \alpha N(k)] D} \ ;$$

$M(k)$ and $N(k)$ are the integrals involved in the previous method for the first iteration. And it is natural to compare the results.

2·3.3. Comparison of the two methods. – If one develops the expressions of $\operatorname{tg} \delta$ in power series of the coupling constant α, the three first coefficients are identical:

$$\operatorname{tg} \delta_l \simeq \frac{k}{8 E_k (2l+1)(2\pi)^5} \big\{ \alpha D^T \Delta(k,k) D + \alpha^2 D^T \Delta(k, k) M(k) D + \alpha^3 D^T \Delta(k, k) N(k) D \big\}.$$

With more parameters for the variational principle (the successive trial functions are the different Born approximations) and more iterations for the approximate method, it is clear that the identification of higher power terms in the coupling constant α in the precedent expansion is realized. This infinite expansion is the Born series. Our two methods give an approximated and closed form for the rest of this series. The question of convergence will not be treated; it depends on the value of α and on the form of the interaction kernel.

2·4. *Scattering length in S-state.* – We shall now compare the numerical results of bothmethods by computing, in each case, the scattering length defined by

$$a = - \lim_{k \to 0} \frac{\operatorname{tg} \delta_0}{k} \ .$$

We choose the second order interaction (see Appendix VI):

$$N(\boldsymbol{p}, \boldsymbol{p}') = \frac{1}{(\boldsymbol{p}' - \boldsymbol{p})^2 + \mu^2 - i\varepsilon} \ ,$$

considering μ as a parameter. The zero energy implies that in the sums over q and q', the only contribution proceeds from the terms $q = q' = 0$. One then sees immediately that:

1) for the first Born approximation:

$$a^{(B)} = - \frac{\alpha}{\mu^2} \frac{\pi^3}{M} \, .$$

2) for the approximate method:

$$a^{(1)} = - \frac{\alpha}{\mu^2} \frac{\pi^3}{M} \frac{1}{1 - \alpha m} \, ,$$

m is a function of $\varrho = \mu/M$;

3) for the first iteration of this method:

$$a^{(2)} = - \frac{\alpha}{\mu^2} \frac{\pi^3}{M} \frac{1}{1 - \alpha m} \left[1 + \alpha^2 \frac{n - m^2}{1 - \alpha m} \right] \, .$$

4) for the variational principle:

$$a^{(v)} = - \frac{\alpha}{\mu^2} \frac{\pi^3}{M} \left[1 + \frac{\alpha m^2}{m - \alpha n} \right] \, .$$

The first problem is to classify the values of a for a given α. We obtain:

$$a^{(B)} < a^{(1)} < a^{(2)} < a^{(v)} \, .$$

The second problem is to determine the values of α reproducing the experimental value of neutron-proton scattering length [22] ($2.32 \cdot 10^{-13}$ cm). After numerical computations, we find:

$$\begin{cases} \alpha^{(B)}/\mu^2 = 3.54 & \alpha^{(1)}/\mu^2 = 0.402 \\ a^{(2)}/\mu^2 = 0.375 & 6a^{(v)}/\mu^2 = 0.357 \, . \end{cases}$$

We note that the two last results are of the same order of magnitude and it is interesting to compare them with the static approximation. If we neglect the motion of the nucleons while the mesons are in flight, we have a local

_____

[22] E. FERMI: _Nuclear Physics_, 242 (1950).

instantaneous interaction which leads to an ordinary Schrödinger equation with Yukawa potential. The corresponding value of $\alpha^{(s)}/\mu^2$ is 0.342.

In summary we can conclude:

1) The variational method, the first iteration and the static approximation are perfectly in agreement.

2) The approximate method and its iteration differ by 10%.

3. – Dirac particles.

The Bethe and Salpeter equation for spin $\frac{1}{2}$ particles involves the spinor wave function $\varphi(p)$. The free propagators are the S_F functions. Let us consider the pseudoscalar theory with pseudoscalar coupling, the kernel of interaction takes the form:

$$W(\mathbf{p}, \mathbf{p}') = \alpha(i\gamma_5^{(1)})(i\gamma_5^{(2)}) N(\mathbf{p}, \mathbf{p}') ,$$

where $N(\mathbf{p}, \mathbf{p}')$ is a scalar function.

With this notation, $\varphi(\mathbf{p})$ satisfies the integral equation:

$$(3.1) \qquad \varphi(\mathbf{p}) = \varphi_0(\mathbf{p}) + \alpha \frac{(-i\gamma^{(1)} \cdot p_1 + M)(-i\gamma^{(2)} \cdot p_2 + M)}{(p_1^2 + M^2 - i\varepsilon_1)(p_2^2 + M^2 - i\varepsilon_2)} \cdot$$
$$\cdot (i\gamma_5^{(1)})(i\gamma_5^{(2)}) \int \varphi(\mathbf{p}') N(\mathbf{p}, \mathbf{p}') \, \mathrm{d}\mathbf{p}' .$$

3˙1. *Scalar integral equation.* – The first problem is to consider the matrix properties of Φ and the mode of operation of the $\gamma^{(1)}$ and $\gamma^{(2)}$ matrices. If the rows Φ are numbered by the a index corresponding to the first particle and the columns by the b index corresponding to the second particle, the γ matrices operate as follows [23,24]:

$$(3.2) \qquad\qquad \gamma_\mu^{(a)}\Phi = \gamma_\mu\Phi , \qquad \gamma_\mu^{(b)}\Phi = \Phi\gamma_\mu^T ,$$

γ_μ is the usual Dirac matrix and γ_μ^T, its transpose. In order to simplify these relations, we introduce the charge conjugate matrix $\gamma_3\gamma_1$ which has the following properties:

$$\gamma_3\gamma_1\gamma_\mu^T = \gamma_\mu\gamma_3\gamma_1 .$$

If we define $\psi = \Phi\gamma_1\gamma_3$ or $\Phi = \psi\gamma_3\gamma_1$, Eq. (3.2) becomes

$$\gamma_\mu^{(a)}\psi = \gamma_\mu\psi , \qquad \gamma_\mu^{(b)}\psi = \psi\gamma_\mu$$

[23] J. S. GOLDSTEIN: *Phys. Rev.*, **91**, 1516 (1953).
[24] L. DE BROGLIE: *Théorie générale des particules à spin, Méthode de fusion* (Paris, 1943).

and it is seen that ψ satisfies:

(3.3) $\qquad \psi(\mathbf{p}) = \psi_0(\mathbf{p}) + \dfrac{\alpha}{(p^2 + M^2 + (P^2/4))^2 - p^2 P^2} \cdot$

$$\cdot \int N(\mathbf{p}, \, \mathbf{p'}) \{ (\gamma \mathbf{p}_1 + iM) \gamma_5 \psi(\mathbf{p'}) \gamma_5 (\gamma \mathbf{p}_2 + iM) \} \, \mathrm{d}\mathbf{p'} \,.$$

We shall begin by taking for ψ a reduced form:

$$\psi = \begin{array}{cc} \psi_{11} & \psi_{12} \\ \psi_{12} & \psi_{22} \end{array} \,.$$

The $\psi_{\alpha\beta}$ are 2×2 square matrices which are decomposed as follows:

(3.4) $\qquad \left\{ \begin{array}{l} \psi_{11} = S_1(\mathbf{p})I + \boldsymbol{\sigma} \cdot \boldsymbol{V}_1(\mathbf{p}) \qquad \psi_{22} = S_2(\mathbf{p})I + \boldsymbol{\sigma} \cdot \boldsymbol{V}_2(\mathbf{p}) \,, \\[2mm] \psi_{12} = \dfrac{B(\mathbf{p}) + C(\mathbf{p})}{2} I + \boldsymbol{\sigma} \cdot \dfrac{\boldsymbol{F}(\mathbf{p}) + \boldsymbol{G}(\mathbf{p})}{2} \\[2mm] \psi_{21} = \dfrac{B(\mathbf{p}) - C(\mathbf{p})}{2} I + \boldsymbol{\sigma} \cdot \dfrac{\boldsymbol{F}(\mathbf{p}) - \boldsymbol{G}(\mathbf{p})}{2} \,, \end{array} \right.$

where $\mathbf{p}$ is the unit-matrix and $\boldsymbol{\sigma}$, the three Pauli's matrices.

Inserting on both sides of Eq. (3.3) and writing $\mathbf{p} = (\boldsymbol{p}, p_4)$, we find a sistem of coupled integral equations for S_1, S_2, $\boldsymbol{V}_1$, $\boldsymbol{V}_2$, B, C, $\boldsymbol{F}$ and $\boldsymbol{G}$.

(3.5) $\qquad \left\{ \begin{array}{l} S_1(\mathbf{p}) = S_1^0(\mathbf{p}) + \dfrac{\alpha}{(p^2 - k^2)^2 + 4p_4^2 E_k^2} \displaystyle\int N(\mathbf{p}, \, \mathbf{p'}) \, \mathrm{d}\mathbf{p'} \cdot \\[2mm] \cdot \{ -|\boldsymbol{p}|^2 S_1(\mathbf{p'}) - [p_4^2 + (E_k + M)^2] S_2(\mathbf{p'}) + (E_k + M)\boldsymbol{p} \cdot \boldsymbol{F}(\mathbf{p'}) + ip_4 \boldsymbol{p} \cdot \boldsymbol{G}(\mathbf{p'}) \} \,, \\[4mm] \boldsymbol{V}_1(\mathbf{p}) = \boldsymbol{V}_1^0(\mathbf{p}) + \dfrac{\alpha}{(p^2 - k^2)^2 + 4p_4^2 E_k^2} \displaystyle\int N(\mathbf{p}, \mathbf{p'}) \, \mathrm{d}\mathbf{p'} \{ |\boldsymbol{p}|^2 \boldsymbol{V}_1(\mathbf{p'}) - 2\boldsymbol{p}[\boldsymbol{p} \cdot \boldsymbol{V}_1(\mathbf{p'})] + \\[2mm] \quad - [p_4^2 + (E_k + M^2)] \boldsymbol{V}_2(\mathbf{p'}) + (E_k + M)\boldsymbol{p} B(\mathbf{p'}) + \\[2mm] \quad + ip_4 \boldsymbol{p} C(\mathbf{p'}) + i(E_k + M) \boldsymbol{p} \times \boldsymbol{G}(\mathbf{p}) - p_4 \boldsymbol{p} \times \boldsymbol{F}(\mathbf{p'}) \} \,, \\[4mm] S_2(\mathbf{p}) = S_2^0(\mathbf{p}) + \dfrac{\alpha}{(p^2 - k^2)^2 + 4p_4^2 E_k^2} \displaystyle\int N(\mathbf{p}, \, \mathbf{p'}) \, \mathrm{d}\mathbf{p'} \cdot \\[2mm] \cdot \{ -[p_4^2 + (E_k - M)^2] S_1(\mathbf{p'}) - \boldsymbol{p}^2 S_2(\mathbf{p'}) + (E_k - M)\boldsymbol{p} \cdot \boldsymbol{F}(\mathbf{p'}) - ip_4 \boldsymbol{p} \cdot \boldsymbol{G}(\mathbf{p'}) \} \,, \\[4mm] \boldsymbol{V}_2(\mathbf{p}) = \boldsymbol{V}_2^0(\mathbf{p}) + \dfrac{\alpha}{(p^2 - k^2)^2 + 4p_4^2 E_k^2} \displaystyle\int N(\mathbf{p}, \, \mathbf{p'}) \, \mathrm{d}\mathbf{p'} \cdot \\[2mm] \cdot \{ -[p_4^2 + (E_k - M)^2] \boldsymbol{V}_1(\mathbf{p'}) + |\boldsymbol{p}|^2 \boldsymbol{V}_2(\mathbf{p'}) - 2\boldsymbol{p}[\boldsymbol{p} \cdot \boldsymbol{V}_2(\mathbf{p'})] + \\[2mm] \quad + (E_k - M)\boldsymbol{p} B(\mathbf{p'}) - ip_4 \boldsymbol{p} C(\mathbf{p'}) - i(E_k - M)\boldsymbol{p} \times \boldsymbol{G}(\mathbf{p'}) - p_4 \boldsymbol{p} \times \boldsymbol{F}(\mathbf{p'}) \} \,, \end{array} \right.$

$$B(\mathbf{p}) = B^0(\mathbf{p}) + \frac{\alpha}{(p^2 - k^2)^2 + 4p_4^2 E_k^2} \int N(\mathbf{p}, \mathbf{p}') \, d\mathbf{p}' \cdot$$
$$\cdot \left\{ (p^2 + k^2) B(\mathbf{p}') - 2i M p_4 C(\mathbf{p}') - (2E_k - M)\mathbf{p} \cdot \mathbf{V}_1(\mathbf{p}') - 2(E_k + M)\mathbf{p} \cdot \mathbf{V}_2(\mathbf{p}') \right\},$$

$$F(\mathbf{p}) = F^\cdot(\mathbf{p}) + \frac{\alpha}{(p^2 - k^2)^2 + 4p_4^2 E_k^2} \int N(\mathbf{p}, \mathbf{p}') \, d\mathbf{p}' \cdot$$
$$\cdot \left\{ [p_4^2 - |\boldsymbol{p}|^2 + k^2] F(\mathbf{p}') + 2\mathbf{p}[\mathbf{p} \cdot F(\mathbf{p}')] - 2i M p_4 G(\mathbf{p}') - \right.$$
$$\left. - 2(E_k - M)\mathbf{p} S_1(\mathbf{p}') - 2(E_k + M)\mathbf{p} S_2(\mathbf{p}') - 2p_4 \mathbf{p} \times \mathbf{V}_1(\mathbf{p}') + 2p_4 \mathbf{p} \times \mathbf{V}_2(\mathbf{p}') \right\},$$

(3.5)

$$C(\mathbf{p}) = C^0(\mathbf{p}) + \frac{\alpha}{(p^2 - k^2)^2 + 4p_4^2 E_k^2} \int N(\mathbf{p}, \mathbf{p}') \, d\mathbf{p}' \cdot$$
$$\cdot \left\{ 2i M p_4 B(\mathbf{p}) + [|\boldsymbol{p}|^2 - p_4^2 - k^2] C(\mathbf{p}') - 2i p_4 \mathbf{p} \cdot \mathbf{V}_1(\mathbf{p}') + 2i p_4 \mathbf{p} \cdot \mathbf{V}_2(\mathbf{p}') \right\}.$$

$$G(\mathbf{p}) = G^\cdot(\mathbf{p}) + \frac{\alpha}{(p^2 - k^2)^2 + 4p_4^2 E_k^2} \int N(\mathbf{p}, \mathbf{p}') \, d\mathbf{p}' \cdot$$
$$\cdot \left\{ -(p^2 + k^4)G(\mathbf{p}') + 2\mathbf{p}[\mathbf{p} \cdot G(\mathbf{p}')] + 2i M p_4 F(\mathbf{p}) - 2i p_4 \mathbf{p} S_1(\mathbf{p}') + \right.$$
$$\left. + 2i p_4 \mathbf{p} S_2(\mathbf{p}') - 2i(E_k - M)\mathbf{p} \times \mathbf{V}_1(\mathbf{p}') + 2i(E_k + M)\mathbf{p} \times \mathbf{V}_2(\mathbf{p}') \right\}.$$

The incident part of the wave function Φ is the product of two spinors describing the spin states of the two free particles as solutions of the Dirac equation.

In order to simplify Eq. (3.5), we attempt to perform the integration over angular variables.

3·2. *Integration over angular variables.* – Let us expand the scalar functions, as $S(\mathbf{p})$, in hyperspherical harmonics and the vector functions, as $V(\mathbf{p})$, in vector hyperspherical harmonics (see Appendix VII):

(3.6)

$$S(\mathbf{p}) = \sum_{n=0}^{\infty} \sum_{J=0}^{n} \sum_{m=-J}^{m=+J} S(p; J, m, n) \mathcal{Y}_{Jn}^m(\Omega_p),$$

$$V(\mathbf{p}) = \sum_{n=0}^{\infty} \sum_{L=0}^{n} \sum_{J=L-1}^{J=L+1} \sum_{m=-J}^{m=+J} V(p; J, L, m, n) \mathbf{Y}_{JL1}^{mn}(\Omega_p).$$

The orthonormalization of the hyperspherical harmonics allows an immediate integration over the two angles θ_p and φ_p. We find again that the total angular momentum J and its component over the z-axis, m, are good quantum numbers.

For the sixteen components of ψ, it is useful to consider a row-matrix $A(p; J, m, n)$ with the respective elements: $S_1(p; J, m, n)$; $S_2(p; J, m, n)$;

$F(p; J, J+1, m, n);$ $F(p; J, J{-}1, m, n);$ $V_1(p; J, J, m, n);$ $V_2(p; J, J, m, n);$,
$G(p; J, J+1, m, n);$ $G(p; J, J{-}1, m, n);$ $V_1(p; J, J+1, m, n);$ $V_1(p; J, J{-}1, m, n$
$V_2(p; J, J+1, m, n);$ $V_2(p; J, J{-}1, m, n);$ $B(p; J, m, n);$ $G(p; J, J, m, n);$
$C(p; J, m, n);$ $F(p; J, J, m, n).$

The matrix $A(p)$ satisfies a matricial integral equation:

$$(3.7) \qquad A(p; J, m, n) = A^0(p; J, m, n) + \frac{\alpha}{p^2 - k^2} \cdot$$

$$\cdot \sum_{n=0}^{\infty} K(p; J, n, n') \int_0^{\infty} \Delta_{n'}(p, p') A(p'; J, m, n') p'^3 \, dp' .$$

The 16×16 matrices $K(p; J, n, n')$ are directly related to the integration over the β angle:

$$\frac{K_{\lambda \mu}(p; J, n, n')}{p^2 - k^2} = \int_0^{\pi} \frac{\mathcal{C}_L^n(\beta) R_{\lambda\mu}(p; \beta, J) \mathcal{C}_{L'}^{n'}(\beta)}{(p^2 + M^2 + (P^2/4))^2 - p^2 P^2 \cos^2\beta} \sin^2\beta \, d\beta .$$

The values of L and L' respectively depend on λ and μ. For $\lambda = 3, 7, 9, 11$, we have $L = J+1$; for $\lambda = 4, 8, 10, 12$, we have $L = J-1$; for the other values, $L = J$. The matrix $R(p; \beta, J)$ is the result of trivial integrations over θ and φ; it possesses various symmetries which are recapitulated in the following table of its non-vanishing elements.

$$R_{11} = -p^2 \sin^2\beta , \quad R_{12} = -[p^2 \cos^2\beta + (E_k + M^2)], \quad R_{13} = p(E_k + M) \sin\beta \sqrt{\frac{J+1}{2J+1}} ,$$

$$R_{14} = p(E_k + M) \sin\beta \sqrt{\frac{J}{2J+1}} ,$$

$$R_{17} = ip^2 \sin\beta \cos\beta \sqrt{\frac{J+1}{2J+1}} , \qquad R_{18} = ip^2 \sin\beta \cos\beta \sqrt{\frac{J}{2J+1}} ,$$

$$R_{21} = -[p^2 \cos^2\beta + (E_k - M)^2], \quad R_{22} = R_{11} , \quad R_{23} = \frac{E_k - M}{E_k + M} R_{13} , \quad R_{24} = \frac{E_k - M}{E_k - M} R_1 ,$$

$$R_{27} = -R_{17} , \qquad R_{28} = -R_{18} ,$$

$$R_{31} = -2R_{23} , \qquad R_{32} = -2R_{13} ,$$

$$R_{33} = k^2 + \frac{p^2}{2J+1} (1 + 2J \cos^2\beta) , \quad R_{34} = \frac{2p^2 \sin^2\beta}{2J+1} \sqrt{J(J+1)} ,$$

$$R_{35} = -2R_{18} , \qquad R_{36} = -2R_{18} , \qquad R_{37} = -2ipM \cos\beta ,$$

$$R_{41} = -2R_{24}, R_{42} = -2R_{14}, \quad R_{43} = R_{34}, \quad R_{44} = k^2 - \frac{p^2}{2J+1}\left(1 - 2(J+1)\cos^2\beta\right),$$

$$R_{45} = 2R_{17} = R_{46}, \qquad R_{48} = R_{37},$$

$$R_{53} = R_{18}, \quad R_{54} = -R_{17}, \quad R_{55} = R_{11}, \quad R_{56} = R_{.2}, \quad R_{57} = R_{14}, \quad R_{58} = R_{13}$$

$$R_{63} = R_{18}, \quad R_{64} = -R_{17}, \quad R_{65} = R_{21}, \quad R_{66} = -R_{11}, \quad R_{67} = -R_{24}, \quad R_{68} = R_{23},$$

$$R_{71} = -2R_{17}, \quad R_{72} = 2R_{17}, \quad R_{73} = -R_{37}, \quad R_{75} = -2R_{23}, \quad R_{76} = 2R_{13},$$

$$R_{77} = -k^2 + \frac{p^2}{2J+1}\left(1 - 2(J+1)\cos^2\beta\right), \qquad R_{78} = R_{34},$$

$$R_{81} = -2R_{18}, \quad R_{82} = 2R_{18}, \quad R_{84} = -R_{37}, \quad R_{85} = -2R_{24}, \quad R_{86} = 2R_{14}, \quad R_{87} = R_{34}$$

$$R_{88} = -k^2 - \frac{p^2}{2J+1}\left(1 + 2J\cos^2\beta\right),$$

$$R_{99} = -p^2\frac{\sin^2\beta}{2J+1}, \qquad R_{910} = -2p^2\sin^2\beta\frac{\sqrt{J(J+1)}}{2J+1},$$

$$R_{911} = -[p^2\cos^2\beta + (E_k + M)^2],$$

$$R_{913} = p(E_k + M\sin\beta)\sqrt{\frac{J+1}{2J+1}},$$

$$R_{9\,14} = p(E_k + M)\sin\beta\sqrt{\frac{J}{2J+1}}, \qquad R_{915} = ip^2\sin\beta\cos\beta\sqrt{\frac{J+1}{2J+1}},$$

$$R_{913} = ip^2\sin\beta\cos\beta\sqrt{\frac{J}{2J+1}},$$

$$R_{10\,9} = R_{9\,10}, \quad R_{10\,10} = -R_{99}, \quad R_{10\,12} = R_{9\,11}, \quad R_{10\,13} = R_{9\,14}, \quad R_{10\,14} = -R_{9\,13},$$

$$R_{10\,15} = R_{9\,16}, \qquad R_{10\,16} = -\Gamma_{9\,15},$$

$$R_{11\,9} = -[p^2\cos^2\beta + (E_k - M)^2], \qquad R_{1111} = R_{99},$$

$$R_{1112} = R_{910}, \qquad R_{1113} = \frac{E_k - M}{E_k + M}R_{913},$$

$$R_{1114} = -\frac{E_k - M}{E_k + M}R_{914}, \quad R_{1115} = -R_{915}, \quad R_{1113} = -R_{913},$$

$R_{12\ 10} - R_{11\ 9}, \quad R_{12\ 11} = R_{9\ 10}, \quad R_{12\ 12} = - R_{99}, \quad R_{12\ 13} = - R_{11\ 14}, \quad R_{12\ 14} = R_{11\ 9}.$

$R_{12\ 15} = - R_{9\ 16}, \quad R_{12\ 16} = - R_{9\ 15},$

$R_{13\ 9} = - 2R_{11\ 13}, \quad R_{13\ 10} = 2R_{11\ 14}, \quad R_{13\ 11} = - 2R_{9\ 13}, \quad R_{13\ 12} = - R2_{9\ 14},$

$R_{13\ 13} = p^2 + k^2, \quad R_{13\ 15} = - 2ip\, M \cos \beta,$

$R_{14\ 9} = 2R_{11\ 14}, \quad R_{14\ 10} = 2R_{11\ 13}, \quad R_{14\ 11} = 2R_{9\ 14}, \quad R_{14\ 12} = - 2R_{9\ 13},$

$R_{14\ 14} \quad - R_{13\ 13}, \quad R_{14\ 15} = - R_{13\ 15},$

$R_{15\ 9} = - 2R_{9\ 15}, \quad R_{15\ 10} = - 2R_{9\ 16}, \quad R_{15\ 11} = 2R_{9\ 15}, \quad R_{15\ 12} = 2R_{9\ 16},$

$R_{15\ 13} = - R_{13\ 15}, \quad R_{15\ 15} = - p^2 \cos 2\beta - k^2,$

$R_{16\ 9} = 2R_{9\ 16}, \quad R_{16\ 10} = - 2R_{9\ 15}, \quad R_{16\ 11} = - 2R_{9\ 16}, \quad R_{16\ 12} = 2R_{9\ 15},$

$R_{16\ 14} = R_{13\ 15}, \quad R_{16\ 16} = - R_{15\ 15}.$

Upon examining this table, it is immediately seen that the matrix K possesses a particular form:

$$K = \begin{array}{cc} K^+ & 0 \\ 0 & K^- \end{array},$$

where K^+ and K^- are now 8×8 matrices. This expresses the existence of two independent systems of coupled equations corresponding to the parities $(-1)^J$ for K^+ and $(-1)^{J+1}$ for K^-.

If we use the same methods as in the previous section (Klein-Gordon particles), we can easily show that the matrix K^+ is also completely reducible:

$$K^+ = \begin{array}{cc} K_s^+ & 0 \\ 0 & K_t^+ \end{array},$$

where K_s^+ and K_t^+ are 4×4 matrices.

To summarize, we have found three disconnected systems of integral equations. The first one, with four components S_1, S_2, $F(J, J+1)$, $F(J, J-1)$, describes the « singlet states »; the second one, with four components $V_1(J, J)$, $V_2(J, J)$, $G(J, J+1)$, $G(J, J-1)$, the « triplet states » of parity $(-1)^J$ $(L = J$ and $m = \pm 1)$; finally, the third set, with eight components, corresponds to the other « triplet states » of parity $(-1)^{J+1}$ $(L = J \pm 1$ and $m = 0, \pm 1)$.

3·3. *Singlet and triplet states.* – The program of computations is the same as for spinless particles. The poles $p = \pm k$ appear when integrating over the β angle and we obtain again an integral equation with its singularity at the point $p = k$, formally equivalent to a Schrödinger equation written in momentum space.

By means of a Fourier transformation, one can return to configuration space. The asymptotic behaviour of the wave function $A(r)$ in this space permits to define quantities independent of n analogous to phase-shifts.

If one first considers the « singlet states », it may be pointed out that the four pseudo-phase-shifts are identical and, after summation of the partial waves over n, one finds that the phase-shift corresponds to a given value of the total angular momentum J ($m = 0$ for the « singlet state »). Furthermore, it is interesting to write the scattering amplitude with a reduced form for the matrices:

$$(3.9) \qquad f_s^+(J) = \begin{vmatrix} \dfrac{E_k + M}{2E_k}\, \mathrm{I} & \dfrac{k}{2E_k}\, \boldsymbol{\sigma}\cdot\boldsymbol{e}_r \\[2mm] \dfrac{k}{2E_k}\, \boldsymbol{\sigma}\cdot\boldsymbol{e}_r & \dfrac{E_k - M}{2E_k}\, \mathrm{I} \end{vmatrix} \frac{[4\pi(2J+1)]^{\frac{1}{2}}}{k} \exp\left[i\delta_J\right] \sin\delta_J\, Y_J^0(\theta)\,,$$

where $\boldsymbol{e}_r$ is a unit vector and δ_J the J phase-shift.

In order to obtain the singlet differential cross-section, we perform the sum over J, as usual, and it is necessary to take the trace of the matrix product:

$$\frac{\mathrm{d}\sigma}{\mathrm{d}\Omega} = \mathrm{Tr}\left[\sum_J f_J\right]^* \left[\sum_J f_J\right].$$

Inserting the above expression of f_J, we find again the well-known result [25]

$$\frac{\mathrm{d}\sigma_s}{\mathrm{d}\Omega} = \frac{4\pi}{k^2}\,\Big|\sum_J (2J+1)^{\frac{1}{2}} \exp\left[i\delta_J\right] \sin\delta_J\, Y_J^0(\theta)\Big|^2\,.$$

The second set of four equations describing the triplet states of parity $(-1)^J$ is entirely similar. We shall only write the scattering amplitude:

$$f_t^+(J, m) = \begin{vmatrix} \dfrac{E_k + M}{2E_k}\, \mathrm{I} & \dfrac{k}{2E_k}\, \boldsymbol{\sigma}\cdot\boldsymbol{e}. \\[2mm] -\dfrac{k}{2E_k}\, \boldsymbol{\sigma}\cdot\boldsymbol{e}_r & -\dfrac{(E_k - M)}{2E_k}\, \mathrm{I} \end{vmatrix} \frac{[2\pi(2J+1)]^{\frac{1}{2}}}{k} \exp\left[i\delta_{JJ}\right] \sin\delta_{JJ}\, \boldsymbol{\sigma}\cdot Y_{JJ1}^m,$$

the phase-shift δ_{JJ} is the same for the four equations.

---

[25] N. F. MOTT and H. S. V. MASSEY: *Theory of Atomic Collisions.*

The last system is more complicated because the orbital angular momentum L is not a good quantum number and we have a mixture of the waves corresponding to $L = J \pm 1$. The treatment is identical for the two cases: $m = 0$ and $m = \pm 1$; we have, each time, five coupled radial equations which call up five pseudo-phase shifts connected by three relations (two of these relations involve Clebsch-Gordan coefficients ([26])). They are of course not the physical phase-shifts; one can nevertheless easily deduce the scattering amplitudes and the differential cross-sections from these quantities.

The coupled integral equations are solved with the approximate method described in Sect. 2. We generalize the matrix formulation with two series of indices: the first one, infinite, corresponding to the values of q and q'; the second one, finite, with the number of components of each system. The method of calculation is at all points identical; the products of matrices involve summations over two indices instead of one only.

3˙4. *Scattering length and phase-shift in the singlet S-state.* – We can compute entirely analytically the scattering length in the S state with the approximate method without iteration. The infinite summations reduce again to the terms $q = q' = 0$; but we consider the four components of the wave function.

By inversion of the matrix $[1 - \alpha M(k)]$ (see Sect. 2), we obtain a scattering length proportional to an expression of the following form:

$$X_{11} = \frac{\alpha m_{21}(1 - \alpha m_3)}{d(\alpha)} ,$$

where $d(\alpha)$ is a third degree polynomial in α. The m_{ij} are the matrix elements of M for $k = 0$ and $q = q' = 0$; they are functions of $\varrho = \mu/M$. If we adopt a phenomenological point of view, we can consider ϱ as a parameter; we then perform the calculations for thee values of ϱ: 0.1, 0.15 and 0.2, the intermediate value corresponding for μ to the π-meson mass. The $d(\alpha)$ function has a zero in the neighbourhood of $\alpha = 0.18$:

$\varrho = 0.1$	$\varrho = 0.15$	$\varrho = 0.2$
$\alpha_c = 0.193$	$\alpha_c = 0.175$	$\alpha_c = 0.178$.

These results show that the critical value for α is practically independent of the value of ϱ. We now try to find a coupling constant α_s that reproduces

([26]) J. M. Blatt and V. F. Weisskopf: *Theor. Nucl. Phys.* (1952).

the correct experimental value of the neutron-proton scattering length ([23]) $(2.32 \cdot 10^{-13}$ cm). We obtain:

$$\begin{array}{ccc}
\varrho = 0.1 & \varrho = 0.15 & \varrho = 0.2 \\
\alpha_s = 0.161 & \alpha_s = 0.164 & \alpha_s = 0.168\,.
\end{array}$$

and the ordinary coupling constant $g^2/4\pi$ is about 20. It is half the value calculated with the static approximation ([5]) ($\simeq 42$). The present situation is entirely different from the Klein-Gordon particle one, where the various coupling constants are of the same order of magnitude. If one remembers that the static approximation does not take into account all components of the wave function ([5]), whereas our treatment includes the intermediate states, one can explain this disagreement.

With this value of α_s (we recall that α is the only parameter of the problem), we have studied the ^1S phase-shift for three values of the energy. Using the I.B.M. 650 to resolve the coupled integral equations, we were obliged to make some approximations: the infinite summations over q are reduced to the first term $q = 0$; this treatment is rigorous at zero-energy, but it does not remain valid at high energy. Newt we use the approximate method and we can evaluate the difference with the first iteration by a factor of 10%. Nevertheless, we can obtain good qualitative results.

The calculations are performed for the following values of the energy (expressed in the laboratory system):

1) $k/M = 10^{-3}$ in order to verify the programs of calculations, we adjust the slope at $k = 0$ of the curve $\delta(k)$.

2) $k/M = 0.08$ or $E = 6$ MeV. At this energy, it is allowed to apply the shape independent approximation and to determine the effective range r_0. The phase-shift is 60° and we obtain:

$$r_0 = 2.43 \cdot 10^{-13} \text{ cm}\,.$$

The experimental value is $(2.5 \pm 0.25) \cdot 10^{-13}$ cm ([27]); we can conclude that this treatment is valid in the range of low energies.

3) $k/M = 0.3$ or $E = 82$ MeV: the calculated phase-shift is 54°.

4) $k/M = 0.43$ or $E = 165$ MeV: the calculated phase-shift is $-27°$.

([27]) H. A. BETHE and P. MORRISON: *Elementary Nuclear Theory*, 2nd edition (New York, 1956).

The evident conclusion is the existence of a zero for the $\delta(k)$ function in the energy region of 140 MeV. For high energies, we are able to explain the experimental results. The phase-shift analysis of nucleon-nucleon experiments ([6.28,29]) points out that the sign of the S phase-shift will change from positive to negative in this energy region. We find that this change and Lévy's conclusions on the existence of a short range strongly repulsive potential, so-called «hard core», are corroborated ([5]).
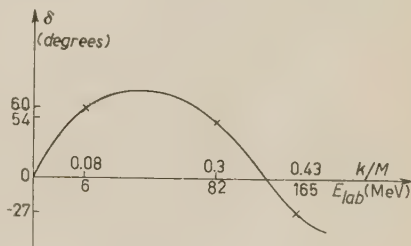
Fig. 3. – ^1S phase-shift.

4. – Conclusion.

The analytic continuation of the wave function permits to extend the method of partial waves to a covariant problem. The definition of quantities, which are analogous to phase-shifts—in some particular cases, they are the physical phase-shifts corresponding to a fixed value of the angular momentum—allows to give explicitly the expression of the nucleon-nucleon differential cross-section.

Nevertheless, to solve our systems of coupled integral equations, we were obliged to make some approximations and it is not possible to determine their domain of validity with certainty. The kernel of the integral equations—directly deduced from the knowledge of the interaction between the particles—is replaced by an approximated kernel that enables an analytical resolution by means of quadratures.

All the formalism has been introduced with an arbitrary interaction which satisfies certain general covariance conditions only. As a matter of fact, we have adopted a phenomenological point of view and our model can be treated with any physically reasonable kernel formulated in a covariant way. For numerical computations such as the singlet ^1S phase-shift and the neutron-proton singlet scattering length, we chose the $\Delta_F(x)$ function which represents the second order interaction as it is directly deduced from the mesic theory of nuclear forces. We have shown that a good agreement can be obtained with the experimental results if the coupling constant $g^2/4\pi$ is of the order of 20. In particular, the ^1S phase-shift involves a change of sign around 140 MeV.

([28]) C. KLEIN: *Nuovo Cimento*, **2**, 38 (1955).

([29]) O. CHAMBERLAIN, E. SEGRÉ, R. D. TRIPP, C. WEEGAND and T. YPSILANTIS: *Phys. Rev.*, **105**, 288 (1957).

This particularity, which is necessary to explain correctly the proton-proton scattering experiments, lead JASTROW a few years ago, to assume the existence of an infinitely repulsive potential acting at short distance only. LÉVY's investigations enabled him to estimate the order of magnitude of the radius of such a « hard core ». Our results confirm the fact that the relativistic matrix elements are equivalent to a source function and that the corrections which we have brought in the S state only corroborate the existence of a hard core.

The numerical computations have also required some approximations. The series have been reduced to their first term and it was impossible to study the convergence of the approximate method by comparing the various iterations. We think however that our results cannot be appreciably modified by these different corrections. Moreover, in order to obtain a more general treatment, we must consider the fourth order interaction terms—in particular, the two pair terms—and we do not know their real magnitude. The results obtained for the ^1S phase-shift incite to extend such developments.

More detailed analysis and computations will be given later (*).

* * *

In am indebted to Professor M.M. LÉVY for many informative and helpful discussions on this subject.

———

(*) M. GOURDIN: Thesis (1957) to be published in the *Ann. Phys.*

APPENDIX I.

The hyperspherical harmonics $\mathcal{Y}_{ln}^m(\beta, \theta, \varphi)$ are the generalization, to four dimensions, of the well known spherical harmonics Y_l^m:

$$\mathcal{Y}_{ln}^m(\beta, \theta, \varphi) = Y_l^m(\theta, \varphi)\mathcal{C}_l^n(\beta) .$$

The function $\mathcal{C}_l^n(\beta)$ is related to the Gegenbauer polynomials of $\cos\beta$ as following [17]

$$\mathcal{C}_l^n(\beta) = \left\{ \frac{2^{l+1}}{\pi} \frac{(n+1)(n-l)![l!]^2}{(n+l+1)!+} \right\}^{\frac{1}{2}} \sin^l\beta\, C_{n-l}^{1+l}(\cos\beta) .$$

The hyperspherical harmonics are orthonormalized on the four dimensional sphere and verify the addition theorem [17]

$$C_n^1(\cos X) = \frac{2\pi^2}{n+1} \sum_{l=0}^{l=n} \sum_{m=-l}^{m=+l} \mathcal{Y}_{ln}^{m*}(\beta\theta, \varphi)\, \mathcal{Y}_{ln}^m(\beta', \theta', \varphi') ,$$

X is the angle between the two unitary four-vectors $\beta\theta\varphi$ and $\beta'\theta'\varphi'$.

APPENDIX II.

The plane wave $\exp[i\mathbf{p}\cdot\mathbf{r}]$ can be expanded in Gegenbauer polynomials of the angle between $\mathbf{p}$ and $\mathbf{r}$ [17]. With the addition theorem we obtain:

$$\exp[i\mathbf{p}\cdot\mathbf{r}] = (2\pi)^2 \sum_{l,m,n} i^n \frac{J_{n+1}(pr)}{pr} \mathcal{Y}_{ln}^{m*}(\Omega) \mathcal{Y}_{ln}^{m}(\Omega_r).$$

With a Fourier transformation, we can easily obtain the expansion of the Dirac $\delta_4(\mathbf{p} - \mathbf{k})$ function in hyperspherical harmonics of the angles of $\mathbf{p}$ and $\mathbf{k}$:

$$\delta_4(\mathbf{p} - \mathbf{k}) = \frac{\delta(p-k)}{k^3} \sum_{lmn} \mathcal{Y}_{lm}^{n*}(\Omega_k) \mathcal{Y}_{lm}^{n}(\Omega_r).$$

APPENDIX III.

We define the Fourier transformation by the two non-symmetrical relations:

$$\begin{cases} \varphi(\mathbf{r}) = \dfrac{1}{(2\pi)^4} \displaystyle\int \exp[i\,\mathbf{p}\cdot\mathbf{r}]\varphi(\mathbf{p})\,\mathrm{d}\mathbf{p}, \\[3mm] \varphi(\mathbf{p}) = \displaystyle\int \exp[-i\,\mathbf{p}\cdot\mathbf{r}]\varphi(\mathbf{r})\,\mathrm{d}\mathbf{r}, \end{cases}$$

We can expand $\varphi(\mathbf{p})$ and $\varphi(\mathbf{r})$ in hyperspherical harmonics of the angles of $\mathbf{p}$ and $\mathbf{r}$ respectively. The relations between the radial functions in the two developments are obtained by using the form $\exp[i\mathbf{p}\cdot\mathbf{r}]$ written in the Appendix II. We finally have:

$$\begin{cases} A(r; l, m, n) = \dfrac{i^n}{(2\pi)^2} \displaystyle\int_0^\infty A(p; l, m, n) \frac{J_{n+1}(pr)}{pr} p^3\,\mathrm{d}p, \\[3mm] A(p; l, m, n) = (-i)^n (2\pi^2) \displaystyle\int_0^\infty A(r; l, m, n) \frac{J_{n+1}(pr)}{pr} r^3\,\mathrm{d}r. \end{cases}$$

APPENDIX IV.

We shall now consider the asymptotic value of the integral:

$$I_n(r) = \text{P.V.} \int_0^\infty \frac{p^3}{p^2 - k^2} \frac{J_n(pr)}{pr}\,\mathrm{d}p.$$

With the integral representation of the Bessel function $J_n(pr)$ (17):

$$J_n(pr) = \frac{1}{\pi} \int_0^\pi \cos\left[pr \sin\beta - n\beta\right] d\beta ,$$

we obtain, for the asymptotic value (3'):

$$I_n(r) \simeq -\frac{k}{2r} \int_0^\pi \sin(kr \sin\beta - n\beta) d\beta + 0\left(\frac{1}{r^2}\right).$$

The irregular Bessel function $N_n(pr)$ possesses an integral representation of this form and we finally obtain:

$$\text{P.V.} \int_0^\infty \frac{p^3}{p^2 - k^2} \frac{J_n(pr)}{pr} dp = -\frac{\pi k^2}{2} \frac{N_n(kr)}{kr} + 0\left(\frac{1}{r^2}\right).$$

In a similar way we can perform an identical integral with spherical Bessel functions:

$$\text{P.V.} \int_0^\infty \frac{p^3}{p^2 - k^2} j_l(pR) dp = -\pi \frac{k^2}{2} n_l(kR) + 0\left(\frac{1}{R^2}\right).$$

APPENDIX V.

In order to calculate the sum:

$$S = \sum_{q=0}^\infty (-1)^q \, \mathcal{C}^{l+2q}\left(\frac{\pi}{2}\right) \frac{J_{l+2q+1}(pr)}{pr} \, \mathcal{C}_l^{l+2q}(\beta) ,$$

we consider the plane wave $\exp[i\mathbf{k}\cdot\mathbf{r}]$ in two expansions. The first one, carried out in the Appendix II, in hyperspherical harmonics of the angles of $\mathbf{k}$ and $\mathbf{r}$:

$$\exp i[\mathbf{k}\cdot\mathbf{r}] - (2\pi)^2 \sum_{l=0}^\infty \sum_{q=0}^\infty i^l (-1)^q \frac{J_{l+2q+1}(kr)}{kr} \left(\frac{2l+1}{4\pi}\right)^{\frac{1}{2}} \mathcal{C}_l^{l+2q}\left(\frac{\pi}{2}\right) \mathcal{Y}_{l\,l+2q}^0(\Omega) .$$

(30) ERDÉLYI: *Tables of Integral Transforms* (New York, 1954).

The second one in ordinary spherical harmonics:

$$\exp\left[i\,\mathbf{k}\cdot\mathbf{r}\right] = 4\pi \sum_{l=0} i^l j_l(kR) \left(\frac{2l+1}{4\pi}\right)^{\frac{1}{2}} Y_l^0(\cos\theta) ,$$

by using

$$\mathbf{k}\cdot\mathbf{r} = kr\sin\beta_r \cos\theta_r = kR\cos\theta .$$

If we identity the terms of same angular momentum, we obtain the infinite sum S:

$$S = \frac{1}{\pi} j_l(pr\sin\beta_r) ,$$

that generalizes the Angel-Jacobi formula ([17]).

APPENDIX VI.

In the case of the « ladder approximation », the kernel $\Delta_n(p, p')$ of the integral equation is given by

$$\Delta_n(p, p) = \frac{4\pi}{n+1} \int_0^\pi \frac{C_n^l(\cos\Theta)\sin\Theta\,\mathrm{d}\Theta}{p^2 + p'^2 + \mu^2 - 2pp'\cos\Theta} .$$

The Gegenbauer polynomials C_n^l are simple trigonometric functions and we make use of the Poisson formula as in Sect. **2**.
By putting

$$S(p, p') = [(p+p')^2 + \mu^2]^{\frac{1}{2}} , \qquad D(p, p') = [(p-p')^2 + \mu^2]^{\frac{1}{2}}$$

we obtain

$$\Delta_n(p, p') = \frac{2\pi^2}{n+1} \left(\frac{2}{S+D}\right)^2 \left(\frac{S-D}{S+D}\right)^n .$$

APPENDIX VII.

The vector hyperspherical harmonics are defined from the hyperspherical harmonics by the relation ([26]):

$$\mathbf{Y}_{JL1}^{mn}(\theta, \varphi, \beta) = \sum_{\mu=-1}^{\mu=+1} C_{L1}(Jm;\ m-\mu, \mu)\mathcal{Y}_{Ln}^{m-\mu} \chi_\mu ,$$

where the $C_{L1}(Jm; m - \mu, \mu)$ are the Clebsch Gordan coefficients and the χ_μ the spin vectors in the triplet state. They are orthonormalized:

$$\int \mathbf{Y}_{JL1}^{mn*} \cdot \mathbf{Y}_{J'L'1}^{m'n'} \, \mathrm{d}\Omega = \delta_{JJ'} \cdot \delta_{LL'} \cdot \delta_{mm'} \cdot \delta_{nn'} \, .$$

RIASSUNTO (*)

Non è possibile spiegare le esperienze di scattering e polarizzazione nucleone-nucleone con un potenziale locale semplice. Questo metodo dà buoni risultati nel campo delle basse energie. Ma è ben noto che, tra 0 e 300 MeV, per esempio, l'equazione di Schrödinger fallisce. È necessario, alle alte energie, di usare per sistemi di due corpi una formulazione completamente covariante — l'equazione di Bethe e Salpeter — per tener conto delle correzioni relativistiche. Con la continuazione analitica dell'ampiezza di scattering per i valori immaginari del tempo relativo (o dell'energia relativa) si può generalizzare il metodo delle onde parziali facendone un problema euclideo a quattro dimensioni. Si dimostra che nel caso semplificato di particelle prive di spin (particelle di Klein-Gordon) è facile ottenere gli spostamenti di fase fisici corrispondenti a un dato valore del momento angolare orbitale. Per il caso più realistico di particelle dotate di spin $\frac{1}{2}$ (particelle di Dirac) è possibile calcolare la sezione d'urto differenziale. Si ottengono soluzioni esplicite con un metodo approssimato di risoluzione delle equazioni integrali. Inoltre, nel caso dell'« approssimazione a gradini » si può determinare il valore della costante d'accoppiamento che dà la lunghezza di scattering sperimentale esatta per l'urto neutrone-protone singoletto. Lo spostamento di fase ^1S calcolato per differenti valori dell'energia cambia di segno nella regione energetica di 140 MeV. Questo risultato s'accorda con l'esperienza e la teoria dell'« hard core » di Lévy.

Dispersione della velocità di propagazione di ultrasuoni in acido propionico.

A. BARONE e G. PISENT

Istituto Nazionale di Ultracustica « O. M. Corbino » - Roma

D. SETTE

Istituto Nazionale di Ultracustica « O. M. Corbino » - Roma
Fondazione Bordoni - Istituto Superiore Poste e Telecomunicazioni - Roma

Riassunto. — Si riportano i risultati di alcune misure della dispersione della velocità di propagazione di ultrasuoni in acido propionico fra 2 e 6 MHz, nel campo di temperatura compreso fra 15 e 30 °C. Essi sono in accordo con le previsioni teoriche basate sui dati dell'assorbimento.

1. - Introduzione.

L'acido propionico è stato oggetto di una ricerca da parte di J. LAMB e H. HUDDART (¹). Tali Autori hanno studiato il comportamento del coefficiente di assorbimento ultrasonoro fra 8 e 51 °C nel campo di frequenze 1 ∶ 15 MHz. Il valore sperimentale del coefficiente di assorbimento (α) supera quello classico dovuto alla viscosità ed alla conducibilità termica e l'eccesso va con sicurezza attribuito ad un fenomeno di rilassamento nel liquido.

Come è noto, fenomeni di rilassamento si presentano durante la propagazione di onde elastiche in un sistema quando nel suo interno esista qualche equilibrio che possa essere turbato dalle variazioni di temperatura e di pres-

---

(¹) J. LAMB and H. HUDDART: *Trans. Faraday Soc.*, **46**, 540 (1950).

sione che accompagnano le onde e quando il sistema perturbato richieda un
tempo finito (di rilassamento, τ) per raggiungere nuove condizioni di equi-
librio. L'esistenza di un fenomeno di rilassamento conduce ad un assorbimento
addizionale e ad una dispersione della velocità di propagazione. Più precisa-
mente questo assorbimento, causato dal ritardo con il quale le condizioni del
sistema seguono le variazioni della pressione e della temperatura, dipende dalla
frequenza (f) ed è tale che il coefficiente di assorbimento per lunghezza d'onda
($\mu = \alpha\lambda$) presenta un massimo per un periodo dell'onda pari al tempo di rilas-
samento.

Le curve sperimentali trovate da LAMB e HUDDART in acido propionico
per μ a diverse temperature, presentano un massimo (μ_m) e sono in accordo
con quelle teoriche per un fenomeno di rilassamento; esse mostrano che l'acido
propionico è uno dei pochi liquidi per i quali le frequenze dei fenomeni di
rilassamento sono comprese nel campo di misura $1 \div 15$ MHz.

Una indagine accurata del sistema in esame sembra indicare che l'equi-
librio in questione è quello fra le forme monomera e dimera nelle quali le mole-
cole dell'acido possono trovarsi: tale equilibrio sarebbe turbato dalle varia-
zioni di temperatura che accompagnano le onde sonore.

I fenomeni di rilassamento conducono, come si è detto, anche ad una
variazione della velocità di propagazione con la frequenza. Quando infatti la
frequenza dell'onda è talmente elevata che l'equilibrio in oggetto non riesce
più a seguire le variazioni di temperatura o di pressione, la velocità di propa-
gazione cresce giacchè diminuisce il calore specifico effettivo o, rispettivamente,
il coefficiente di compressibilità.

La differenza fra la velocità di propagazione a bassa frequenza (v_0) e la
velocità (v_∞) a frequenza molto al disopra di quella di rilassamento ($1/\tau$), è
notevole nel caso di fenomeni di rilassamento termico nei gas, sicchè la deter-
minazione della dispersione costituisce il metodo più esatto per lo studio di
questo tipo di fenomeni. Nel caso dei liquidi le variazioni di velocità attendi-
bili, anche in quei pochi esempi di fenomeni di rilassamento che avvengono
con frequenze caratteristiche nel campo di frequenze oggi producibili, sono
talmente piccole da non potere, in genere, essere misurate con i normali mezzi
di indagine. Per queste ragioni sono molto scarse le misure di dispersione della
velocità nei liquidi.

Appare quindi interessante cercare di studiare con i migliori metodi di
misura oggi disponibili, la velocità in funzione della frequenza in qualcuno
dei pochi liquidi nei quali le misure di assorbimento mostrano che le frequenze
di rilassamento si trovano in una gamma facilmente accessibile.

Noi abbiamo preso in esame il caso dell'acido propionico. È facile valu-
tare, sulla base dei valori del coefficiente di assorbimento, la variazione di velo-
cità attendibile quando si passa da una frequenza molto bassa ad una molto
alta ($\gg 1/\tau$). Nel caso dell'acido propionico, presentandosi per quanto si è

detto, un fenomeno di rilassamento termico, si può fare uso delle formule originariamente stabilite da KNESER ([2]) per il rilassamento legato alla distribuzione di energia fra gradi di libertà esterni e di vibrazione delle molecole.

La formula che interessa per il calcolo della dispersione, è:

$$(1) \qquad \left(\frac{v_f}{v_0}\right)^2 = \frac{1 + f^2\tau^2}{1 + f^2\tau^2(1-\varepsilon)},$$

in cui v_f è la velocità alla frequenza f ed

$$(2) \qquad \varepsilon = \frac{v_\infty^2 - v_0^2}{v_\infty^2} = \frac{2\mu_m^2}{\pi}.$$

Facendo uso dei valori sperimentali dell'assorbimento in acido propionico, si sono calcolate con la (1) le dispersioni attendibili, a tre diverse temperature (Fig. 1). Come si vede, la variazione totale di velocità fra basse ed alte frequenze è molto piccola (circa 0.5%). Se si desidera fare misure nell'interno della regione di rilassamento, la variazione di velocità fra due frequenze si riduce ovviamente in modo notevole.

Nella presente nota vengono riferiti i risultati ottenuti, usando un metodo di misura molto sensibile, nella rivelazione della dispersione in acido propionico in funzione della temperatura.
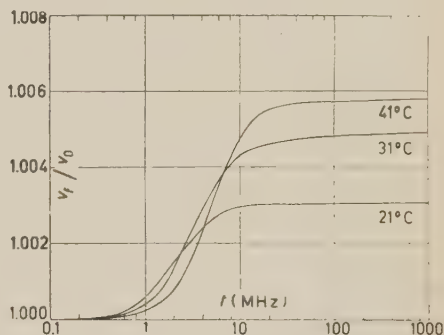
Fig. 1.

Dispersione della velocità calcolata in base alle misure di assorbimento.

2. - Metodo sperimentale.

Si sono eseguite misure della velocità in funzione della temperatura alle frequenze di 2 e 6 MHz, su diversi campioni di acido propionico forniti dalle Ditte Merck e Fluka. Le misure sono state fatte entro i limiti di temperatura fra 15 e 30 °C.

Lo strumento di misura è uno speciale tipo di interferometro di elevata precisione che è stato dettagliatamente descritto in un precedente lavoro ([3]). Nella loca-

---

([2]) H. O. KNESER: *Erg. Ex. Naturw.*, **22**, 121 (1949).

([3]) A. BARONE: *Nuovo Cimento*, **5**, 717 (1957).

zione citata ed in occasione di altre ricerche effettuate con lo stesso metodo ([4]), sono state discusse le principali cause di errore. Per quanto riguarda le misure qui riportate, ricorderemo l'importanza dell'errore che si commette nel traguardare le frange di interferenza: la larghezza di tali frange aumenta infatti con il coefficiente di assorbimento del liquido e, nel caso dell'acido propionico, il coefficiente di assorbimento è molto elevato per frequenze vicine a quella di rilassamento. La precisione conseguita nelle presenti misure è risultata del 0.5 ‰.

Le onde ultrasonore erano generate da un unico quarzo a 2 MHz, il quale veniva eccitato una volta sulla prima e una volta sulla terza armonica. Le frequenze di 2 e 6 MHz si ottenevano con opportune moltiplicazioni dal medesimo campione di frequenza a quarzo termostatato. La frequenza era quindi stabile e conosciuta entro l'1 su 100 000.

Stabilizzata la temperatura con un termostato a circolazione d'acqua, si eseguivano due misure consecutive, una a 2 e l'altra a 6 MHz; si incrementava quindi la temperatura, ripetendo la misura dopo la successiva stabilizzazione. In tal modo si aveva, per ogni fissata temperatura, una coppia di determinazioni rispettivamente a 2 e 6 MHz ottenute nelle medesime condizioni sperimentali. Ne consegue che, eventuali cause accidentali di errore nel confronto fra le misure a temperature diverse, non influiscono sull'entità della dispersione misurata ad ogni singola temperatura.

3. - Risultati.

In Fig. 2 sono riportati i risultati di una misura relativa ad un campione di acido propionico « purissimo » della Fluka. Le due serie di punti sperimentali a 2 e 6 MHz, mostrano chiaramente l'esistenza della dispersione. Per confrontare questi dati con la teoria, si è proceduto nel modo seguente: poichè la teoria del rilassamento prevede l'entità della dispersione, ma non dà alcuna informazione sul valore assoluto della velocità, si è tracciata la retta congiungente i punti sperimentali a 2 MHz, e si è assunta questa retta come base per il calcolo delle dispersioni. Usando quindi le formule (1) e (2) ed i valori di τ e μ_m dati da LAMB per 21 °C e 31 °C si è tracciato l'andamento teorico della velocità a 6 MHz. I punti sperimentali a 6 MHz riportati nel grafico vanno quindi confrontati con la retta superiore.

Si noti che l'andamento previsto di v in funzione di T, pur non essendo rigorosamente lineare, può essere ritenuto approssimativamente tale nei ristretti limiti di temperatura da noi esplorati.

([4]) A. BARONE, G. PISENT e D. SETTE: *Acustica*, **7**, 109 (1957).

In Fig. 3 è riportato, in funzione della temperatura, il rapporto fra i valori della velocità a 6 e a 2 MHz. A differenza dei risultati della Fig. 2,
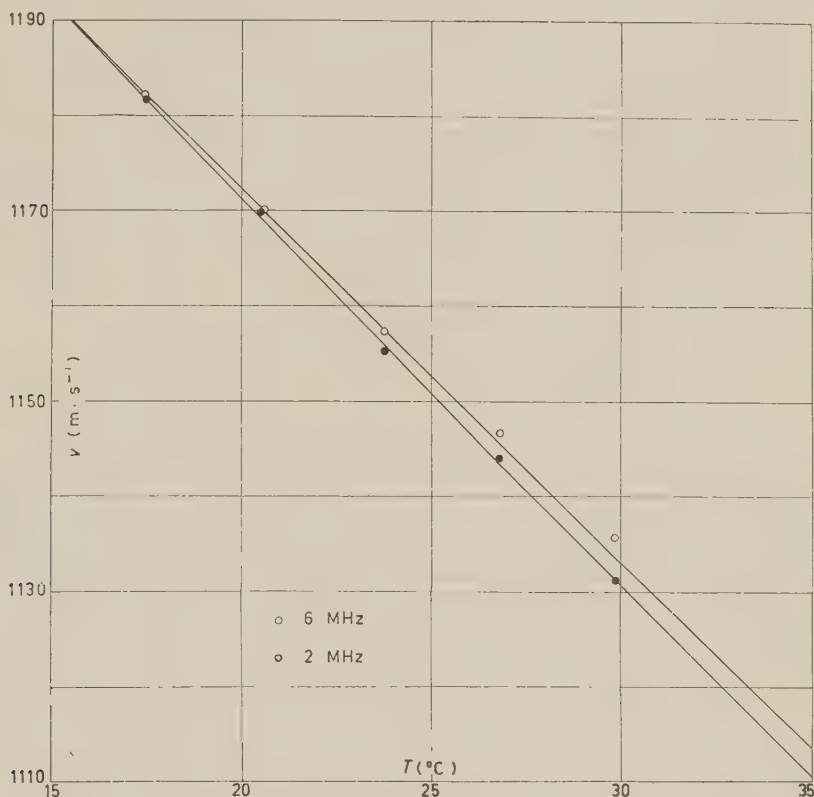
Fig. 2. – Velocità di propagazione degli ultrasuoni a 2 e 6 MHz in funzione della temperatura.

qui i punti sperimentali non appartengono ad una sola serie di misure, ma a molte serie eseguite in momenti diversi su campioni diversi.

Malgrado questa disparità di condizioni sperimentali, l'andamento medio dei valori misurati si accorda abbastanza bene con quello previsto in base alle misure di assorbimento rappresentato in figura dalla linea a tratto continuo.
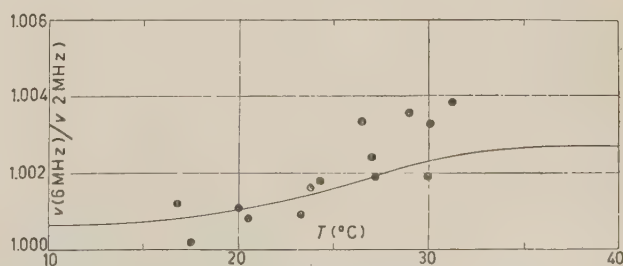
Fig. 3. – Rapporto delle velocità a 2 e 6 MHz in funzione della temperatura.

Dall'esame dei risultati sperimentali possiamo trarre le seguenti conclusioni:

1) In acido propionico la dispersione esiste, ed è dell'ordine di grandezza che le misure di assorbimento facevano prevedere.

2) L'andamento della dispersione in funzione della temperatura, è pure in accordo con le previsioni.

3) Alle alte temperature, l'entità della dispersione sembra tendere ad un valore più grande del previsto, ma tale effetto supera di poco gli errori sperimentali, per cui quest'ultimo risultato può essere considerato solo come indicativo.

SUMMARY

Sound dispersion in propionic acid has been studied between 2 and 6 MHz in the temperature range $15 \div 30$ °C. The results agree with theoretical expectations based on the absorption coefficient's data.

On the Charge and Energy Spectrum
of Heavy Primaries in Cosmic Radiation.

R. Cester, A. Debenedetti, C. M. Garelli, B. Quassiati,
L. Tallone and M. Vigone

Istituto di Fisica dell'Università - Torino
Istituto Nazionale di Fisica Nucleare - Sezione di Torino

Summary. — 529 tracks of heavy primaries in the cosmic radiation have
been studied. Charge measurements have been carried out on all tracks
with a photometric method, and independent checks with gap counting
have been performed on Boron and Carbon tracks. All tracks have been
followed through and a total of 331 nuclear collisions observed. From
the analysis of these interactions, the interaction mean free paths and
fragmentation probabilities in emulsion and in air have been determined.
The results are in good agreement with those of other workers and have
been used to extrapolate the charge distribution at the top of the atmo-
sphere: the ratios of light nuclei and of heavy nuclei to medium nuclei,
at the top of the atmosphere, are 0.30 ± 0.09 and 0.51 ± 0.11 respect-
ively. Results of energy determination on 275 tracks give a value
$1.54^{+0.16}_{-0.13}$ for the exponent of the integral energy spectrum. Some diffi-
culties in the application of Peters' relation between the energy of primary
and the angles of emission of the fragmentation products are discussed.

1. - Introduction.

The knowledge of the relative abundance of the heavy primaries and of
their energy spectrum is very important in order to study the origin of the
cosmic radiation. Experimental data on this subject have been given by many

authors ([1,8]), but the results are not in perfect agreement. This discrepancy is probably due to the difficulty of avoiding systematic errors and of having a large statistics.

The present work will add some experimental results to the ones that have already been collected. In order to reduce the uncertainty due to possible errors in the measurements, we divided the charge spectrum in three groups: L group ($3 \leqslant Z \leqslant 5$); M group ($6 \leqslant Z \leqslant 9$); H group ($Z \geqslant 10$). We discuss carefully all the types of measurements made, and we try to check the results with independent methods every time it is possible.

2. - Exposure details.

Two stacks flown at high altitude at the same latitude were used in this work. One, which we shall indicate as Y-stack, was a stack of 38 stripped Ilford G5 emulsions (38 cm × 25 cm × 0.06 cm.). It was exposed with vertical orientation of the 38 cm side, over Northern Italy ($\lambda = 46°$ N) at an atmospheric depth of about 15 g/cm². To the amount of atmosphere above the stack must be added the thickness of the packing material which was 2 g/cm². The other stack, indicated as B-stack, of 70 stripped 15 cm × 15 cm × 0.06 cm Ilford G5 emulsions, was flown at the same latitude of 46° N, under a depth of 12 g/cm² of air and packing material.

3. - Detection of particles.

All plates of the Y-stack were scanned along a line parallel to and 3 mm below the upper edge, for tracks satisfying the following criteria:

1) Projected length > 2 mm/plate.

2) Grain density greater than about nine times the minimum value.

The total area scanned in this way was 55 cm².

The scanning of the B-stack was made, under the same criteria, on all

([1]) H. L. BRADT and B. PETERS: *Phys. Rev.*, **80**, 943 (1950).

([2]) A. D. DAINTON, P. H. FOWLER and D. W. KENT: *Phil. Mag.*, **43**, 729 (1952).

([3]) M. F. KAPLON, B. PETERS, H. L. REYNOLDS and D. M. RITSON: *Phys. Rev.*, **85**, 295 (1952).

([4]) K. GOTTSTEIN: *Phil. Mag.*, **45**, 347 (1954).

([5]) M. F. KAPLON, J. H. NOON and G. W. RACETTE: *Phys. Rev.*, **96**, 1408 (1954).

([6]) J. H. NOON and M. F. KAPLON: *Phys. Rev.*, **97**, 769 (1955).

([7]) H. FAY: *Zeits. f. Naturf.*, **10a**, 572 (1955).

([8]) J. H. NOON, A. J. HERTZ and B. J. O'BRIEN: *Nuovo Cimento*, **5**, 854 (1957).

plates of the stack along a 5 cm long line, 1 cm below the top edge of the emulsions (total area scanned 21 cm²). The total depth under which the scanning of the B-stack was performed was about 16 g/cm² (3.8 g/cm² of emulsion and 12 g/cm² of air and packing material).

Only the tracks that had a projected length $l \geqslant 3$ mm/plate were considered in this work. They were followed through the stack until they left or interacted; if a heavy fragment emerged from an interaction, this fragment was also followed.

A special scanning for Li and Be tracks was made in the Y-stack on an area of 23 cm² and all tracks of $I/I_0 > 7$ were detected. In order to distinguish the Li-tracks from the background of singly charged and α-particles, all tracks of $I/I_0 > 7$ were followed through a range $\geqslant 5$ cm and those stopping or showing a change in ionization were rejected. The remaining tracks were accepted for measurements and followed through the whole stack. We believe that no Li and Be tracks in the area re-scanned in this way could be missed.

No special scanning for Li and Be tracks was made in the B-stack.

On the whole a total of 529 tracks (415 in the Y-stack and 114 in the B-stack) of particles ranging from Li to Fe were detected and studied in this work.

4. - Charge measurements.

Since the cut-off energy for 46° N latitude has been shown to be 1.55 GeV per nucleon ([9]), nearly all the primary heavy nuclei which entered the stack were relativistic and charge can be determined without ambiguity from ionization.

4˙1. *Photometric measurements.* – Charge determinations were made on all tracks with a photoelectric device that has been previously described ([10]). Details on these measurements will be given elsewhere ([11]). The photometric absorption of all tracks was determined at the same depth below the emulsion surface. As the results are sensitive to the dip of the track, the plates were inclined so that the section of the track that was measured was adjusted nearly parallel to the photomultiplier slit. In order to reduce the effect of background and of local fluctuations in the development, a total length of 3 000 μm of each track was measured, the measurements being performed (whenever possible)

([9]) P. H. FOWLER and C. J. WADDINGTON: *Phil. Mag.*, **1**, 637 (1957).

([10]) M. ARTOM and C. GENTILE: *Suppl. Nuovo Cimento*, **4**, 254 (1956).

([11]) M. ARTOM, V. BISI and C. GENTILE: *Ric. Scient.*, (1957) (in the press).

in four different emulsion sheets. On some of the tracks a total length shorter than 3 mm was available, or measurements could be performed only in one or two different emulsion sheets. In these cases gap or δ-rays counting was carried on.
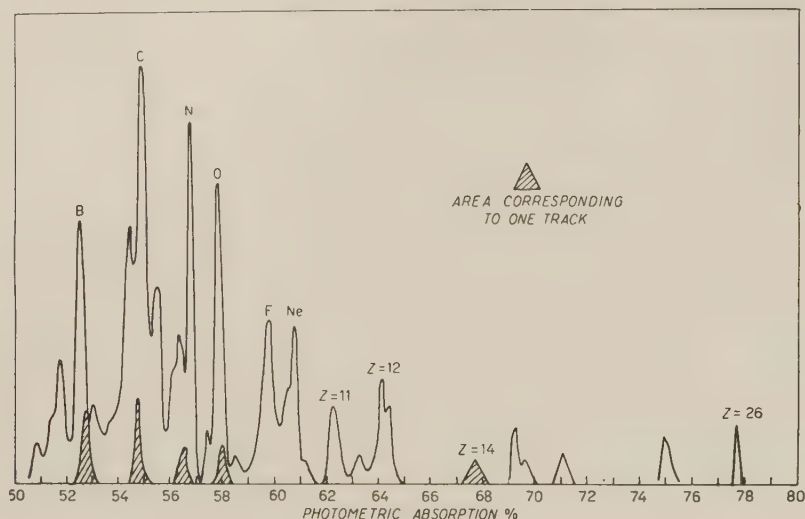
Fig. 1.

The results of the photometric measurements are shown in the two hystograms of Fig. 1 and Fig. 2 in which each track is represented as a triangle of
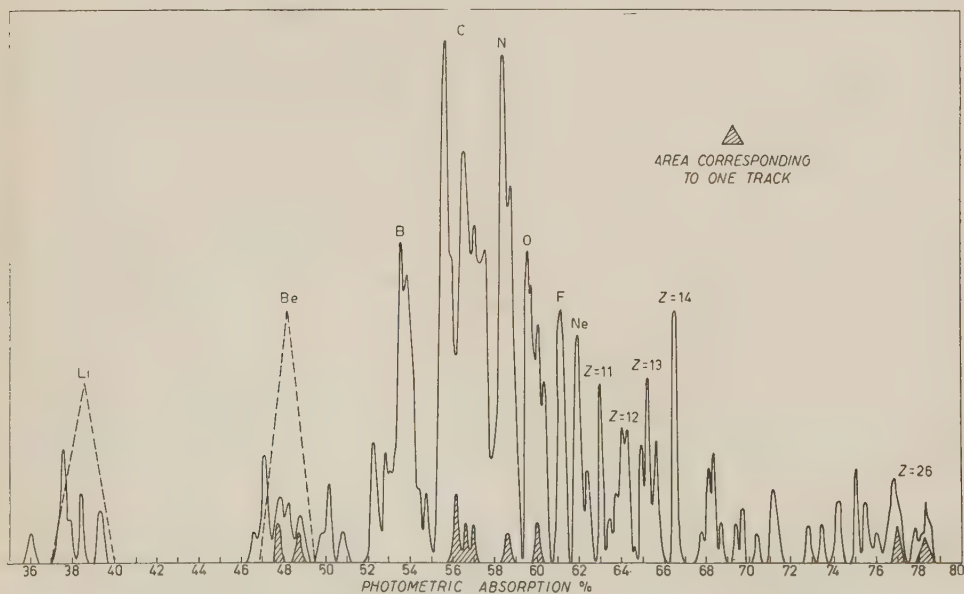
Fig. 2.

constant area with a base equal to twice the standard deviation. The resolution is better in the hystogram of the B-stack (Fig. 1) owing to the very good development of this stack. In this hystogram however we do not report the Li and Be tracks as in the B-stack no special scanning for these tracks was carried out and the scanning efficiency in this charge interval was not very good.

Fig. 3.

In Fig. 2 the area under the dashed curve represents the number of Li and Be particles increased by the corresponding loss correction factors that take into account the results of the special scanning.
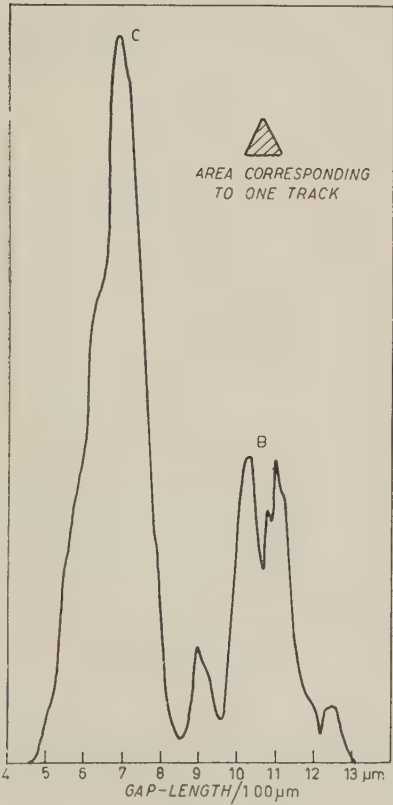
Fig. 4.
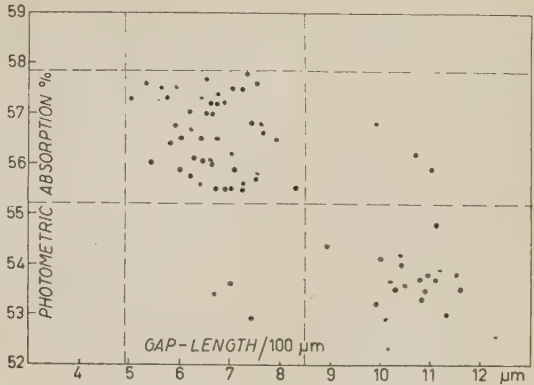
Charge calibration has been made on the splitting tracks whose charge could be unambiguously determined from the products of fragmentation. The corresponding interactions are indicated by a star in Table III-*a* and III-*b* of Sect. **6** and the corresponding area is dashed in the hystograms. These tracks were also used to obtain the calibration for δ-rays and gap-length measurements.

The identification of charges is reliable up to about $Z = 14$; for greater atomic number, owing to low statistics and lack of calibration tracks, the determination of charge is more uncertain.

4·2. *Gap length measurements.* – In order to have a further check on the charge determination and to improve the resolution between Boron and Carbon, gap length measurements were carried out on all the Boron and Carbon tracks (in the Y-stack) which made an angle $\leqslant 30°$ with the vertical. For each track a total of about $300 \div 400$ gaps, corresponding to a total track length of $3\,000$ μm, in at least three different

emulsion sheets was measured. The gap length obtained (length of gaps per 100 μm of track) are plotted against the photometric absorption in Fig. 3 which shows a good agreement between the two types of measurements. Of the total of 65 particles, 58 have the same charge in both determinations, while for 8 tracks the two methods give two values of Z differing by one.

In Fig. 4 the results of gap length measurements are shown in the form of an hystogram.

5. - Scanning efficiency.

To check the scanning efficiency we determined for the Y-stack the distribution in length per plate of the particles. We divided the tracks in the following three groups of dip angles ξ: $6°50' \leqslant \xi < 11°$; $3°30' \leqslant \xi < 6°50'$; and $0° \leqslant \xi < 3°30'$; corresponding to lengths per plate l of $3 \div 5$ mm, $5 \div 10$ mm, > 10 mm respectively. If the efficiency of detection is the same for all plates, the number n of tracks per plate and per unit solid angle (*) must be practically the same for all groups. A certain loss for very flat tracks and for the shorter ones is evident from the results of Table I.

TABLE I. – *Number of tracks per plate and per steradian.*

	$3 \text{ mm} \leqslant \dfrac{\text{lenght}}{\text{plate}} < 5 \text{ mm}$	$5 \text{ mm} \leqslant \dfrac{\text{length}}{\text{plate}} < 10 \text{ mm}$	$\dfrac{\text{length}}{\text{plate}} \geqslant 10 \text{ mm}$	$\dfrac{\text{lenght}}{\text{plate}} \geqslant 3 \text{ mm}$
All observers	4.4 ± 0.2	5.6 ± 0.3	3.6 ± 0.3	4.5 ± 0.2
Good observers	4.8 ± 0.3	5.9 ± 0.4	3.8 ± 0.3	4.8 ± 0.2

We also compared the values of n for the various scanners and they turned out to be the same for all but one. We can try to evaluate a correction factor for scanning loss, dividing the value of n for good observers and for l ranging from 5 mm to 10 mm, by the value of n for all tracks and for all observers. This correction factor turns out to be $5.9/4.5 = 1.3$.

_____

(*) The solid angle corresponding to each interval $\Delta\xi = \xi_1 - \xi_2$ has been evaluated, and for small values of ξ is simply related to ξ_1 and ξ_2:

$$\Delta\Omega \cong 2\pi \left(\cos \xi_1 - \cos \xi_2\right) + 4 \left(\xi_2 - \frac{\pi}{2}\right) \sin \xi_2 - 4 \left(\xi_1 - \frac{\pi}{2}\right) \sin \xi_1 .$$

It is anyhow important to note that the relative abundances of light, medium and heavy nuclei do not vary, within statistical errors, with the angle of dip, as it is shown in Table II.

TABLE II. – *Scanning efficiency with regard to the relative abundance.*

	$3 \text{ mm} \leqslant \dfrac{\text{lenght}}{\text{plate}} < 5 \text{ mm}$	$5 \text{ mm} \leqslant \dfrac{\text{lenght}}{\text{plate}} \leqslant 10 \text{ mm}$	$\dfrac{\text{length}}{\text{plate}} \geqslant 10 \text{ mm}$	$\dfrac{\text{length}}{\text{plate}} \geqslant 3 \text{ mm}$	
N_L/N_M	0.59 ± 0.08	0.53 ± 0.08	0.61 ± 0.10	all observers	0.55
				good »	0.56
N_H/N_M	0.43 ± 0.09	0.29 ± 0.05	0.31 ± 0.10	all observers	0.34
				good »	0.34

So that it seems reasonable to assume that the missing of tracks does not affect the determination of charge distribution. The scanning loss has to be taken into account, of course, in the evaluation of the total flux of particles entering the stack.

6. - Nuclear interactions.

331 primary and secondary interactions of heavy nuclei ($Z \geqslant 3$) were found on a total track length of 4 660 cm traced through the Y and B-stacks. The details of each interaction are reported in Table III-*a* (Y-stack) and in Table III-*b* (B-stack).

All interactions were divided in two groups called respectively « splittings » and « stars ».

We indicate by splitting every interaction where in the direction of the primary or very close to it (within 9°) one can see:

a) one or more tracks of fast nuclei of $Z \geqslant 2$ with or without relativistic tracks;

b) a group of minimum tracks sharply divided from the other tracks of the star.

The total charge of the secondary tracks which we call splitting tracks must be compatible with the measured charge of the primary.

We call star every interaction were it is not possible to distinguish a group of fast particles in a narrow cone.

TABLE IIIa. — *Characteristics of each of the 265 nuclear interactions found in the Y-sta[...] α-particles in the splitting; p = number of protons in the splitting; r = tot[...]*

	Li					Be					B					C			
f	α	p	r	N_h	f	α	p	r	N_h	f	α	p	r	N_h	f	α	p	r	N_h
	1	1			2				4*	1	3	2	3			2	2	2	4
	1	1	2	3	1	2			5	2	1					2	2		
	1	1			1	2				1	3	8	3			3			
	3			6	1	2		5		1	3		2			3		1	1*
	1	1		5	2		1			2	1	?				2	2		2
Li		?		6	1	2			*	2	1	1				1	4	2	3
					1	2			5	2	1	1	4			2	2	1	5
		3	?	13	1	2		3	11		4		7			2	2		
		3		12	1	2					5	17	19			1	4	8	2
		3	2	31	2			4	4	2	1	3			Li		3	5	3
	?	?	?	?	1	2	?		2	2	1		2						?
					2			4	15	1	3	3				2	2		
							4	5	19	Li / B		2	5	7			6	5	8
								1	19			5	1	3		1	4	7	1
					1				2	Be		1					6	14	3
						?	?		10		1	3	4	2		2	2	5	
										B				4		1	4	?	3
											1	3	4	19	Li		3		
												5		9		2	2	5	5
											1	3	16	3		1	4		4
											2	1				1	4	11	15
											2	1			C				1
															C			3	4
												5	7	13			6	2	18
												5	5	14			6	3	23
												5	14	17			6	12	17
												5	5	8			6	2	18
												5	2	7			6	9	1
												5	3	15		1	4	8	4
											1	3	5	24			6	3	2
											1	3	10	14			6	4	4
												5	8	18			6	4	14
												5	1	4			6	4	24
												5	5	14		1	4	5	4
												5	12	19			6	17	18
												5	7	7			3		?
												?	?	6					

h interaction is classified in terms of: f = number of heavy fragments; α = number of
...ber of relativistic tracks minus p; N_h = number of black and grey tracks.

C f	C α	C p	C r	C N_h	N f	N α	N p	N r	N N_h	O f	O α	O p	O r	O N_h	F f	F α	F p	F r	F N_h
e	1			*		1	5		1		4			*		1	7	30	?
		6	2	1		1	5	1			4		2	4	Li		6	4	4
e		1		6			7	3	3		2	4	2	11	N	1			
	3			4*	Be	1	1		*		1	6			N	1			
	2	2	2		B	1			1	C	1						9	12	4
	1	4	2	1			7	9	15	B		3	2	5	C		3	4	4
	2	2		*		1	5	3	5		3	2	1	2	F				2
		6	3	4		1	5	3	9	N		1	4		O		1	9	16
			3	3	Be		3	5	3		1	6	3	8	C	1	1		2
i	1	1	2	3		1	4		8		2	4	4	3	N		2		7
	3				B		2	4	4			8	5	1	Be		5	5	12
		3	2	4		3	1			C	1		2				9	7	20
i		1	5	1	B	1						8	7	16			9	9	21
	1	4	4	3			7	8	3	Be		4	7	4			8		10
		6	3	6	C	1		1	8	Li	1	3		6		1	7	1	11
		6	27	20		1	5		8		2	4	1	1					
i					N			3	5		3	2	3	7					
i										C		2	?						
	3			1	N				3			3	6	6					
i		3	2	8	Li		4	4	12	B		1	5	6					
i		3	1	5		1	5	6	16	B	1	8		2					
e		2	6	8	C		1	2	7	N		1		1					
				2		1	5	6	16											
					Li	1	2	10	13											
		6	60	2								8	15	10					
		6	18	20			7	29	14			8	27	18					
		6	8	13			3		13		1	6	9	16					
		6	9	24		1	5	4	9		1	6	10	10					
		6	10	12		1	5	26	4			8	15	16					
	2	2	1	3			7		9										
		6	8	11															
	?	?	?	2															
	?	?	?	?															
		6	11	12															
		6	4	1															
	1	2		8															
	?	?	?	>10															

TABLE IIIa (continued).

	Ne					Na					Mg					Al			
f	α	p	r	N_h	f	α	p	r	N_h	f	α	p	r	N_h	f	α	p	r	N_h
C	2					2	7	4	8	C	1	4		5		1	11		
$\begin{cases}\text{Li}\\\text{Li}\end{cases}$		4	6	3	C	1	3	2				12	18	31		1	11		3
		10	10	19	O	1	1					12	10	9	Na		2	3	1
	2	6		4	F	1				Li	1	7	8	16		2	9	10	13
O	1		2		Na			2	5	$\begin{cases}\text{Be}\\\text{Li}\end{cases}$	1	3				3	7		1
	1	8	36	21								12	70	>10			13	38	21
Ne				1								12	13	10					
Ne				1							1	10	19	12					
		10	6	22															
		10	34	26															

	A					K					Ca					Ti			
f	α	p	r	N_h	f	α	p	r	N_h	f	α	p	r	N_h	f	α	p	r	N_h
$\begin{cases}\text{B}\\\text{Li}\end{cases}$	1	8	16	17	Si	2	1	2	4	Si	2	2	2	3		1	20	5	2
A				4							2	16	15	3					
											4	12	2						

In the first part of Tables III-*a* and III-*b* the 242 splitting events, which were studied carefully, are collected. The available information relative to the 89 stars is reported in the second part of Tables III*a* and III-*b*.

7. – Interaction mean free paths.

The mean free paths λ_i where $i = L$, M, H) in emulsion obtained in the Y- stack are reported in Table IV.

This result must be considered as an upper limit since we did not take into account those events in which one evaporation track only is noticed and no change of charge is detected in the incoming nucleus. Such events, as

	Si				Ph					S					Cl				
	α	p	r	N_h	f	α	p	r	N_h	f	α	p	r	N_h	f	α	p	r	N_h
a	1	6	1		Al	1		4	5	Ne		6	1	5	Ne		7	2	2
	1	1				3	9	4		N	2	5		6	Na	1	4	9	16
1	1	12	3	3											B		12	26	5
1	1	12	9				15	2	18										23
		14	4	13															
		14	66	13															
		14		12															

	Cr					Mn					Fe			
f	α	p	r	N_h	f	α	p	r	N_h	f	α	p	r	N_h
Sc	1	1	2	1	Cl	2	4			Mg	3	8	11	23*
S		8	16	3	Ti	1	1			Be	5	12	10	4*
N	3	11									1	24	7	8
Ph	3	3		3								26	5	13

some author pointed out [12], could in fact be due to a physical process some-
what different from the collision processes.

Our results for L and M incoming nuclei agree with those found by other
authors [6,12,13] and with the values calculated by using for an estimate of the
cross-section the empirical expression given by BRADT and PETERS [14]:

$$(1) \qquad \sigma_i = \pi(R_i + R_t - 2\Delta R)^2 , \qquad R = r_0 A^{\frac{1}{3}} \qquad (r_0 = 1.45 \cdot 10^{-13} \text{ cm}),$$

[12] P. H. FOWLER, R. R. HILLIER and C. J. WADDINGTON: Phil. Mag., 2, 293 (1957).

[13] V. Y. RAJOPADHYE and C. J. WADDINGTON: Private communication.

[14] H. L. BRADT and B. PETERS: Phys. Rev., 77, 54 (1950).

TABLE IIIb. – *Characteristics of each of the 66 nuclear interactions found in the B-stack* α-*particles in the splitting;* p = *number of protons in the splitting;* r = *tota[...]*

Be					B					C					N				
f	α	p	r	N_h	f	α	p	r	N_h	f	α	p	r	N_h	f	α	p	r	N_h
		4		6		2	1		*		3			*	Be			3	3
	2			1		1	3	2	6			6	4	21		1	5	2	5
	1	2	10	12		2	1	6	1		2	2		1*	C		1		5
Li		1	3			2	1	1				6	4	3			7	7	13
		5	2	7		2	1		1*	C		6		2	7	B		2		2
								2	1			6		16		3	1	2	1
					B	1	3	7	18			6	19	20	B		2	1	1
											2	2	1	6	Be	1	1	1	4
										Be	1					2	3		2*
												6	19	1			7	11	22
											2	2	4	5					
											2	2	4	17					
											2	2	4	3					
										Li	1	1		3					
											3			5					
											1	4	2	2					
											1	4	1	3					
												6	13	19					
												6	38	19					
												6	18	38					
												6	17	24					
												6	10	19					

where R_i is the radius of the incoming nucleus, R_t is the radius of the target nucleus and ΔR has the empirical value of $0.86 \cdot 10^{-13}$ cm. Experiments [15,16] of different kind have proved this expression to be appliable over a large range of target and incident nuclei, including the type of nuclei we are dealing with. An exception must be made for the process in which hydrogen nuclei are interested. In this case the experimental value of the σ found by CHEN and co-workers [17] by exposing a heavy nucleus target to a 860 MeV proton beam was used.

The mean free path for heavy incident nuclei found in this work is larger than the experimental and calculated values we are comparing with. This could be explained with the loss of some interactions and the only events

[15] Y. EISENBERG: *Phys. Rev.*, **96**, 1378 (1954).
[16] F. B. McDONALD: *Phys. Rev.*, **104**, 1725 (1956).
[17] F. F. CHEN, C. P. LEAVITT and A. M. SHAPIRO: *Phys. Rev.*, **99**, 857 (1955).

...interaction is classified in terms of: f = number of heavy fragments; α = umber of ...ber of relativistic tracks minus p; N_h = number of black and grey tracks.

O α	O p	O r	O N_h	F f	F α	F p	F r	F N_h	Ne f	Ne α	Ne p	Ne r	Ne N_h	Na f	Na α	Na p	Na r	Na N
2	4	22	4	N		2	1	2	Be	1	4	12	11		3	5	5	
	2	2	5	N	1				O	1			2	N	4	10		16
	1		1*	N	1						10	9	16	B	2	3	1	11
	8	10	18								10	6	19			11	69	31
	8	14	3															

Mg α	Mg p	Mg r	Mg N_h	Si f	Si α	Si p	Si r	Si N_h	Cl f	Cl α	Cl p	Cl r	Cl N_h	Ca f	Ca α	Ca p	Ca r	Ca N_h
	5	3		C	2	4		7*	Mg	2	1	1	1	F	4	3	3	8
	12	2	31															
	12	43	36															

TABLE IV. – *Mean free paths in emulsion and in air.*

Charge group	λ (g/cm^2) emulsion Turin (Y-stack)	λ (g/cm^2) emulsion Bristol	λ (g/cm^2) emulsion Rochester	λ (g/cm^2) emulsion calculated value	λ (g/cm^2) air calculated value
L	60.0 ± 5.7	51.6 ± 6.1	61.7 ± 19.4	60.1	33.6
M	51.6 ± 3.3	51.9 ± 3.8	59.6 ± 6.0	49.7	26.9
H	42.5 ± 4.1	37.0 ± 3.1	36.5 ± 4.8	35.2	19.0

which we feel could be missed are those in which one or two relativistic part-icles only are emitted. If this is so, on the other side, we should notice also a

discrepancy between our value of the fragmentation probabilities of H nuclei in H secondaries and those found by other authors, which is not the case. We conclude then that such a high value of λ_{H} must be due to a statistical fluctuation.

In Table IV the values calculated from formula (1) of the mean free paths in air, to be used in the extrapolation of the charge spectrun to the top of the atmosphere, are also reported.

8. - Fragmentation probabilities.

In Table V are reported the fragmentation probabilities in emulsion obtained by analysing the interactions found in the Y and B-stacks. Our results are in good agreement with those of the Bristol group ([12,13]), while there appears to be a discrepancy between our values of P_{HL}, P_{ML} and those found by the Rochester group ([6]).

TABLE V. – *Fragmentation probabilities in emulsion.*

	P_{LL}	P_{ML}	P_{MM}	P_{HL}	P_{HM}	P_{HH}
Turin	0.11 ± 0.04	0.18 ± 0.03	0.16 ± 0.03	0.13 ± 0.04	0.18 ± 0.05	0.25 ± 0.06
Bristol	0.10 ± 0.04	0.12 ± 0.03	0.11 ± 0.03	0.11 ± 0.04	0.25 ± 0.06	0.16 ± 0.04
Rochester	—	0.32 ± 0.05	0.08 ± 0.03	0.43 ± 0.07	0.21 ± 0.05	0.18 ± 0.05

In order to estimate the fragmentation probabilities in air to be used for the extrapolation of the charge spectrum to the top of the atmosphere we have taken into account only those events in which $N_h \leqslant 7$ (l-events) neglecting the ones with $N_h > 7$ (h-events). The l-events are found to be 58.5% of the total number of interactions. From the emulsion composition and from the evaluation of the cross-section in emulsion, the percentage of collisions with a light target (H, C, O, N) is estimated to be 33.3%. This means that 43% of l-events are peripherial collisions with a heavy target. In order to estimate the fragmentation probabilities in air, we have assumed that peripheric collisions with a heavy target are felt by the incident nucleus as collisions with a light target, and therefore, we have taken as fragmentation probabilities in air those obtained by analysing l-events in emulsion. Our data compare with those obtained making the same assumption by the Bristol group and, since the experimental conditions and the criteria in selecting the

heavy nuclei tracks are very similar, we have used for the extrapolation to the top of the atmosphere the values obtained averaging over the results of the Turin and Bristol groups (Table VI).

TABLE VI. – *Fragmentation probabilities in l-events.*

	P_{LL}	P_{ML}	P_{MM}	P_{HL}	P_{HM}	P_{HH}
Turin	$\dfrac{7}{48}=0.15$	$\dfrac{27}{119}=0.23$	$\dfrac{23}{119}=0.19$	$\dfrac{6}{44}=0.14$	$\dfrac{12}{44}=0,27$	$\dfrac{15}{44}=0.34$
Bristol	$\dfrac{5}{31}=0.16$	$\dfrac{18}{100}=0.18$	$\dfrac{16}{100}=0.16$	$\dfrac{5}{42}=0.12$	$\dfrac{19}{42}=0.45$	$\dfrac{12}{42}=0.29$
Turin and Bristol (averaged values)	0.15 ± 0.03	0.21 ± 0.02	0.18 ± 0.02	0.13 ± 0.03	0.36 ± 0.04	0.31 ± 0.04

It must be added that the impact parameter may play an important role, as regards the fragmentation, the fragmentation being increased when the parameter decreases. In this case the previous assumption would result in an overestimate of the P_{HH}, P_{MM}, P_{LL} and in an underestimate of the P_{HL}, P_{ML}, $P_{M\alpha}$, $P_{L\alpha}$.

We did not attempt to extrapolate the charge spectrum from the top of the atmosphere to the cosmic rays origin since fragmentation probabilities of heavy primaries in hydrogen would be needed. We have reported in Table XVI (*a, b*) (Appendix II) the interactions with a proton target in emulsion but we feel that their number is much too low to give a satisfactory indication of the fragmentation probabilities in hydrogen.

9. – Charge spectrum.

The results obtained, in the Y-stack only, by measuring the heavy nuclei tracks with zenith angle $\leqslant 60°$ were taken into account in order to determine the charge spectrum. The number of particles of each charge entering the stack at flight altitude are given in Table VII.

In the extrapolation of the charge spectrum to the top of the atmosphere we have taken in consideration only the tracks with zenith angle $\leqslant 30°$. In this case the path in air for heavy nuclei is practically the same for all zenith angles, with a maximum spread of 8%, and therefore the computation is more

TABLE VII. – *Numbers of particles at flight altitude with zenith angle* $\leqslant 60°$.

	Li	Be	B	C	N	O	F	$Z \geqslant 10$
Number of particles N_z	27	37	52	110	43	35	19	74
Relative frequencies $\dfrac{N_z}{\text{Total number}}$	0.07 ± 0.01	0.09 ± 0.01	0.13 ± 0.01	0.27 ± 0.02	0.11 ± 0.01	0.09 ± 0.01	0.05 ± 0.01	0.18 ± 0.02

straightforward. Moreover, as already mentioned, we have divided all tracks in three intervals of charge, L, M, H, where: the L group includes Li, Be, B $(3 \leqslant Z \leqslant 5)$; the M group includes C, N, O, F $(6 \leqslant Z \leqslant 9)$; the H group includes all elements with charge $Z \geqslant 10$.

We used the diffusion equation reported by KAPLON *et al.* [5] and the fragmentation probabilities and mean free paths discussed in Sect. **8** and **7** and quoted in Tables VI and IV. In Table VIII the relative abundances of the three groups are given, both at flight altitude and at the top of the atmosphere.

TABLE VIII. – *Relative abundances of light, medium and heavy particles with zenith angle* $\leqslant 30°$.

	N_L	N_M	N_H	N_L/N_M	N_H/N_M
Flight altitude	60 ± 6	130 ± 8	52 ± 5	$0.46 + 0.07$	$0.40 + 0.07$
Top of the astmosphere	58 ± 12	193 ± 15	99 ± 15	0.30 ± 0.09	0.51 ± 0.11

We quote the statistical errors on the number of tracks for the values at flight altitude; the errors computed for the results at the top of the atmosphere take into account statistical errors on the fragmentation probabilities as well.

To obtain the fluxes of the various components of the cosmic radiation at the top of the atmosphere, we must take in consideration the loss in the detection of particles, which was found in Sect. **5** not to be negligible. The flux for each charge component will be given by:

$$\Phi = \frac{N^0 K}{\Delta t \cdot \Delta \Omega \cdot A} \; \frac{\int_0^{\theta_{max}} \sec \theta \, \mathrm{d}\theta}{\int_0^{\theta_{max}} \mathrm{d}\theta} \quad ,$$

where N^0 is the total number of particles belonging to that charge group, A the receiving area, Δt the duration of exposure, $\Delta \Omega$ the allowed solid angle, K the correction loss factor. If we take for K the value $K = 1.3$ which results from the analysis of Sect. **5**, we obtain for the three components the flux values:

$$\Phi_{\mathrm{L}^0} = 1.67 \pm 0.39 \;\; \text{particles/m}^2 \text{ sterad s}$$

$$\Phi_{\mathrm{M}^0} = 5.52 \pm 0.40 \qquad \text{»} \qquad\qquad \text{»} \quad \text{»}$$

$$\Phi_{\mathrm{H}^0} = 2.82 \pm 0.40 \qquad \text{»} \qquad\qquad \text{»} \quad \text{»}$$

that are not inconsistent with the values of previous experiments.

10. – Zenith angle dependence.

The dependence of the flux of particles from the thickness of air traversed would give a check of the calculated values of the mean free paths and fragmentation probabilities in air. Therefore we studied the dependence of the heavy nuclei flux from the zenith angle θ. The weak point of this method is that, since the number of tracks decreases very rapidly with increasing zenith angles, the values corresponding to a long path of air traversed are affected by a large statistical error. In Fig. 5 the experimental quantity

$$\frac{\Delta N(\theta)}{\Delta \Omega \cos \theta}$$

(which is proportional to the flux of particles arriving at flight altitude in the solid angle $\Delta \Omega(\theta)$ (*) in a direction between θ and $\theta + \Delta \theta$) is plotted for the three groups of charges versus $x/x^0 = 1/\cos\theta$ ($x =$ thickness of air traversed; $x^0 =$ thickness of air in the vertical direction). The statistical errors in the points are indicated.
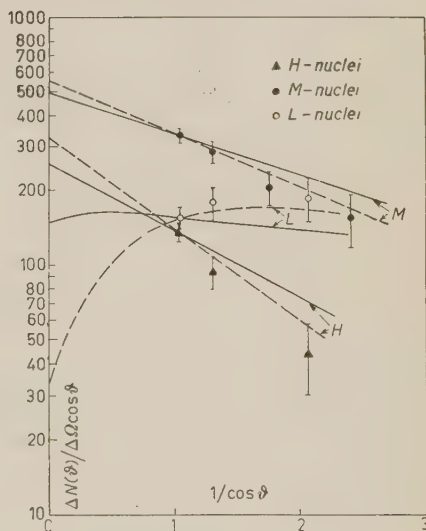
Fig. 5.

The theoretical curves calculated from the diffusion equation are also plotted in the diagram. The full line corresponds to the values of the fragmentation

---

(*) In computing the solid angles $\Delta \Omega$ we took into account the fact that only tracks having an angle of dip $\leqslant 11° 30'$ were accepted in this experiment.

probabilities of Table VI. The agreement is not bad, but an improvement could be reached (dashed curve) assuming for the fragmentation probabilities the values: $P_{LL} = 0.15$; $P_{ML} = 0.30$; $P_{MM} = 0.10$; $P_{HL} = 0.40$; $P_{HM} = 0.20$; $P_{HH} = 0.10$ that is for an increase in the P_{HL} and P_{ML}, and a reduction of the P_{MM}, P_{HH}, P_{HM}. This variation of the P_{IJ} (I, J = L, M, H) should be expected as a consequence, as we already pointed out in Sect. 8, of the inclusion in l-events of a 43% of peripherial collisions with heavy nuclei.

In spite of low statistics we report these results as a possible indication that the values of fragmentation probabilities deduced from the analysis of the interactions in the emulsion give only approximately the values in the atmosphere.

11. - Meson production.

In Tables III-a and III-b we have indicated with N_r all the relativistic prongs outcoming from the interaction, which could not be considered as splitting products. We now assume that N_r is the number of mesons produced in the interaction, neglecting the presence, between them, of some relativistic protons of the target nucleus. In order to estimate the variation of the meson production with energy and charge of the incoming nucleus, we proceeded as follows: we have tried to give a rough estimate of the average number $\overline{N}_{Np}$ of nucleon pairs interested in any single collision. In our estimate the simdlifying hypothesis that $A = 2Z$ for all incident and target nuclei, was made.

It seems then reasonable to define in every collision:

$$N_{Np} = Z_i + Z_t - Z_{z>1} - Z_{ev},$$

where: Z_i is the charge of the incoming nucleus; Z_t is the number of charged non-relativistic prongs outcoming from the interaction; $Z_{z>1}$ is the sum of the charges of the splitting products with $Z > 1$; Z_{ev} is the number of tracks of the target nucleus emitted with low energy ($I/I^0 > 4$) which could be considered as evaporation tracks.

We assume the average number of nucleon-nucleon collisions in every interaction to be equal to the number of above defined nucleon pairs. The average number $\overline{N}_\pi$ of mesons produced in every nucleon-nucleon collision is then estimated.

In Table IX are reported the values of $\overline{N}_\pi$ as a function of the energy and of the group of charge (L, M, H) of the incident nucleus for l-events and h-events. The data include all the interactions collected in Table III-a and III-b.

As mentioned in Sect. 16, the energy of the incoming nucleus was estimated in 242 cases (195 splitting of primaries and 47 splitting of secondaries) with

TABLE IX. – *Energy dependence of meson production.*

Energy (GeV per nucleon)	Charge group	l-events				h-events			
		No. of mesons in every collision	Total number of interactions	$\bar{N}_{Nb}$	$\bar{N}_\pi$	No. of mesons in every interaction	Total number of interactions	$\bar{N}_{Nb}$	$\bar{N}_\pi$
1.5— 4	L	1.7	23	3.3	0.49±0.07	5.1	16	10.9	0.47±0.15
	M	2.6	66	4.4	0.61±0.05	7.3	49	11.7	0.64±0.08
	H	2.7	23	7.3	0.36±0.07	10.1	23	19.4	0.56±0.08
1.5— 4	averaged value over *L, M, H*				0.52±0.03				0.58±0.04
4 —10	L	1.7	13	2.5	0.69±0.15	10.0	4	9.5	1.1 ±0.4
	M	2.9	31	2.6	1.15±0.15	14.7	8	13.0	1.1 ±0.3
	H	3.1	15	5.7	0.54±0.15	27.4	5	15.6	1.8 ±0.6
4 —10	averaged value over *L, M, H*				0.80±0.08				1.3 ±0.2
> 10	L	1.3	8	1.9	0.7 ±0.2	0	0	0	
	M	4.5	9	3.0	1.6 ±0.3	12	2	11	
	H	6.0	8	3.0	2.0 ±0.5	36	1	16	
> 10	averaged value over *L, M, H*				1.5 ±0.2				1.5 ±0.7

methods independent from the number of relativistic particles outgoing from the interactions. In the remaining 89 cases this could not be done and an estimate of the energy was given by attributing to every relativistic track an energy of 1,0 GeV and correcting by a factor 2 for the neutral particles. In Table X we have compared the results of Table IX with those obtained excluding the 89 doubtful cases.

TABLE X. – *Check on meson production.*

Energy (Gev/nucleon)	Charge group	$\overline{N}_\pi$ (l-events)		$\overline{N}_\pi$ (h-events)	
		splitting	splitting and stars	splitting	splitting and stars
1.5 — 4	L	0.71 ± 0.15	0.49 ± 0.07	1.82 ± 0.08	0.47 ± 0.15
	M	0.48 ± 0.05	0.61 ± 0.05	0.75 ± 0.15	0.64 ± 0.08
	H	0.35 ± 0.06	0.36 ± 0.07	0.66 ± 0.14	0.56 ± 0.08
1.5 — 4	averaged value over L, M, H	0.45 ± 0.04	0.52 ± 0.03	0.71 ± 0.08	0.58 ± 0.04
4 — 10	L	0.68 ± 0.15	0.69 ± 0.15	1.1 ± 0.4	1.1 ± 0.4
	M	1.12 ± 0.15	1.15 ± 0.15	0.6 ± 0.3	1.1 ± 0.3
	H	0.56 ± 0.11	0.54 ± 0.15	1.1 ± 0.4	1.8 ± 0.6
4 — 10	averaged value over L, M, H	0.81 ± 0.08	0.80 ± 0.08	0.9 ± 0.2	1.3 ± 0.2
> 10	L	0.7 ± 0.2	0.7 ± 0.2		
	M	1.6 ± 0.4	1.6 ± 0.3		
	H	2.0 ± 0.5	2.0 ± 0.5		
> 10	averaged value over L, M, H	1.5 ± 0.2	1.5 ± 0.2	1.5 ± 0.7	1.5 ± 0.7

The comparison clearly indicates that adding these events we do not affect the results excepts obviously for an improvement of the statistics.

As it was to be expected, the average number of mesons produced in every so called nucleon-nucleon collision is roughly independent, within the limits of errors, from the group of charge of the incident nucleus and from the size of the target (l-events, h-events) and increases with the energy of the incoming nucleus. The value $\overline{N}_\pi$ cannot be compared directly with the average number of mesons produced in free p-p or p-n collisions of the same energy but, if the

above given arguments are correct, should have the same dependence on the energy.

In Table IX, the average number N_{Np} of nucleon pairs for every collision is reported. Such a number decreases as the energy increases. This effect could have a physical meaning, but no conclusion can be drawn until Peters' relations used for the determination of the energy in most of the cases reported, are proved to be generally correct (cfr. Sect. **15**).

12. – Ratio of even charged to odd charged secondaries.

It has been pointed out by GOTTSTEIN [4] that, in the fragmentation of the heavy primaries, the probability of splitting into even charge fragments is greater for even charged primaries than for odd charged ones. In order to check this effect we collected our data in a diagram to be compared with the one given by GOTTSTEIN. In Fig. 6 the ratio N_{even}/N_{odd} of the number of secondaries of even charge to that of secondaries of odd charge (including protons) is plotted versus the charge Z of the primary nucleus. The figures in parenthesis represent the number of events on which the statistics is based. Only interactions in which the number of grey and black prongs is equal to or lower than seven (l-events) are taken into account.
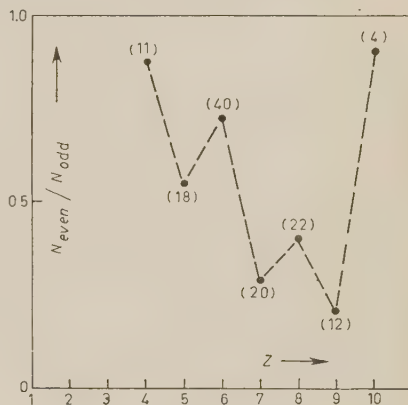
Fig. 6.

As one sees, we find the same result as GOTTSTEIN with a greater statistical weight. This seems to confirm the existence of the effect.

13. – Energy determination.

The determination of the energy of fast particles is a weak point in the emulsion technique, because all the methods which can be used are affected by errors whose magnitude is only very roughly established.

The energy of the tracks that do not interact in the emulsion can be determined only by scattering measurements. For energies certainly higher than 1 GeV, like the ones we have to study (the cut-off energy for this latitude was determined by FOWLER and WADDINGTON [9] to be 1.55 GeV per nucleon) one must use cell sizes of 1 mm or more and therefore only very flat tracks can be analysed. Consequently we decided to neglect the few measurable

non-interacting tracks and to investigate the energy determination only on the interacting particles.

The measurements that one can make in order to determine the energy of an interacting heavy nucleus are the following:

1) For splitting events (where we assume that the energy of the primary and those of the splitting products are of the same order):
   — scattering on the primary and on the secondary tracks;
   — relative scattering on the splitting tracks;
   — angle of emission of the splitting tracks.

2) For star events:
   — scattering on the primary track;
   — number of black, grey and minimum prongs (from which the visible energy of the star can be derived (^{4})).

14. - Scattering measurements.

Relative scattering measurements have been carried out with the usual method (^{18}). They give very reliable results because they are not affected by spurious scattering and distorsion of the plates. Unfortunately the measurements have to be confined to tracks fulfilling rather strict geometrical conditions: the distance between the two tracks must not exceed 50 μm in the y direction and 20 μm in the z direction (the direction of the primary defines the x-axis). This limitation results in a bias towards the tracks which, being emitted in a very narrow angle, are likely to be the most energetic ones.

Scattering measurements on individual tracks give reasonable results only if it is possible to eliminate the influence of spurious scattering. Since on the plates of stack Y the value of the spurious scattering has been already found to be small (^{18}) and reliable results have been obtained for the energy of very fast protons, we felt justified in estimating the energy of the heavy primaries in the same stack with the same method. We selected for the measurements, tracks whose length per plate is greater than 2 cm and whose total path in the stack is longer than 5 cm. Moreover we compared the results with those obtained following the procedure proposed by FOWLER and WADDINGTON (^{9}). The value of the mean sagittae obtained by the two methods are usually in good agreement within the statistical errors; the energy was derived by using the scattering constant ($K = 32$) proposed by the Bristol group (^{9}).

(^{18}) A. DEBENEDETTI, C. M. GARELLI, L. TALLONE and M. VIGONE: *Nuovo Cimento*, **4**, 1142 (1956).

15. – Mean angle of emission of the α-particles.

The measurement of the angle of emission of the secondaries with respect to the direction of the primary, does not present any experimental difficulties and the error is usually small. We restrict ourselves to the study of the α-particles emitted in the splitting events because in the case of plateau ionization tracks it is impossibile to distinguish between protons and created mesons.

The angle of emission of the α-secondaries in the laboratory system is related to the energy of the primary particle, but depends also from other factors (angle of emission and energy of the secondaries in the centre of mass system) that it is not possible to determine for each case. A very simple relation between the angle of emission and the primary energy has been given by PETERS ([19]) assuming that the α-particles are emitted isotropically and with a mean energy of 12 MeV in the centre of mass system. Peters' formula gives a result which is valid as a mean value, when the angles of many α-tracks are taken into account; but in the case of few tracks, as PETERS pointed out, this formula can easily give a large overestimate of the energy when the α-particles are emitted in the forward or backward direction in the centre of mass system. On the other hand, FOWLER et al. ([12]) observed that the mean angle of emission of the α-particles increases with increasing primary charge; using the integral energy spectrum proportional to $E^{-1,5}$ previously determined ([9]), they found that the mean energy of the α-particles in the centre of mass system increases with the primary charge and that in any case its value seems to be greater that 12 MeV. This effect would mean that the energy calculated with Peters' formula is understimated.

Using our experimental data we looked for the effect of the primary charge on the mean angle of emission, and our results, collected in Table XI, are in perfect agreement with Fowler's ones ([12]).

TABLE XI. – *Dependence of the mean angle of emission of α-particles from the charge of the primary.*

Charge group	L	M	H
θ_x (degrees)	1.11 ± 0.12	1.35 ± 0.10	2.11 ± 0.19
No. of α-particles	49	115	69

([19]) B. PETERS: *Progress in Cosmic Ray Physics*, Vol. **1**, 193 (1952).

In the interpretation of the results we thought that the mean angle of emission of the secondary α-particles may not be a function of the charge of the primary, as it seems from the preceding table, but more likely a function of the number of nucleon pairs involved in the interaction. In order to prove if this assumption is correct, we divided the interactions in groups for which the number of nucleons is the same. This number has been determined for each event in Sect. **11** of the present work. For each group we calculated the mean angle of emission of the α-particles, and the results are given in Table XII.

TABLE XII. – *Dependence of the mean angle of emission of α-particles from the number of nucleon pairs interested in the collision.*

No. of nucleon pairs interested in the collision	$0-1$	$2-3$	$4-5$	$6-7$	$\geqslant 8$
θ_α (degrees)	0.92 ± 0.08	1.16 ± 0.12	1.66 ± 0.19	2.17 ± 0.38	2.46 ± 0.26
No. of α-particles	72	48	43	19	48

The increasing of the mean angle of emission of the α-particles when the number of nucleons involved in the collision increases, might be due to a corresponding increase of the mean energy of the α's in the centre of mass system as suggested by FOWLER ([12]), or to some other effect. The energy of emission of the α-particles has been studied by some authors ([20-22]) but we do not know if their results can be applied to the stars produced by the heavy primaries. For this reason we think that it will be worthwhile to investigate this point using the interaction of the heavy primaries. Only after this analysis, that we plan to carry out in a next work, it will be possible to see if the number of nucleons involved in the interaction has to be accounted for in the determination of the energy.

16. – Energy spectrum.

On 275 interacting tracks measurements could be performed. In 80 events the energy of the primary was derived from the calculation of the visible energy of the star. In 195 splitting events, the energy was obtained from the angles of emission of the secondary nuclei by using Peters' formula.

([20]) N. PAGE: *Proc. Phys. Soc.*, A **63**, 250 (1950).
([21]) D. H. PERKINS: *Phil. Mag.*, **41**, 138 (1950).
([22]) G. BERNARDINI, G. CORTINI and A. MANFREDINI: *Phys. Rev.*, **79**, 952 (1950).

Moreover, in 69 out of the 195 splitting events, either scattering measurements or the study of secondary interactions gave independent values of the energy of the primary. Therefore the energy of these particles is better known, but we cannot base on them an investigation on the energy spectrum of the heavy particles, because, as we said before, the selection of tracks for relative scattering measurements introduces a bias towards the high energy region. Consequently we made use of these 69 tracks only to check if the statistical uncertainty introduced by Peters' formula has a great influence on a distribution of the tracks in wide energy intervals.

In Table XIII we compare the distribution obtained when we attribute to each track the energy evaluated from the angle of emission (distribution A), with the one obtained when the energy of the same tracks is estimated in an independent way (distribution B).

TABLE XIII. – *Check on energy distribution.*

Intervals of energy (GeV/nucleon)	$1.5 \leqslant E \leqslant 4$	$4 < E \leqslant 10$	$E > 10$
No. of tracks (distribution A)	36	24	9
No. of tracks (distribution B)	38	24	7

From the table one can see that if the tracks are divided in wide enough intervals of energy, the various independent methods of evaluating the energy give roughly the same number of tracks in each group. Therefore we think that an attempt to draw the slope of the energy spectrum of the primary particles can be reasonably made; using all the 275 tracks for which we have at least one estimate of the energy and distributing them in the same intervals of energy as in Table XIII we obtain the integral energy spectrum shown in Table XIV.

TABLE XIV. – *Integral energy spectrum.*

Energy (GeV/nucleon)	$E \geqslant 1.55$	$E > 4$	$E > 10$	$E > 50$
Number of tracks	275	91	26	2

Taking for the integral energy spectrum the expression:

$$N(E) = C(E + m_p c^2)^{-k},$$

(where $N(E)$ is the number of heavy primaries with an energy greater than E; $(E + m_p c^2)$ is the total energy in GeV per nucleon, C and k are constants)

we find:

$$k = 1.54^{+0.16}_{-0.13}.$$

This value of the exponent k has been calculated under the assumption that the energy distribution does not depend on the charge of the primaries. Although we know that the statistics is very poor we did the same calculation for the primaries of charge $Z \geqslant 10$. We found for the exponent k the value: $1.5^{-0.3}_{-0.2}$ that seems to indicate that the above mentioned assumption is correct.

* * *

We wish to express our thanks to Prof. R. DEAGLIO and G. WATAGHIN for their constant interest and encouragement.

Thanks are due also to the President of the « Istituto Elettrotecnico Nazionale Galileo Ferraris » for the hospitality given in the photometric laboratory where charge measurements have been carried out with the valuable technical assistence of the photometric staff. We are greatly indebted to Prof. R. DEAGLIO for his helpful suggestions in the design of the photometric device.

The contribution of the scanner's team of our laboratory has to be acknowledged.

APPENDIX I

Comparison B-stack/Y-stack.

As the B and Y stacks have been exposed at the same latitude, the experimental data of the two stacks can be added to derive the energy spectrum and to increase the statistics in the analysis of interactions. On the contrary, to obtain the charge spectrum, we used only the results of the Y-stack. However, as the scanning in both stacks has been made under a nearly equal amount of matter ($\sim 16 \div 17$ g/cm²) the relative abundance of various elements obtained in the two experiments should not be very different except for Lithium and Berillium (owing to the bad scanning efficiency in the B-stack). A comparison of the results seems therefore to be useful, on account of the good resolution obtained in ionization measurements, for the B-stack. The comparison is shown in Table XV in which the errors quoted are the statistical ones.

TABLE XV. – *Comparison between B-stack and Y-stack.*

	No. of B tracks / No. of C tracks	No. of B tracks / No. of M tracks	No. of C tracks / No. of M tracks	No. of N tracks / No. of M tracks	No. of O tracks / No. of M tracks	No. of H tracks / No. of M tracks
B-stack	0.59 ± 0.17	0.28 ± 0.07	0.52 ± 0.05	0.24 ± 0.02	0.13 ± 0.03	0.34 ± 0.08
Y-stack	0.47 ± 0.08	0.24 ± 0.04	0.51 ± 0.04	0.21 ± 0.02	0.17 ± 0.02	0.35 ± 0.04

APPENDIX II

Interactions with a nucleon target.

In Tables XVI (a, b) are given those interactions which can be interpreted as collisions with a single nucleon target (with no meson production). The

TABLE XVI-a. – *Interactions with a nucleon target in the Y-stack.*

Incoming nucleus	Target nucleon	Splitting	Charge identification
Li	n	$\alpha + p$	Photometric measurement
Li	n	$\alpha + p$	» »
Be	n	$\alpha + 2p$	$C \to \alpha + Be$; C: Photometric measurement and δ-ray counting; Be: δ-rays
Be	p (rel.)	2α	Gap counting
Be	n	$\alpha + 2p$	Photometric measurement
Be	n	$\alpha + 2p$	» »
B	n	$2\alpha + p$	Gap and δ-ray counting
B	p (rel.)	$2\alpha + p$	Photometric measurement and δ-rays
B	n	$Be + p$	Photometric measurement
B	p (rel.)	$5p$	» »
C	p (black)	3α	» »
C	n	$2Li$	C: splitting; Li: photometric measur.
C	n	3α	Photometric measurement
C	n	$2\alpha + 2p$	» »
C	n	$Be + \alpha$	» » and gap counting
C	n	$2\alpha + 2p$	Photometric measurement
C	n	$2\alpha + 2p$	» »
C	n	3α	δ-ray counting
C	n	$2\alpha + 2p$	Photometric measurement
C	n	$Li + 3p$	C: Photom. measur.; Li: photom. measur.
N	n	$B + \alpha$	N: δ-ray and gap counting B: δ-rays and photometric measurement
N	n	$3\alpha + p$	Photometric measurement
N	n	$Be + \alpha + p$	N: Photom. measur.; Be: gap counting
N	p (rel.)	$B + \alpha$	N: δ-rays; B: photometric measurement
N	p (rel.)	$\alpha + 5p$	Photometric measurement
N	p (black)	$\alpha + 5p$	» »
O	n	4α	» »
O	n	$C + \alpha$	O: splitting; C.: Photometric measurement
O	p (grey)	$N + p$	O: Photom. measur.; N: Photom. measur.
F	n	$N + \alpha$	F: splitting; N: δ-rays
F	n	$N + \alpha$	F: Photom. measur.; N: Photom. measur.
Ne	n	$C + 2\alpha$	Ne: δ-rays; C: Photometric measurement
Na	n	$F + \alpha$	Na: δ-rays; F: δ-rays

collisions with a single proton target include collisions either with a free proton in the emulsion or with a bound proton of the emulsion nuclei.

We tried to estimate the cross-section of the heavy incoming nuclei with a proton target in emulsion and to compare our results with the experimental cross-section obtained by exposing a heavy nucleus target to a 860 MeV proton beam ([17]). In order to do this, we must also take into account the inter-actions which can be interpreted as collisions with a proton target where some mesons were produced. Such events can not be positively identified and we

TABLE XVI-b. – *Interactions with a nucleon target in the B-stack.*

Incoming nucleus	Nucleon target	Splitting	Charge identification				
Be	p (black)	2α	Photometric measur. and δ-ray counting				
B	n	$2\alpha + p$	»	»	»	»	»
B	p (rel.)	$2\alpha + p$	»	»	»	»	»
B	p (grey)	$2\alpha + p$	»	»	»	»	
C	n	3α	»	»	»	»	»
C	p (black)	$2\alpha + 2p$	»	»	»	»	»
C	n	$Be + \alpha$	C: Photometric measurement and δ-rays				
			Be: »		»	»	»
O	p (black)	$N + p$	O: Photometric measurement and δ-rays				
			N: »		»	»	»
F	n	$N + \alpha$	F: »		»	»	»
			N: »		»	»	»
F	n	$N + \alpha$	F: »		»	»	»
			N: »		»	»	»

can only set an upper limit to their number. This was done by selecting all the events in which the number of outgoing charges exceeded the charge of the incoming nucleus and where at most one non-realtivistic track was noticed. In order to avoid errors due to some imprecision in the determination of charge we restricted our analysis to incoming charges $3 \leqslant Z \leqslant 10$.

The values of the total cross-section (with and without meson production) of heavy nuclei with a proton target emulsion is reported in Table XVII.

TABLE XVII. – *Collision with proton target in emulsion* $(3 \leqslant Z_i \leqslant 10)$.

	No. of collisions with no meson production	Max. number of collisions with meson production	Total range (cm)	σ_H (cm·10^{-25}) elastic (no mesons)	σ_H (cm·10^{-25}) total (max. value)	σ_p (cm·10^{-25}) experimental value of CHEN ([17])
Y + B stack	16^{+2}_{-3}	22	3752	1.5 ± 0.6	3.5 ± 0.5	2.1

This value compared with the correspondent one obtained in [17] shows that at most 40% of the collisions with a proton target in emulsion occurs with a bound proton of an emulsion nucleus. This results is in good agreement with what found independently by other authors [23].

— ———

[23] R. CESTER, T. F. HOANG and A. KERNAN: *Phys. Rev.*, **103**, 1443 (1956).

———————

RIASSUNTO

Sono state analizzate 529 tracce di nuclei pesanti, primari della radiazione cosmica. Su tutte le tracce sono state eseguite misure di carica utilizzando un dispositivo fotometrico; per controllo si sono eseguite misure di carica con conteggio di gap su tracce di boro e carbonio. Tutte le tracce sono state seguite nell'emulsione; nel corso delle osservazioni sono state rilevate 331 interazioni nucleari. L'analisi di queste interazioni ha permesso di determinare il libero cammino medio e le probabilità di frammentazione in emulsione ed in aria. I risultati, che sono in buon accordo con quelli ottenuti in altri laboratori, sono stati utilizzati per estrapolare al top dell'atmosfera lo spettro di carica. Al top dell'atmosfera il valore del rapporto tra nuclei leggeri e nuclei medi è 0.30 ± 0.09, quello del rapporto tra nuclei pesanti e nuclei medi è 0.51 ± 0.11. È stata misurata l'energia di 275 tracce per determinare l'esponente K che compare nella formula $N(E) = C(E + m_p C^2)^{-K}$ dello spettro integrale. Il risultato è $K = 1.54^{+0.16}_{-0.13}$. L'analisi è stata eseguita utilizzando la relazione di Peters tra l'energia del primario e l'angolo di emissione dei prodotti di frammentazione. I limiti di validità di tale relazione sono discussi nel corso del lavoro.

Further Measurements on n, p Reactions at 14 MeV: Ti, Rh, Sn, Ta, Au and Angular Distribution of Protons Emitted in the Ca (n, p) and Ni (n, p) Reactions.

L. Colli, U. Facchini, I. Iori, G. Marcazzan and A. Sona

Laboratori CISE - Milano

M. Pignanelli

Istituto di Scienze Fisiche dell'Università - Milano
Istituto Nazionale di Fisica Nucleare - Sezione di Milano

Summary. — This paper will present the spectra of protons emitted by (n, p) reactions with 14 MeV energy neutrons on the medium weight and heavy elements: Ti, Rh, Sn, Ta, Au. Angular distributions are also presented on the two elements: Ca, Ni. This spectra have been obtained by improving the technique already employed for lighter elements, which makes use of coincidence between scintillating and gas counters.

1. - Introduction.

This work is a continuation of previous researches to investigate the mechanism of nuclear reactions at intermediate energies [1-3].

For the measurements reported here a new type of spectrometer was used to detect the emitted protons, which was modified with respect to the type used in previous works.

The new apparatus made it possible to obtain an appreciable reduction in the background, so that we could measure the spectrum of the protons emitted

[1] L. Colli and U. Facchini: *Nuovo Cimento*, **4**, 671 (1956).
[2] C. Badoni, L. Colli and U. Facchini: *Nuovo Cimento*, **4**, 1618 (1956).
[3] L. Colli and U. Facchini: *Nuovo Cimento*, **5**, 309 (1957).

in the reaction (n, p) by heavy nuclei such as Ta and Au, having for this reaction a cross-section many times smaller than that of nuclei previously investigated. Moreover it was possible to measure the angular distribution of the protons emitted in these reactions in the case of the nuclei Ca and Ni.

2. - Experimental apparatus.

The spectrometer used, shown in Fig. 1, consists of a chamber containing a target of the element under study, two proportional counters and a CsI crystal, connected externally with a photomultiplier. The walls of the chamber are lined with graphite, so is the target support.

The targets are carried on a wheel inside the chamber, which can be turned from outside by means of a magnet, and permits the replacement of the target without opening the spectrometer. The wheel carries 6 different targets, one of which of graphite to measure the background and one of polythene furnishing hydrogen recoil protons that are used for energy calibration.

The wires of the counter are of platinum while their supporting rods are of gold. The chamber is filled with CO_2 at 7 cm Hg pressure. The CsI(Tl) crystal is cut out in the form of a disc of 40 mm diameter and 2 mm thickness, and in order to screen it

Fig. 1. – Proton detector: 1, chamber with two proportional counters; 2, Stupakoff seals with pulse output; 3, CsI crystal; 4, photomultiplier; 5, container; 6, target; 7, wheel with target support.

from the light produced by the Townsend avalanches in the counters, an aluminum sheet of 0.02 mg/cm² is placed over it.

The voltage and the bias of the counter are so adjusted as to count pulses greater than or equal to those due to 14 MeV protons. The protons then give out their energy in the crystal, which then gives a pulse proportional to the energy of the protons.

The pulses given by the photomultiplier in coincidence with both counters are analyzed by a 99 channel pulse analyzer.

The targets of the element under study are thin with respect to the range

of 4 MeV protons. By crossing the targets and all through the instrument before entering the crystal, these protons lose 0.5 MeV of energy.

The element under study is bombarded with neutrons of 14.5 MeV energy, produced by the reaction $D+T = n+\alpha$, utilizing a deuteron beam of a few μA accelerated by 200 keV over a tritium-zirconium target of 1 cm diameter.

The intensity of the emitted neutrons is monitored by a scintillating counter consisting of an anthracene crystal and a photomultiplier.

The measurements consist in detecting successively the spectrum of the recoil protons of hydrogen, the spectrum of the background and that of the element under study.

In the series of measurements that give the spectrum of the elements Ti, Rh, Sn, Ta and Au, the target to be irradiated is placed at a 3 cm distance form the source of 14.5 MeV neutrons.

Thus, the protons emitted forward with angles between 0° and 40° are detected.

The measurements that give the spectrum of Ca and Ni at various angles are made with better angular precision, and therefore the target was placed at 10 cm distance from the neutron source. To obtain various emission angles, the entire instrument is turned around an axis passing over a diameter of the target. The protons are thus taken with an angular opening corresponding to about 20° for 0° position, to 30° for the 45° position, and to 20° for the two other positions studied.

The calibration of the energy scale is made by measuring the recoil protons of hydrogen. In order to obtain a well-defined line of monoenergetic protone by this measurements it is necessary to use a very good collimation for the proton emitted. The measurement was therefore made by using a polythens target of 1 cm diameter as a radiator, placing it at 10 cm distance from the neutron source. The scintillator in the apparatus was screened by a Pb diaphragm with a 1 cm hole so that only the uncovered central region is efficient. With this arrangement the spectrum shown in Fig. 2 was obtained,
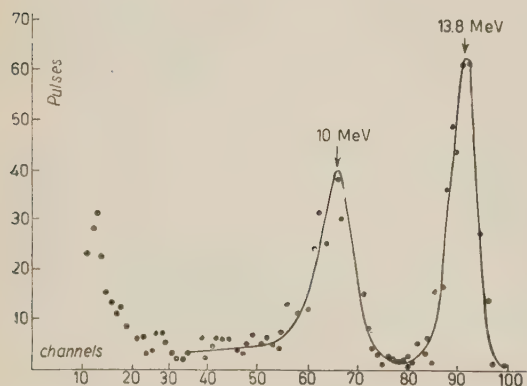
Fig. 2.—Spectrum of hydrogen recoils for calibration. The higher energy line (right) corresponds to 13.8 MeV protons, that is protons scattered at about 0° with the incident beam. The other line corresponds to the same protons absorbed by a layer of lead 22/100 mm. thick. In both cases, the width of the line is mostly due to the angular width.

where the higher energy line corresponds to protons emitted at 0° and the lower energy line to the same protons absorbed by a layer of lead 22/100 mm thick.

The width of the lines can be attributed to a large extent to the angular opening.

As the energy of the protons emitted by the polythene in this arrangement is known, and since the CsI crystal is linear, the entire energy scale is therefore known. Furthermore, the spectra were corrected for proton absorption in the targets and in the counter.

To give an idea of the quantity of the effect observed with respect to the background, we are reporting in Fig. 3 the background spectrum (graphite target) and that of the protons emitted by an aluminium target of 11.9 mg/cm². For heavier elements (Ta and Au) the counting with the target under study was about double that with graphite.

The time required to obtain the spectrum of the protons emitted by an element varies between 5 and 20 hours. The results were obtained with good reproducibility.

As can be seen in Fig. 3 the background is very low above the 20° channel, corresponding to protons of 4 MeV energy, and presents a steep rise at lower energies. This rise has prevented the study of the parts of the spectra below 4 MeV.

Fig. 3. – Proton spectrum of Al (n, p) given by a target 11.9 mg/cm² thick (2) and the background spectrum (1) corresponding to the same amount of irradiation.
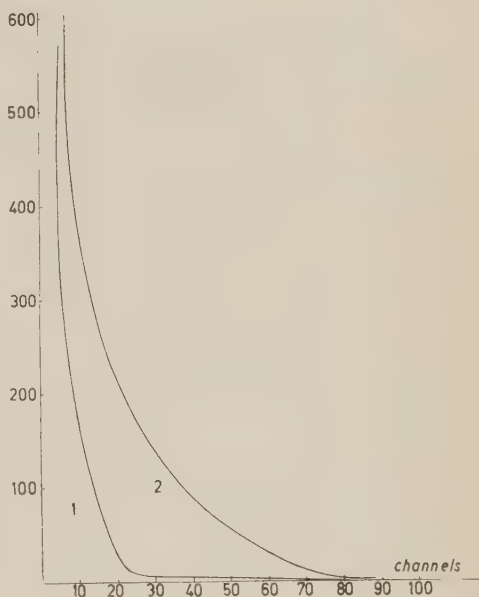
3. - Results for elements Ti, Rh, Sn, Ta, Au.

The proton spectra of the elements Ti, Rh, Sn, Ta, Au were obtained in analogous conditions with an angle for proton direction including protons emitted between 0° and 40°. These spectra are shown in Fig. 4, 5, 6, 7, 8.

The experimental conditions applied here are not much different from those described in the previous works excepted the useful angle, that was between 0° and 60°. The spectra of Ni, Al, Zr and Fe were taken again
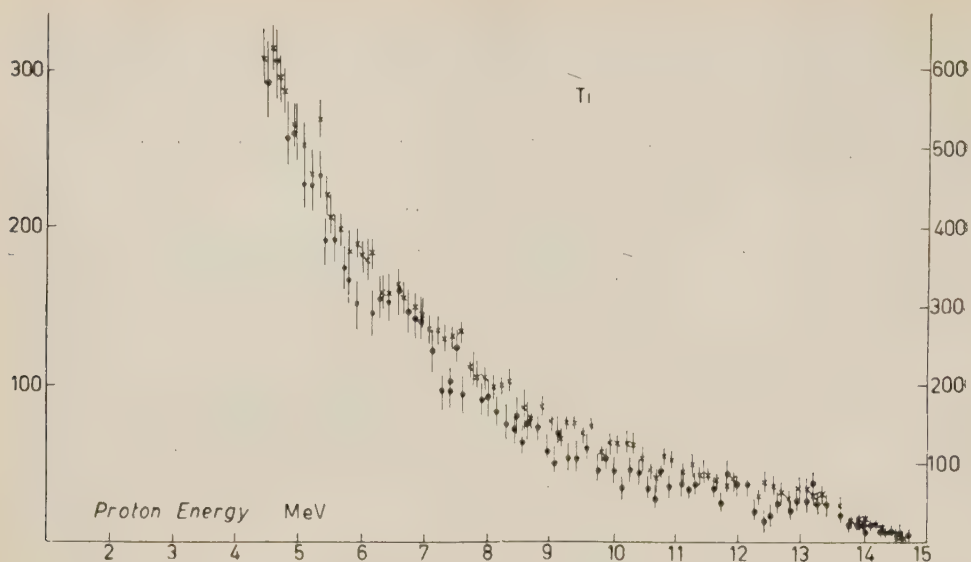
Fig. 4 to 8. – Proton spectra from Ti (n, p), Rh (n, p), Sn (n, p), Ta (n, p), Au (n, p). The two series of points for Ti (n, p) have been obtained with two different target thicknesses (10.35 and 20.7 mg/cm²).
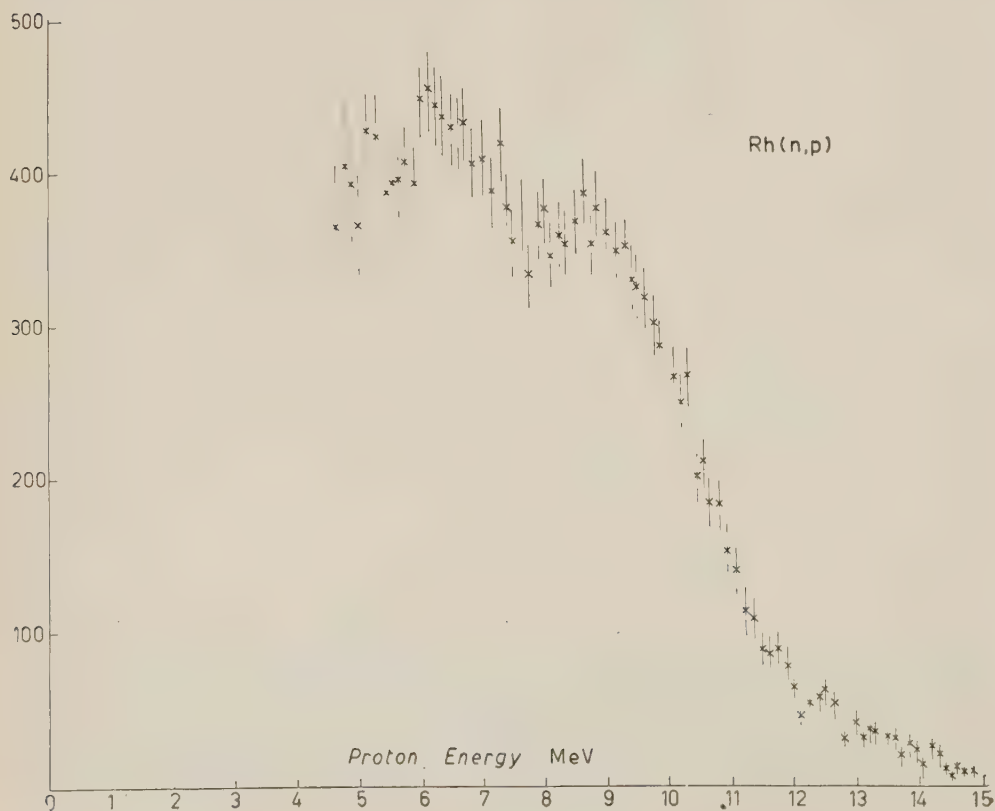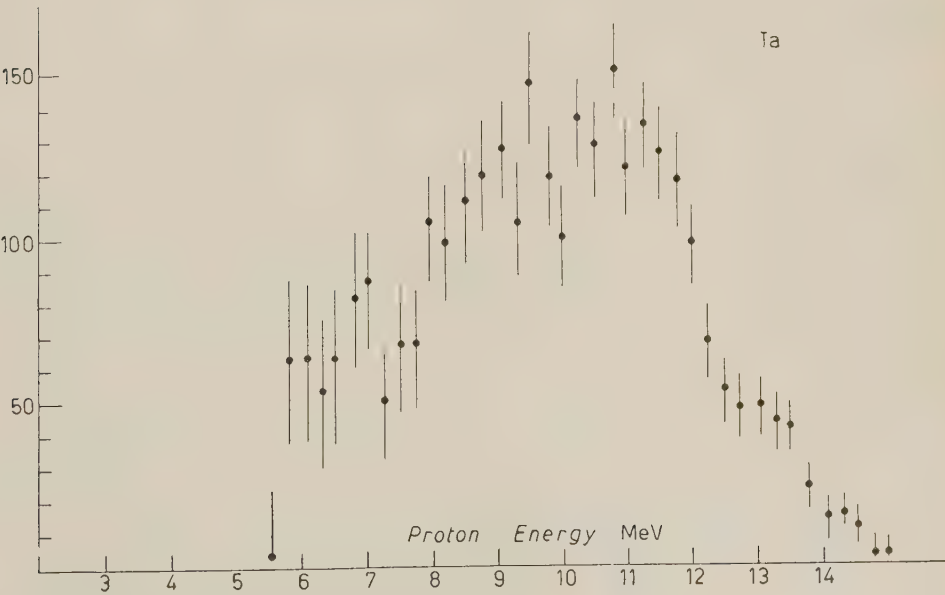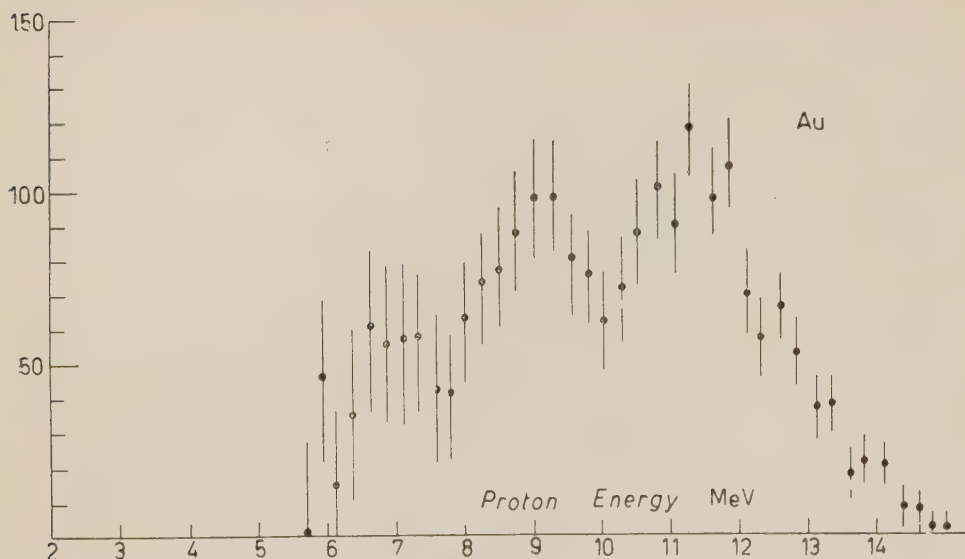

Fig. 5.
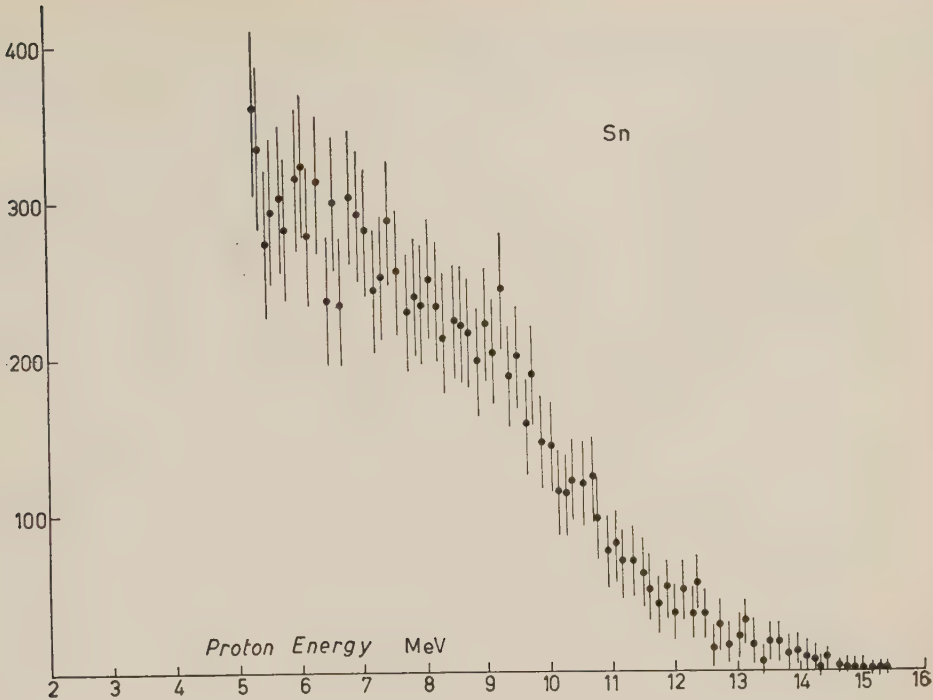
Fig. 6.

Fig. 7.

Fig. 8.

under the new conditions and the results were found identical to those already published.

Ti.   75% of the isotopic mixture is made up of ^{48}Ti which for ^{48}Ti(n, p)^{48}Sc reaction has $Q = -3.2$ MeV. The other isotopes ^{46}Ti (7.9%) and ^{47}Ti (7.7%), have a Q value respectively -1.58 and ~ 0.

As the spectrum extends up to 14 MeV, it seems that the isotope ^{47}Ti contributes notably to the reaction. The reaction Ti(n, n p) is not possible for proton energies over 4 MeV.

Rh. ^{103}Rh is the only isotope and has $Q \sim 0$.

This spectrum is very interesting because it shows a rather pronounced bump at about 8.5 MeV energy. These deviations from the monotonous form in the case of some spectra have not received any explanation on the basis of nuclear reaction theories under discussion at present (^{2}).

The fall under 6.5 MeV is in agreement with the existence of Coulomb barrier.

The spectrum of (n, p) reaction in the case of Rh was measured with the method of nuclear plates by G. BROWN and al. (^{4}) who obtained results in good agreement with ours.

The reaction Rh (n, np) can take place under 8.5 MeV.

(^{4}) G. BROWN, G. C. MORRISON, H. MUIRHEAD and W. T. MORTON: *Phil. Mag.*, **2**, 785 (1957).

Sn. Since natural tin is a mixture of various isotopes, it is not possible to attribute the reaction to anyone of them in particular. The descent in the case of lower energies due to Coulomb barrier is hardly visible.

Ta and Au. The spectra of Ta and Au are very similar. In both cases the Q of reaction (n, p) is ~ 0 and the reaction (n, np) can contribute at energies respectively below 8 and 8.5 MeV. The action of Coulomb barrier under 9 MeV is clearly visible.

TABLE I. – *Relative cross-sections for protons of energy above 5 MeV and emitted in the solid angle accepted by the counter. Same relative unity as in (3).*

Nucleus	Z	Relative cross-section (Nickel = 3.1)
Al	13	0.830 ± 20%
Ti	22	0.66 »
Fe	26	0.94 »
Ni	28	3.1 »
Zr	40	0.8 »
Rh	45	0.53 »
Sn	50	0.45 »
Ta	73	0.12 »
Au	79	0.08 »

In Table 1 the cross-section relative to various elements measured under the conditions described are shown. They were calculated for protons emitted with energy greater than 5 MeV.

It is not possible to calculate the absolute value of the cross-sections since our results refer to protons emitted in the forward direction with an angle between 0° and 40°, and it is possible that the cross-section for this reaction varies with the variation of the emission angle (⁴).

The value of the relative cross-sections for heavy elements and especially the disappearance of low energy protons indicate that proton emission is affected by Coulomb barrier.

4. – Results on angular distribution for Ca and Ni.

The measurements of the angular distribution of these two elements have been made with the geometrical arrangement described in part 2.

In Figs. 9, 10, the spectra obtained for the elements Ca and Ni at various angles are shown.
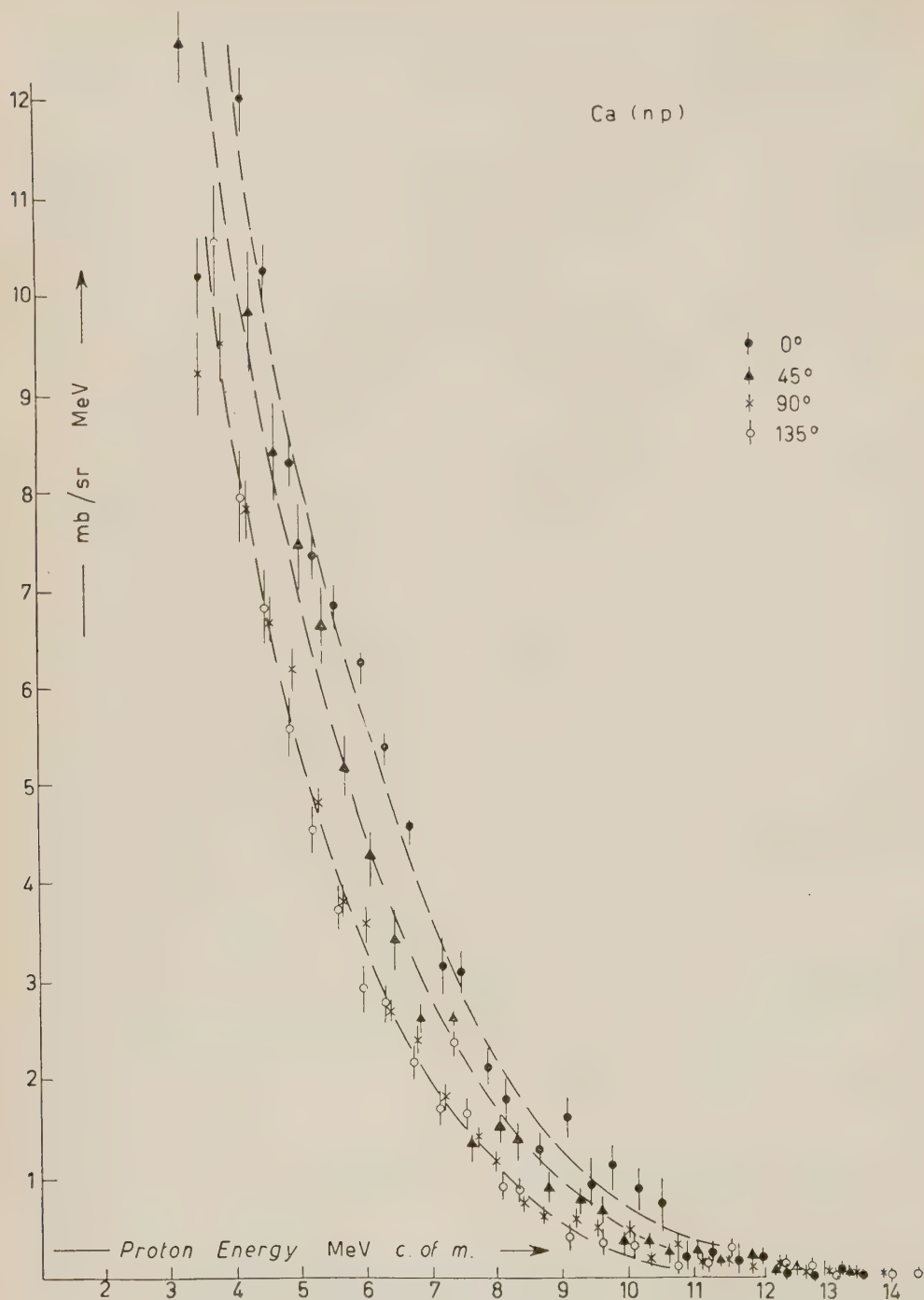
Fig. 9. – Spectrum from Ca (n, p) taken at four different angles in the center of
mass system.

Our results show that in these two cases the spectrum of protons is more intense in the forward direction than in the backward. The form of the spectrum, however, remains pratically unchanged at various angles in the case
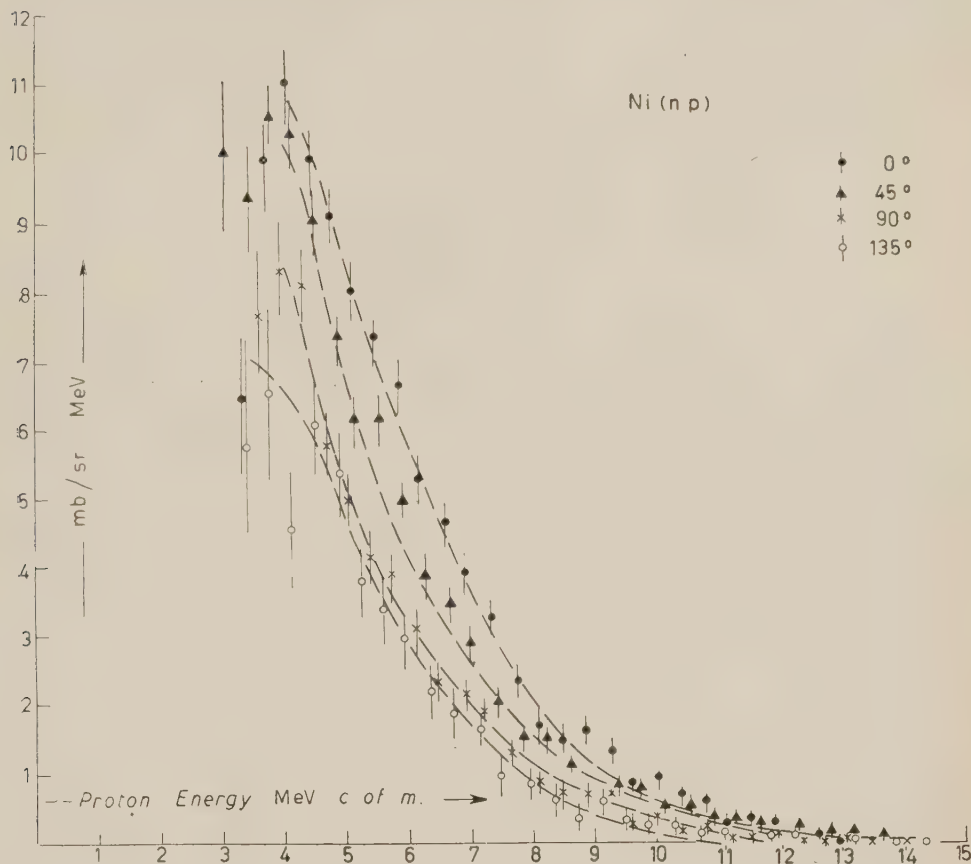

Fig. 10. – Spectrum of Ni (n, p) taken at four different angles in the center of mass system.

of Ca, while in the case of Ni a slight increase in the section at higher energies is observed for the spectrum emitted forward. Similar results were obtained for Cu by ALLAN (⁵) and for Al, Fe, Rh by BROWN *et al.* (⁵) using the method of nuclear plates.

(⁵) D. L. ALLAN: *Proc. Phys. Soc.*, A **70**, 195 (1957) and private communication.

* * *

RIASSUNTO

In questo lavoro sono presentati gli spettri di protoni prodotti in reazioni (n, p) ottenuti con neutroni da 14 MeV sugli elementi medi e pesanti: Ti, Rh, Sn, Ta ed Au. Vengono anche presentate le distribuzioni angolari per il Ca ed il Ni. Questi spettri sono stati ottenuti mediante un perfezionamento di una tecnica, già impiegata per gli elementi più leggeri, che fa uso di coincidenze fra contatori a scintillazione e contatori proporzionali.

LETTERE ALLA REDAZIONE

Relation of Charge Independence and Baryon Conservation to Pauli's Transformation (*).

Feza Gürsey (+)

Brookhaven National Laboratory - Upton, N.Y.

Pauli [1] has recently introduced a 4-parameter group, isomorphic to the group of unitary 2×2 matrices, which leaves the neutrino equation invariant. These generalized gauge transformations have been used in connection with β interactions by several authors [2]. The purpose of this note is twofold. First we devise a formalism in which the Pauli transformations are actually represented by 2×2 unitary matrices. Then we show that this group can be extended to particles with mass and charge. As applied to the nucleon, this formalism implies the separation of the 8-component nucleon wave function into two 4-spinors χ and ζ, the first involving only the even components of the proton and neutron wave functions, and the second only their odd components. It then appears that the equation of the nucleon interacting with a pion field is invariant against a 4-parameter generalized gauge group which is closely related to the Pauli transformations and leads directly to charge independence as well as baryon conservation, thus combining isotopic spin rotations and baryon gauge transformations in a single unitary group.

In order to represent the Pauli group by unitary 2×2 matrices, we choose the Weyl representation for the γ operators:

$$(1) \qquad \gamma_0 = \begin{pmatrix} 0 & I \\ I & 0 \end{pmatrix}, \qquad \gamma_n = \begin{pmatrix} 0 & -\sigma_n \\ \sigma_n & 0 \end{pmatrix}, \qquad \gamma_5 = \begin{pmatrix} I & 0 \\ 0 & -I \end{pmatrix}.$$

Let ψ denote a 4-spinor. Then, the projection operators $(1 \pm \gamma_5)$ select the first two (ψ_1, ψ_2) and the last two (ψ_3, ψ_4) components of ψ respectively. The two spinors thus defined will be called even or odd components of ψ according as they cor-

---

(1) W. Pauli: *Nuovo Cimento*, **6**, 204 (1957).

(2) C. Enz: *Nuovo Cimento*, **6**, 250 (1957); D. L. Pursey: *Nuovo Cimento*, **6**, 266 (1957).

respond to the eigenvalues ± 1 of γ_5. To exhibit this separation explicitly we represent ψ by the 2×2 matrix Ψ (wave matrix),

$$(2) \qquad\qquad \Psi = \begin{pmatrix} \psi_1 & -\psi_4^* \\ \psi_2 & \psi_3^* \end{pmatrix}$$

the first column of which is even and the second one odd. The Dirac equation can be written in terms of Ψ ([3]) and various operations on ψ induce corresponding operations on Ψ. A list of such correspondences has already been given ([4]). In particular, if ψ undergoes a Lorentz transformation

$$(3) \qquad\qquad \psi' = \mathcal{L}\psi = \left(\exp\left[\tfrac{1}{2}\sigma_{\mu\nu}a_{\mu\nu}\right]\right)\psi ,$$

the transformation induced on Ψ is

$$(3') \qquad\qquad \Psi' = L\Psi ,$$

where L is a constant 2×2 matrix whose determinant is $+1$. We note that L multiplies Ψ *to the left*. Now, because of the correspondences

$$(4) \qquad\qquad \gamma_5\psi \leftrightarrow \Psi\sigma_3 ,$$

$$(5) \qquad\qquad i\psi \leftrightarrow \Psi i\sigma_3 ,$$

$$(6) \qquad\qquad \psi^c = C\bar\psi = \gamma_2\psi^* \leftrightarrow \Psi\sigma_2 ,$$

the 1-parameter transformation

$$(7) \qquad \text{I:} \qquad \psi \to \psi\cos\lambda + i\gamma_5\psi\sin\lambda \qquad\qquad (\lambda\text{: real}),$$

and the 3-parameter transformation

$$(8) \qquad \text{II:} \qquad \psi \to a\psi + b\gamma_5\psi^c \qquad\qquad (|a|^2+|b|^2=1),$$

correspond respectively to

$$(7') \qquad \text{I':} \qquad \Psi \to \Psi\exp[i\lambda] ,$$

$$(8') \quad \text{and II':} \qquad \Psi \to \Psi R = \Psi\exp[i\boldsymbol\sigma\cdot\boldsymbol l] \qquad\qquad (\boldsymbol l\text{: real}).$$

Here R is the 2×2 rotation matrix. Combining I' and II' we obtain the following representation of the Pauli group:

$$(9) \qquad G_P: \qquad \Psi \to \Psi R\exp[i\lambda] = \Psi U \qquad\qquad (UU^\dagger=1).$$

([3]) F. GÜRSEY: *Nuovo Cimento*, **3**, 988 (1956).
([4]) F. GÜRSEY: *Rev. Fac. Sci. Univ. Istanbul*, A **21**, 33 (1956).

Consequently, under an operation of the Pauli group, the wave matrix Ψ is multiplied *to the right* by a 2×2 unitary matrix.

An obvious generalization of (9) is provided by

$$(10) \qquad\qquad \mathcal{G}: \qquad\qquad\qquad\qquad \Psi \to \Psi S , \qquad\qquad\qquad\qquad (|\operatorname{Det} S| = 1),$$

where S is a unimodular matrix. This 7-parameter group also leaves the neutrino equation invariant but does not preserve the commutation relations. $\mathcal{G}$ may be written as the combination of $(7')$ and the 6-parameters group

$$(11) \qquad\qquad \mathcal{G}_\Lambda: \qquad\qquad\qquad\qquad \Psi \to \Psi \Lambda , \qquad\qquad\qquad\qquad (\operatorname{Det} \Lambda = + 1),$$

which, on comparison with $(3')$ is seen to be isomorphic to the Lorentz group. The transformations (8) isomorphic to rotations form a subgroup of $\mathcal{G}_\Lambda$.

We now treat the case of a particle with finite rest mass. Consider two 4-spinors χ and ζ to which correspond the wave matrices X and Z, Let $\overline{X} = X^{-1} \operatorname{Det}(X)$ denote the adjoint matrix of X. The system of equations

$$(12) \qquad \begin{cases} D\overline{Z}^{\dagger} = \quad imX \\ D\overline{X}^{\dagger} = - imZ \end{cases} \quad \text{or} \quad \begin{cases} \gamma_\mu \partial_\mu \zeta = \quad im\gamma_5\chi , \\ \gamma_\mu \partial_\mu \chi = - im\gamma_5\zeta , \end{cases}$$

where $D = \partial_0 - \boldsymbol{\sigma} \cdot \boldsymbol{\nabla}$, leads to the Klein-Gordon equations for a particle of mass m. If we introduce new wave matrices by

$$(13) \qquad \begin{cases} \mathrm{p} = \tfrac{1}{2}X(1 + \sigma_3) + \tfrac{1}{2}Z(1 - \sigma_3) , \\ \mathrm{n} = [\tfrac{1}{2}X(1 - \sigma_3) - \tfrac{1}{2}Z(1 + \sigma_3)]\sigma_1 , \end{cases}$$

we obtain the equivalent equations

$$(14) \qquad \begin{cases} D\overline{\mathrm{p}}^{\dagger} = im\mathrm{p}\sigma_3 \\ D\overline{\mathrm{n}}^{\dagger} = im\mathrm{n}\sigma_3 \end{cases} \quad \text{or} \quad \begin{cases} \gamma_\mu \partial_\mu \psi_\mathrm{p} = im\psi_\mathrm{p} , \\ \gamma_\mu \partial_\mu \psi_\mathrm{n} = im\psi_\mathrm{n} , \end{cases}$$

where ψ_p and ψ_n are the 4-spinors which correspond to p and n and may be regarded as the wave functions of the proton and the neutron. We note that the form (12) of the nucleon equation corresponds to the separation of the proton and neutron 4-spinors into even and odd components since we have

$$(15) \qquad \begin{cases} \chi = \tfrac{1}{2}(1 + \gamma_5)\psi_\mathrm{p} + \dfrac{i}{2}[(1 + \gamma_5)\psi_\mathrm{n}]^e , \\ \zeta = \tfrac{1}{2}(1 - \gamma_5)\psi_\mathrm{p} - \dfrac{i}{2}[(1 - \gamma_5)\psi_\mathrm{n}]^e . \end{cases}$$

Now Eq. (12) is obviously invariant against the 4-parameter group

$$(16) \quad \begin{cases} Z \to ZU = ZR \exp\left[i\lambda\right], & (UU^\dagger = 1) \\[2mm] X \to X\overline{U}^\dagger = XR \exp\left[-i\lambda\right], \end{cases}$$

which is a modification of the Pauli group as applied to massive particles. The analogue of (7) is obtained by taking $U = \exp\left[i\lambda\right]$. This induces the transformation

$$(17) \qquad \psi_\mathrm{p} \to \psi_\mathrm{p} \exp\left[i\lambda\right], \qquad \psi_\mathrm{n} \to \psi_\mathrm{n} \exp\left[i\lambda\right],$$

which is the baryon gauge transformation connected with the conservation of the baryon number. The special case $U = R$ gives rise to transformations isomorphic to rotations and corresponds to (8) and (8'). It can be shown immediately that these transformations induce isotopic spin rotations of ψ_p and ψ_n. Another special case

$$(18) \qquad U = \exp\left[\frac{i}{2}\left(1 + \sigma_3\right)\right],$$

which is the analogue of the Nishijima transformation [5] $\psi \to \{\exp\left[i/2(1+\gamma_5)\alpha\right]\}\psi$, leads to the ordinary gauge transformation.

$$(19) \qquad \psi_\mathrm{p} \to \psi_\mathrm{p} \exp\left[i\alpha\right], \qquad \psi_\mathrm{n} \to \psi_\mathrm{n},$$

connected with charge conservation.

The nucleon interacting with pseudoscalar pions obeys the equation

$$(20) \quad \begin{cases} D\overline{Z}^\dagger = iX(m + ig\boldsymbol{\sigma}\cdot\boldsymbol{\pi}), \\[2mm] D\overline{X}^\dagger = -iZ(m - ig\boldsymbol{\sigma}\cdot\boldsymbol{\pi}), \end{cases}$$

or,

$$(20') \quad \begin{cases} \gamma_\mu\partial_\mu\zeta = i\gamma_5[(m + ig\pi_3)\chi + g(\pi_1 + i\pi_2\gamma_5)\chi^c], \\[2mm] \gamma_\mu\partial_\mu\chi = i\gamma_5[(-m + ig\pi_3)\zeta + g(\pi_1 + i\pi_2\gamma_5)\zeta^c], \end{cases}$$

which is invariant under the simultaneous transformation (16) and

$$(21) \qquad \boldsymbol{\sigma}\cdot\boldsymbol{\pi} \to U\boldsymbol{\sigma}\cdot\boldsymbol{\pi}\,\overline{U}^\dagger = R\boldsymbol{\sigma}\cdot\boldsymbol{\pi}\,R^{-1},$$

which is just an isotopic spin rotation of the meson field wave function $\boldsymbol{\pi}$ (π_1, π_2, π_3).

It is an interesting fact that Eq. (20), unlike the free particle equation (12), admits an enlarged group isomorphic to 4-dimensional rotations and mixing m

---

[5] K. NISHIJIMA: *Nuovo Cimento*, **5**, 1349 (1957).

and π, whereas a scalar meson theory would lead to invariance with respect to a group isomorphic to the Λ-transformations (11).

Another result which proves to be useful in the formulation of weak interactions is that interaction terms in the Lagrangian involving only the χ or ζ components of the nucleon wave function lead to the violation of both parity and charge conjugation but to the conservation of their product CP.

The application of these methods to the strong and weak interactions of other elementary particles will be discussed in a more detailed communication.

* * *

It is a pleasure to thank Prof. YANG, Dr. NISHIJIMA and Prof. DYSON for valuable discussions.

Note added in proof:

Strictly speaking, transformation (17) is the nucleon number gauge transformation, which, in a generalization of the theory, may be regarded as corresponding to the conservation of either baryons or isofermions. In a theory involving strange particles it is only in the latter case that the Nishijma transformation (18) represents the charge gauge transformation.

A Circular Polarimeter for Low Energy γ-Rays.

M. Bernardini, P. Brovetto, S. Debenedetti (*) and S. Ferroni

Istituto di Fisica dell'Università - Torino

The measurement of circular polarization of γ-rays is of interest in connection with the new ideas on parity non-conservation in β-decay [1,2]. For this purpose we have built a γ-circular polarimeter based on Compton back-scattering from iron magnetized parallel and antiparallel to the incident radiation. This design presents two advantages over polarimeters previously described [3]: it makes use of the maximum percentage difference for the two directions of polarization, and can be employed at relatively low energy.

The Compton cross section, as a function of the momenta k_0 and k of the incident and scattered γ-ray, is given by [4]:

$$\frac{d\sigma}{d\omega} = \frac{1}{2}\left(\frac{e}{m_0 c^2}\right)^2 \left(\frac{k}{k_0}\right)^2 \left\{\left[\frac{k_0}{k} + \frac{k}{k_0} - \sin^2 \vartheta\right] \pm \right.$$

$$\left. \pm \left[\left(\frac{k_0}{k} - \frac{k}{k_0}\right)\cos \vartheta \cos \Psi + \left(1 - \frac{k}{k_0}\right)\sin \vartheta \, \sin \Psi \sin \varphi\right]\right\},$$

where ϑ is the scattering angle, Ψ the angle between k_0 and the electron's spin, φ the azimuth, and the signs $+$ and $-$ refer respectively to right and left circular polarization.

Fig. 1 shows the percentage difference between the atomic cross sections of saturated Fe for $\Psi = 0$ and for $\Psi = 180°$, as a function of ϑ. Saturation is obtained in iron with $B = 21\,600$ G and in these conditions 2 electrons out of 26 are polarized. For very high energies the effect becomes 15.38% both for forward and back-

---

(*) Fulbright Scholar 1956-57; permanent address, Physics Department, Carnegie Institute of Technology, Pittsburgh 13 - Pennsylvania.

[1] T. D. Lee and C. N. Yang: *Phys. Rev.*, **104**, 254 (1956).

[2] M. Goldhaber, L. Grodzins and A. W. Sunyar: *Phys. Rev.*, **106**, 826 (1957).

[3] S. B. Gunst and L. A. Page: *Phys. Rev.*, **92**, 970 (1953); J. C. Wheatley, W. J. Huiskamp, A. N. Diddens, M. J. Steenland and H. A. Tolhoek: *Physica*, **21**, 841 (1955).

[4] W. Franz: *Ann. d. Phys.*, **33**, 698 (1938).

scattering. However, at these energies it is more convenient to use forward scattering since backscattering cross sections become smaller with increasing energy.
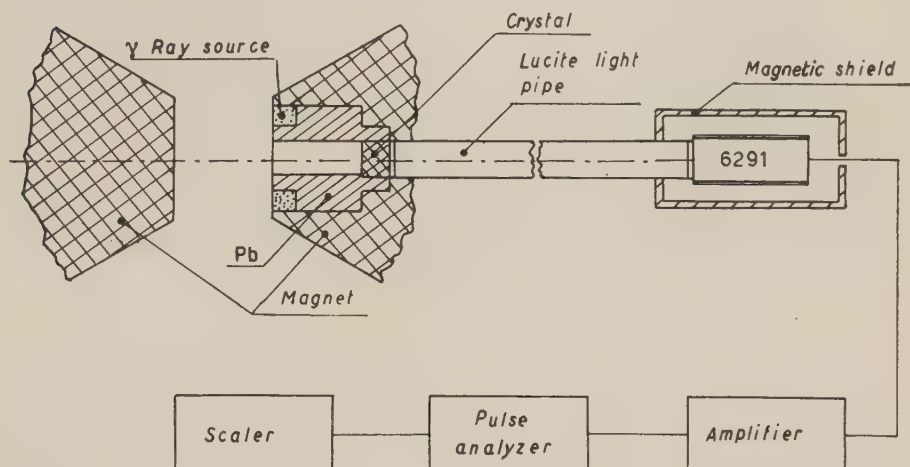

Fig. 1. – The curves represent the computed effect for scattering from saturated Fe (1 electron on 13 aligned). The function plotted as a function of θ is:

$$F(\theta) = \frac{2}{13} \left[\left(\frac{d\sigma}{d\omega} \right)_{\psi=0} - \left(\frac{d\sigma}{d\omega} \right)_{\psi=\pi} \right] \Big/ \left[\left(\frac{d\sigma}{d\omega} \right)_{\psi=0} + \left(\frac{d\sigma}{d\omega} \right)_{\psi=\pi} \right].$$

The energy in $m_0 c^2$ is indicated for each curve.

The advantage of working at $\vartheta = 180°$ is obvious at low energies. For a scattering angle of $180°$ the expected effect, as a function of incident photon energy, is in $m_0 c^2$ units:

$$\frac{2}{13} \left\{ 1 + \left[2 \frac{k_0}{m_0 c^2} \left(1 + \frac{k_0}{m_0 c^2} \right) \right]^{-1} \right\}^{-1},$$

of course experimentally such an effect will be found smaller because of multiple scattering in iron.

In our instrument (Fig. 2), a toroidal radioactive source is located on one of the pole pieces of a magnet, and the γ-rays are back-scattered from the other pole piece. They are detected by a NaI scintillator situated in an axial hole in the first pole and shielded with Pb from the direct radiation of the source. The iron acting as back scatterer can be magnetized to saturation. A light-pipe 100 cm long
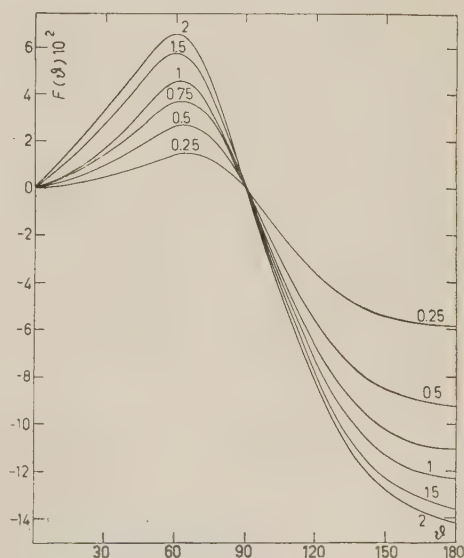

Fig. 2. – Experimental arrangement.

leads the light from the scintillator to a 6291 photomultiplier, protected by a magnetic shield from the fringing field of the magnet. For unpolarized γ-rays the effect of reversing the field is about 0.2%. The photomultiplier pulses are amplified, fed to a single channel pulse-height-selector, and then to a scaler. The response of the experimental equipment was calibrated with the X-rays of ^{180}Ta (prepared with the Turin's betatron) and with the annihilation line of ^{22}Na.

The pulse height selection eliminates or at least greatly reduces the background due to impurities of the source, to natural radioactivity and to the dark current of the phototube.

The geometry of the polarimeter and of the shielding can be varied according to the energy of the γ-rays to be studied. The range of usefulness of the instrument is limited by shielding difficulties on the high energy side, and by the predominance of photo-effect in Fe, on the low energy side.

* * *

Non-Conservation of Parity in K-Capture.

M. Bernardini, P. Brovetto, S. Debenedetti (*) and S. Ferroni

Istituto di Fisica dell'Università - Torino

The effects of non-conservation of parity in β-decay have been experimentally observed for β⁻ and β⁺ emission. We are going to report here an experiment which shows non-conservation of parity in K-capture, through the observation of the circular polarization of internal bremsstrahlung. This effect has been theoretically predicted by Cutkosky [1]; in the case of a two component neutrino theory the internal bremsstrahlung is expected to be 100% right-handedly polarized.

The source chosen was ^{71}Ge, selected mostly because of ease of procurement and convenience of half life (12 days). Since the maximum energy of internal bremsstrahlung is 230 keV [2] we had to design a γ-ray circular polarimeter suitable for use at low energy. This is based on backward Compton scattering, and is described in the preceding note.

Our source consisted of 20 g of natural GeO_2 irradiated at Harwell for three weeks, in a flux of $3.5 \cdot 10^{11}$ neutrons/cm² s. The isotopic mixture contained 500 mC of ^{71}Ge and some impurities of ^{77}Ge (12.8 h; several intense and energetic γ) and ^{77}As (39 h; 245 keV γ, 1.4%; 525 keV γ, 0.5%). Since the internal bremsstrahlung of ^{71}Ge is emitted only in 0.004% of the disintegrations, the presence of impurities is important.

The radiations of ^{77}Ge penetrated our Pb shield, and the decay of this isotope was followed with a Pb plug in front of the scintillator. A half life of 12.73 h was found. Five days after the end of irradiation this activity was negligible and we began analyzing, as a function of the energy, the radiation back scattered from the iron. For energies larger than 120 keV (maximum energy of back-scattered bremsstrahlung from ^{71}Ge), a mean life of 39 h was found, attributable to ^{77}As. For energies smaller than 120 keV the decay has been found to correspond to a mixture of ^{77}As and ^{71}Ge.

---

[1] R. E. Cutkosky: *Phys. Rev.*, **107**, 330 (1957). We thank Professor Cutkosky for having informed us of his results previous to publication. See also: G. W. Ford: *Phys. Rev.*, **107**, 321 (1957); J. Sawicki and J. Szymansky: *Nuovo Cimento*, **6**, 982 (1957).

[2] A. Bisi, E. Germagnoli, L. Zappa and E. Zimmer: *Nuovo Cimento*, **2**, 290 (1955). See this paper for references to previous work.

In particular, we obtained some information on the ratio of the γ activities of the 2 isotopes present in the mixture by using the expression:

$$\frac{A_{77As}(t_2)}{A_{71Ge}(t_2)} = \frac{A_{mix}(t_2) \exp\left[\lambda_{71Ge}(t_2 - t_1)\right] - A_{mix}(t_1)}{A_{mix}(t_1) - A_{mix}(t_2) \exp\left[\lambda_{77As}(t_2 - t_1)\right]},$$

in which the λ's are the decay constants, $A_{mix}(t_1)$, $A_{mix}(t_2)$ are the measured activities of the mixture at times t_1 and t_2 respectively.

In this way, the ^{77}As activity eight days after the end of irradiation was found to be reduced to a 70% of the ^{71}Ge bremsstrahlung activity in the energy range between 60 and 100 keV.

The above data are to be understood as indicative, however they enabled us at least to assume that in the energy range which is significant for the measurement, the activity of the impurities would not cancel a possible effect.

The same conclusion is reached by an evaluation of the activity of the impurities present in the mixture for energies lower than 120 keV, based on the initial isotopic abundances.

The energy range which seemed the most convenient for the polarization measurement was between 70 and 120 keV. A first measurement on the fifth day yielded negative result.

Polarization measurements were performed systematically starting with the seventh day. They consisted of a series of two minute counts with alternate magnetic field. The results are reported in Table I.

TABLE I. – *Total counts for the two orientations of magnetic field.*

Days after end of irradiation	Counts $\psi = 0$	Counts $\psi = \pi$	Counts/min	Effect
7	27.327	26.757	300	$2.1 \pm 0.9\%$
8 (*)	5.154	5.063	232	$1.8 \pm 2\ \%$
9	19.149	18.596	157	$2.9 \pm 1\ \%$
10	15.615	15.095	128	$3.4 \pm 1.1\%$
11	19.059	18.681	105	$2\ \pm 1\ \%$
Total	86.304	84.192		$2.5 \pm 0.5\%$

(*) The counts of the eighth day are low because of a failure in the magnet's cooling system.

A check of the effect of dispersed magnetic field on the apparatus was performed before, during and at the end of the polarization measurements by counting non polarized γ's. The deviation was constantly of the 0.2%. Moreover this effect was of the opposite sign as the effect due to polarized γ's.

The sign of the effect corresponds to right circular polarization of the γ-rays. It agrees with the theoretical prediction, and thus with the experimental evidence according to which negative β-rays are always left-handed and positive γ-rays always right-handed.

The magnitude of the effect predicted from two-component neutrino theory and from the estimated efficiency of the polarimeter is 6%.

It seems plausible to attribute the difference between the theoretical value of 6% and the observed value of 2.5% entirely to the background due to ^{77}As impurities, to multiple scattering in iron and to natural radioactivity, (this last very nearly negligible 13 counts/min, between 70 and 120 keV). A more accurate evaluationof the effect can be performed only by using a ^{71}Ge source depurated of ^{77}As.

* * *

The Relativistic Limit of the Theory of Spin $\frac{1}{2}$ Particles.

M. Cini and B. Touschek

Istituto di Fisica e Scuola di Perfezionamento in Fisica Nucleare dell'Università di Roma
Istituto Nazionale di Fisica Nucleare - Sezione di Roma

The transformation of Foldy and Wouthuysen [1] has greatly contributed to the understanding of the non-relativistic limit of the theory of spin $\frac{1}{2}$ particles. This transformation leads to a form of the Hamiltonian in which positive and negative energy states are separately described by two component wave functions; this is achieved at the expense of the locality in the description of the Dirac field. Recently the two component representation of the relativistic limit behaviour of a Dirac particle has received considerable attention [2]. In this note we want to point out that there exists a transformation very similar to the one considered by Foldy and Wouthuysen which leads to a form of the Hamiltonian in which positive and negative spirality states are separately described by two component wavefunctions. Using the notation of F.W. we choose

$$(1) \qquad S = -\frac{i}{2m}\beta(\boldsymbol{\alpha}\cdot\boldsymbol{p})\,w(p/m)\,.$$

---

[1] L. L. Foldy and S. Wouthuysen: *Phys. Rev.*, **78**, 29 (1950), referred to as FW. M. H. L. Pryce: *Proc. Roy. Soc.*, A **150**, 166 (1935); S. Tani: *Prog. Theor. Phys.*, **6**, 267 (1951).

[2] T. D. Lee and C. N. Yang: *Phys. Rev.*, **105**, 1671 (1957); A. Salam: *Nuovo Cimento*, **5**, 299 (1957); L. Landau: *Nuclear Phys.*, **3**, 127 (1957).

Then

$$(2) \qquad H' = \exp[iS]H\exp[-iS]\,,$$

becomes

$$(3) \qquad H' = \frac{E_p}{p}(\boldsymbol{\alpha}\cdot\boldsymbol{p})\,,$$

provided that w is chosen to be

$$(4) \qquad w = -\frac{m}{p}\operatorname{cotg}^{-1}(p/m)\,.$$

In this new representation the Dirac equation becomes

$$(5) \qquad (\boldsymbol{\alpha}\cdot\boldsymbol{p})\Psi' = p\Psi'\,,$$

which is identical to the Dirac equation for a massless neutrino. The actual separation in two components is effected by means of the projection operators $(1\pm\gamma_5)$ according to

$$(6) \qquad \begin{cases} \Psi' = \Phi' + X'\,, \\[4pt] \Phi' = \frac{1}{2}(1-\gamma_5)\Psi'\,, \\[4pt] X' = \frac{1}{2}(1+\gamma_5)\Psi'\,. \end{cases}$$

It should, however, be observed that γ_5 here refers to the new representation. In the old (conventional) representation

this operator has the form

$$(7) \quad \Gamma_5 = \exp\left[-iS\right]\gamma_5 \exp\left[iS\right] =$$

$$= -\frac{(\boldsymbol{\alpha}\cdot\boldsymbol{p}) + \beta m}{E_p} \frac{(\boldsymbol{\sigma}\cdot\boldsymbol{p})}{p} = -\varepsilon s \, ,$$

where ε is the sign of the energy and s the spirality of the state.

    If one is willing to speculate on the possible applications of this transformation to the actual problems of particle physics one might be tempted to try to replace γ_5 by Γ_5' in the projection operators appearing in the weak inter-action Hamiltonians of parity non conserving processes not involving neutrinos. (Clearly $\gamma_5 = \Gamma_5$ in the case of a massless neutrino). The introduction of Γ_5 would lead one to expect a maximum asymmetry in all decay processes leading to an angular distribution of the form $(1 \pm \overline{P} \cos\theta)$ where P is the average polarization in the production process. However, the introduction of the operator Γ_5 instead of γ_5 may meet considerable difficulties owing to the apparent non-covariance of the transformation (2) and its non-locality.

LIBRI RICEVUTI E RECENSIONI

JENAER ZEISS – *Jahrbuch 1950* - Kommissionsverlag von Gustav Fischer, Jena.

W. FALTA - *Ricerche per la pratica eliminazione dell'effetto direzionale negli sviluppi invertitori.*

G. MESTWERDT - *Il « Kolposkopio » nella lotta contro i tumori nella donna.*

H. BOEGEHOLD - *Per la storia dell'obbiettivo apocromatico.*
L'immagine del microscopio.

H. HARTING - *Indici di rifrazione di alcuni cristalli di alogenuri.*

R. TIEDEKEN - *Sulle formule di approssimazione del terzo grado per l'interno di un raggio principale in sistemi aventi simmetria di rotazione.*

E. WANDERSLEB - *I diversi tipi di ingrandimento di un cannocchiale a grande campo.*

F. FERTSCH - *Un binocolo di tipo particolare.*

A. KÖHLER - *Una generalizzazione della teoria del telemetro a cannocchiale e la sua applicazione pratica alle misure di distanza.*

A. POHLACK - *Metodi analitici e grafici per la soluzione di problemi di interferenza ottica su superfici sottili.*

H. K. ZINSER - *Studi di microscopia clinica col procedimento del contrasto di fase.*

C. BÜTTNER - *Contributi al controllo di superfici lavorate.*

A. SCHORSCH - *Sull'influenza delle tolleranze di rifinitura nell'errore di misura di strumenti tecnici di precisione.*

J. BITTNER - *Sulle proprietà della pirite sintetica come raddrizzatori.*

Per celebrare il centenario della fondazione degli stabilimenti ottici Carlo Zeiss di Jena, avvenuto il 17 Novembre 1946, era stata predisposta la pubblicazione di un certo numero di lavori scientifici riguardanti lo stato delle ricerche che vengono eseguite in quegli importanti laboratori.

Varie difficoltà sorte in conseguenza della recente guerra impedirono allora la realizzazione di questo progetto, nonostante che la C. Zeiss di Jena avesse ripreso a pieno ritmo l'attività di produzione e di ricerca.

Solo nel 1950, col miglioramento della situazione generale e per il notevole interessamento dello Stato fu resa possibile la pubblicazione in forma di Annuario, lo « Jenaer Jahrbuch » di alcuni dei più interessanti lavori.

Com'è naturale, si tratta prevalentemente dello studio e della soluzione di problemi particolari d'ottica geometrica e di tecniche strumentali connesse con la fabbricazione di strumenti ottici di gran classe.

Non mancano tuttavia lavori di carattere più generale, sia di ricerca, sia di rielaborazione sistematica in campi più o meno attinenti all'attività della Zeiss.

I quattordici lavori riportati nel primo volume, pubblicato nel 1950, di notevole interesse per gli specialisti, copre un po' tutto il campo applicativo della Zeiss di Jena. Nel campo dello studio dei materiali per scopi ottici ci sono misure di alta precisione e indici di rifrazione di alcuni alogenuri (NaF, LiF) impiegati in varie maniere in vetri d'ottica e in sistemi disperdenti, mentre per quel che riguarda l'impiego degli apparecchi di ottica si hanno osservazioni sull'impiego del microscopio elmico a contrasto di fase ed uno studio sull'impiego per scopi diagnostici nella lotta contro il cancro di un microscopio Zeiss detto « Kolposcopio ».

Uno studio analitico molto circostanziato determina l'influenza della tolleranza nelle rifiniture delle parti degli strumenti di misura di ottica di precisione sull'errore con cui si ricavano le misure stesse.

Sempre nel campo del controllo della qualità della produzione è notevole un lavoro di Büttner per l'esame di superfici lavorate col metodo interferenziale, per evitare la distruzione del materiale stesso: è stata usata la tecnica della « replica » colloidale della superficie in esame, analoga a quella impiegata in microscopia elettronica. I risultati conseguiti con questo sistema di controllo della produzione sono molto convincenti.

Oltre a questi lavori di carattere vario, una parte notevole dell'attività di ricerca della Zeiss è dedicato allo studio dei sistemi ottici, ed è intesa al miglioramento di particolari apparecchi, obiettivi, ecc.

Pur trattandosi di lavori altamente specializzati, taluni di essi risultano di lettura interessante, specie in quanto di un determinato problema (p. es. la costruzione di obiettivi Apocromatici) viene fatta la storia dei vari tentativi e studi fatti precedentemente. È inutile dire che, indietro nel tempo, si ritrovano sempre più frequenti i nomi di ABBE, SCHOTT, ZEISS.

U. ASCOLI

JENAER ZEISS – *Jahrbuch 1952* - Kommissionsverlag von Gustav Fischer, Jena.

H. BENZINGER - *Nuovi metodi per la determinazione delle costanti ottiche dei metalli.*

P. GÖRLICH e A. KROHS - *Sulle misure su cellule fotoconduttive.*

R. MEIER - *Ricerche nel campo delle onde di lunghezza dell'ordine del decimo di millimetro.*

H. POHLACK - *La sintesi di sistemi di superfici interferenziali di proprietà spettrali prestabilite.*

H. HASSELMEIER - *Il centraggio mediante superfici coniche e suo controllo.*

W. BAUER e F. NESSLER - *Trasmissione del calore attraverso lastre anisotrope.*

H. SCHRADE -

F. HANSER - *Lo sviluppo degli apparati per microfotografia della società Zeiss nel suo primo secolo di vita.*

J. FOCKE - *Sulle aberrazioni di un sistema ottico centrato. Un contributo alla Teoria dell'eiconale e delle aberrazioni.*

A. KNESCHKE - *Sulla relazione tra il problema di integrazione differenziale e il problema dell'interpolazione.*

H. POHLACK - *Sul problema della diminuzione della riflessione di vetri d'ottica mediante incidenza non ortogonale della luce.*

L'annuario 1952 (non risulta pervenuto quello del 1951) dedica una notevole parte dello spazio alla storia dello sviluppo degli apparecchi per microfotografia della Zeiss.

Forse, di un articolo reclamistico quale questo si deve ritenere, la ditta Zeiss, che può vantare ben un secolo di

accurata esperienza in questo campo, poteva non aver bisogno!

Uno studio di notevole interesse, oltre che in vista delle applicazioni anche per l'elegante sviluppo logico, è quello di H. Pohlack sulla trasparenza spettrale di un sistema composto da un numero qualunque di superfici interferenziali omogenee, prive di assorbimento. In questo lavoro, mediante opportune definizioni, si trasferisce la trattazione del problema a quella ben nota del quadripolo: un'applicazione, tra le possibili, è fatta, in un altro articolo pubblicato sempre nello Jenaer Jahrbuch 1952, al problema della riduzione della riflessione della luce incidente sui vetri di ottica.

L'applicazione della teoria del quadripolo allo studio dei problemi della riduzione o dell'aumento della riflessione e dei fattori interferenziali era già nota [cfr. p. es. SCHUSTER: *Ann. d. Phys.*, **6**, Folge 4, H. 6 (1949)]; questa di Pohlack costituisce una notevole, anche se non definitiva generalizzazione.

Alle tecniche sperimentali connesse con lo studio della riflessione metallica è dedicato un interessante lavoro nel quale è data sia la trattazione teorica della questione, che la descrizione di alcuni strumenti, che permettono di raggiungere notevole precisione. Viene riportata la determinazione di n e x per il cromo, l'alluminio, l'argento ed il platino.

U. ASCOLI

A. H. WILSON – *Thermodynamics and Statistical Mechanics*. 495 pagg., Cambridge University Press 1957. Prezzo 50 scellini.

Si tratta di un libro non certo raccomandabile agli studenti che iniziano questi studi, e che interesserà pochi specialisti. La parte più pregevole è costituita dalla termodinamica classica, sviluppata lungo la maniera ossiomodica.

A noi sembra che proprio la presenza della meccanica statistica renda questo rigore logico e astratto piuttosto superato; ma i cultori di questo genere di termodinamica troveranno una trattazione ad alto livello.

La meccanica statistica è pure trattata ad un livello elevato, ma non con altrettanto rigore per quanto riguarda i fondamenti. Le applicazioni sono numerosissime, ma ci lasciano assai insoddisfatti.

Per esempio: la superconduttività è trattata in otto pagine, e le proprietà dell'olio in nove; il tutto da un punto di vista termodinamico e analitico, e mai in quei termini molecolari che rendono questa parte della fisica così viva e interessante.

G. CARERI

M. BORN – *Physics in My Generation*. Vol. I in-16°, di pp. 232 (Pergamon Press, London - New York, 1958).

Si tratta di una raccolta di vari scritti divulgati o di circostanza, pubblicati da BORN tra il 1921 e il 1951, cioè in un periodo particolarmente « avventuroso » per la Fisica. Tra la prefazione del volume sulla relatività einsteiniana e l'appendice di quello sul « Restless Universe », che costituiscono rispettivamente il primo e l'ultimo degli scritti qui riportati in ordine cronologico, vengono toccati gli argomenti che più spesso hanno costituito oggetto di accesi dibattiti intorno alla Fisica moderna, dai riflessi filosofici della meccanica quantistica, della relatività e delle nuove cosmologie, alle conseguenze politiche e sociali dell'avvento dell'era atomica.

Sull'interpretazione statistica della funzione d'onda di Schrödinger, da BORN stesso proposta nel 1926, egli fornisce interessanti dettagli storico-critici, che chiariscono il passaggio dai tentativi

prima compiuti da lui e WIENER per rendere applicabile ai processi aperiodici il metodo delle matrici, alla riuscita estensione dell'idea avuta da Einstein, di interpretare i quadrati delle ampiezze d'onda ottiche come densità di probabilità della presenza di fotoni.

Altri saggi di notevole valore didattico sono quelli dedicati a « Causa, fine ed economia nelle leggi di natura » (cioè ai principi di minimo e di massimo della meccanica analitica e della meccanica statistica), alle teorie statistiche di Einstein ed a varie questioni concettuali del genere di quelle trattate, in forma più approfondita, nel volume *Natural Philosophy of Cause and Chance*, pubblicato da BORN nel 1949.

V. SOMENZI

O. R. FRISCH – *Progress in Nuclear Physics*, Vol. V (Pergamon Press, London and New York, 1956), $ 12.50 (pp. VII-325).

Il quinto volume di questa serie comprende una selezione di articoli su vari argomenti di grande attualità fisica nucleare.

Nel primo articolo di W. W. BUECHNER vengono descritti i vari metodi per la determinazione della energia di particelle emesse in reazioni nucleari, i selettori di energia per i fasci di particelle e gli analizzatori per i prodotti delle reazioni nucleari.

Il secondo articolo di JOAN M. FREEMAN è dedicato alla diffusione anelastica di neutroni veloci. L'articolo riassume i più recenti risultati sperimentali seguiti da discussioni teoriche e da una tabella riassuntiva delle sezioni d'urto per collisione anelastica di numerosi elementi.

K. KANDIAH e G. B. B. CHAPLIN nel terzo articolo espongono le più moderne tecniche elettroniche usate nella fisica nucleare. Sono discussi alcuni circuiti rapidi, quali coincidenze e circuiti a

scatto e gli elementi decimali di conteggio; una larga parte dell'articolo è dedicata ai transistori ed ai loro possibili impieghi nella fisica nucleare.

Segue un articolo di C. DODD sulla camera a bolle.

Il quinto articolo di J. M. C. SCOTT riguarda il raggio del nucleo. In esso vengono esaminati i vari metodi usati per la determinazione del raggio del nucleo in funzione del numero atomico cui segue una discussione dei risultati.

Il sesto articolo di B. W. RIDLEY ha per titolo: « Il Neutrino ». In esso tutti i fatti teorici e sperimentali connessi con il neutrino vengono presentati e discussi con profondità.

Il settimo ed ultimo articolo scritto da F. D. BROOKS è dedicato ai scintillatori organici. Il processo di luminescenza al passaggio di una particella in un mezzo organico è discusso sia nel caso di cristalli sia nel caso di liquidi organici. Sono dati per le varie sostanze spettri, vite medie.

Ogni articolo è seguito da una assai vasta e completa bibliografia, cosicchè ciascun articolo rappresenta per lo specialista, una rassegna che lo mette al corrente dei recenti progressi nei singoli campi di ricerca.

BRUNELLO RISPOLI

Progress in Cosmic Ray Physics – Vol. III edito da J. G. WILSON North-Holland Publishing Company, Amsterdam, 1956), pagine XII-420. Fiorini olandesi 38.

Questo libro è il terzo rapporto sullo stato di conoscenza della Fisica dei raggi cosmici edito da J. G. WILSON; esso è stato scritto nei primi mesi del 1955 sebbene in esso si trovino inserite alcune citazioni di lavori posteriori; poichè la conoscenza del mondo fisico si evolve in questo settore assai rapidamente il volume vuole cristallizzare la situazione

nell'anno 1955; esso contiene i più re-centi dati sperimentali, molti dei quali appaiono per la prima volta raccolti in un libro insieme con una vasta biblio-grafia cosicchè il volume risulta utilis-simo per gli studiosi dei raggi cosmici non solo per gli ottimi articoli generali in esso contenuti, ma anche per la grande quantità di dati sperimentali e di rife-rimenti bibliografici.

Il volume contiene i seguenti articoli: 1) *Gli sciami estesi* di K. GREISEN; 2) *Risultati sperimentali sui mesoni* K *ed iperoni* di H. BRIDGE; 3) *Processi di de-cadimento di particelle neutre instabili* di R. W. THOMPSON; 4) *Il bilancio energe-tico della radiazione cosmica* di G. PUPPI.

Nel primo articolo vengono ripor-tati i risultati delle teorie degli sciami estesi nei riguardi dello sviluppo longi-tudinale, laterale ed angolare di una cascata elettronica insieme con la descri-zione degli esperimenti effettuati dai vari autori; sono successivamente prese in considerazione la densità dello sciame, e le variazioni di intensità con l'altezza, con il tempo e gli effetti barometrici, nonchè le componenti mesoniche e nu-

cleoniche e lo spettro della componente primaria.

Il secondo articolo contiene una ras-segna critica assai completa, ed ottima da ogni punto di vista, dei risultati teo-rici e sperimentali ottenuti recentemente sulle particelle strane; sono esaminati i mesoni τ, la disintegrazione dei mesoni K, gli eventi S, le particelle V cariche, e gli iperoni.

Nel terzo articolo R. W. THOMPSON dopo una introduzione a carattere sto-rico sulle particelle V^0 esamina con no-tevole profondità le tecniche sperimentali (ed i loro limiti) usate nella investiga-zione delle particelle V^0. Segue una ana-lisi delle particelle Λ^0, θ^0 e dei decadi-menti anomali delle V^0.

Conclude il volume un attento ed approfondito esame del bilancio energe-tico della radiazione cosmica a 50° di latitudine geomagnetica. I vari fatti spe-rimentali e le interpretazioni teoriche sono prese in considerazione per la com-ponente mesonica, la componente elettro-fotonica, e la componente nucleonica.

BRUNELLO RISPOLI